Environmental Controls on Alternating Aragonite-calcite Laminations in Notch-speleothems from Cayman Brac, Cayman Islands, British West Indies

by

ERJUN ZHENG

A thesis submitted in partial fulfillment of the requirements for the degree of

Master of Science

Department of Earth and Atmospheric Sciences
University of Alberta

ABSTRACT

Speleothems that grow in semi-exposed surface environments, such as wave-cut notches, are not well understood despite their widespread distribution. The +6.4 m-high wave-cut notch on Cayman Brac, that formed ~ 125 ka ago, is decorated with stalactites, stalagmites, and columns that grew between ~50 ka and ~45 ka ago. These speleothems are formed of calcite, aragonite, and mixed calcite-aragonite laminae, that are commonly separated by unconformities. The mineralogy, crystal morphologies, and fabrics vary between laminations in the same speleothem and from speleothem to speleothem.

The calcite and aragonite laminae in the Cayman notch-speleothems are primary precipitates with minimal alteration by diagenesis or microbial processes. The $\delta^{18}O$ values of these precipitates range from -6.5 to +0.3‰ VPDB, and the $\delta^{13}C$ values range from -11.4 to +1.9‰ VPDB. The strong positive co-variation between $\delta^{18}O$ and $\delta^{13}C$ indicates that evaporation and/or kinetic fractionation was involved in the precipitation processes. Growth of the speleothems spans the warm and wet Dansgaard/Oeschger interstadial 13 (D/O-13), the cooler and drier Heinrich stadial 5 (HS-5), and the warm and wet Dansgaard/Oeschger interstadial (D/O-12), that are millennial-scale climate events. Comparison of stable-isotopic variations from the notch-speleothems with other paleoenvironmental proxies suggests that their growth was controlled by the paleoclimate variation, and confirms the global teleconnection between the tropical Caribbean and the high-latitude North Atlantic. The cooler and drier HS-5 period with enhanced evaporation potentially led to the elevated Mg/Ca and elevated saturation states, that may have been the main control over aragonite precipitation. In contrast, precipitation of calcite was typically favored during the warm and wet periods (D/O-13 and D/O-12) when evaporation was lower.

PREFACE

This thesis is an original work completed by Erjun Zheng, with the assistance of Dr. Brian Jones. The notch-speleothem samples were collected by Dr. Jones, and he also provided the field photographs of wave-cut notch and notch-speleothems used in this study. The overall theme of the thesis was initially outlined by Dr. Jones and then developed through discussions between the two of us.

ACKNOWLEDGEMENT

I really appreciate all the help and support of so many people throughout my thesis.

First and foremost, I want to thank my supervisor Dr. Brian Jones for offering me the o - portunity to work on this project. I would like to thank you for all the valuable guidance on this study. Thanks to Brian for his enlightening advice, consecutive encouragement and criticism, patience and numerous hours of editing. Without his help, I would never be able to finish this thesis.

I would like to thank Dr. Karlis Muehlenbachs and Dr. Long Li for generously allowing me to use their laboratory for the stable isotope analysis; Mrs. Diane Caird for running the XRD samples; Dr. Gerein Nathan for taking the SEM photomicrographs used in this study; Mr. Mark Labbe and Mr. Martin Von Dollen for cutting my samples and preparing the thin sections; and Mr. Igor Jakab, who provided help for thin section scanning.

It has been great to work with all the people of our Carbonate Research Group - Ting Liang, Min Ren, and Simone Booker. Thanks for their kind help, suggestions, and advice.

I am grateful to the Natural Sciences and Engineering Research Council of Canada, which funded this study (Grant ZA635 to Jones); and Mr. Hendrik van Genderen (Water Authority, Cayman Islands) who helped collect the samples used in this study.

Finally, thanks to my family for their love, patience, constant support, and encouragement throughout my study.

TABLE OF CONTENTS

LIST OF TABLES

LIST OF FIGURES

CHAPTER 1: INTRODUCTION

1. Introduction

One of the most spectacular features on Cayman Brac (Fig. 1.1C) is the wave-cut notch, 6.4 m above sea-level (asl) that is cut into the cliff faces around the island (oodroffe et al., 1983; Jones and Hunter, 1994; Tarhule-Lips, 1999). In many areas, this notch is adorned with stalactites, stalagmites, columns, and flowstone that have been collectively referred to as notch speleothems (Jones, 2010a). Although speleothems like these are common in coastal marine notches (Mylroie and Carew, 1991; Taboroši et al., 2003), studies focusing on these deposits are scarce and still in their infancy.

Freshwater carbonate deposits are important paleoenvironmental archives (Hendy and Wilson, 1968; Ford and Pedley, 1996; Andrews, 2006; Pedley and Rogerson, 2010; Dabkowski et al., 2015). Diverse proxies, including the $\delta^{18}O$ and $\delta^{13}C$ isotopes, obtained from carbonate deposits have been widely used to reconstruct the paleoclimate and paleoenvironmental evolution (e.g., McDermott, 2004; Fairchild et al., 2006; Andrews, 2006). The Cayman notch-speleothems are prime candidates for investigating paleoclimate changes because their growth was directly linked to the rainfall that occurred during their growth (Jones, 1994). Potentially, the oxygen and carbon isotopes of the notch speleothems can yield valuable information regarding the changes in the precipitation, temperatures, and vegetation of Cayman Islands during the period of their growth. Such information also allows comparisons with other paleoclimatic information from across the Caribbean and will contribute to the understanding of regional paleoclimatic variation.

2. Geography and physiography

Cayman Brac (19°43' N, 79°48' W), the easternmost of the Cayman Islands, is ~ 19 km long and 1.5 to 3.0 km wide with a surface area of ~36 km^2 (Fig. 1.1B). This island is situated about

240 km south of Cuba and 290 km northwest of Jamaica (Fig. 1.1A). Cayman Brac is characterized by its spectacular cliff, with the island name *Cayman Brac*" being deriving from Gaelic word for the "*bluff*". Abundant caves decorated with speleothems are present in the carbonate successions (Tarhule-Lips, 1993, 1999). A wave-cut notch, about 6 m above sea level is evident in the cliff faces around much of the island (oodroffe et al., 1983)

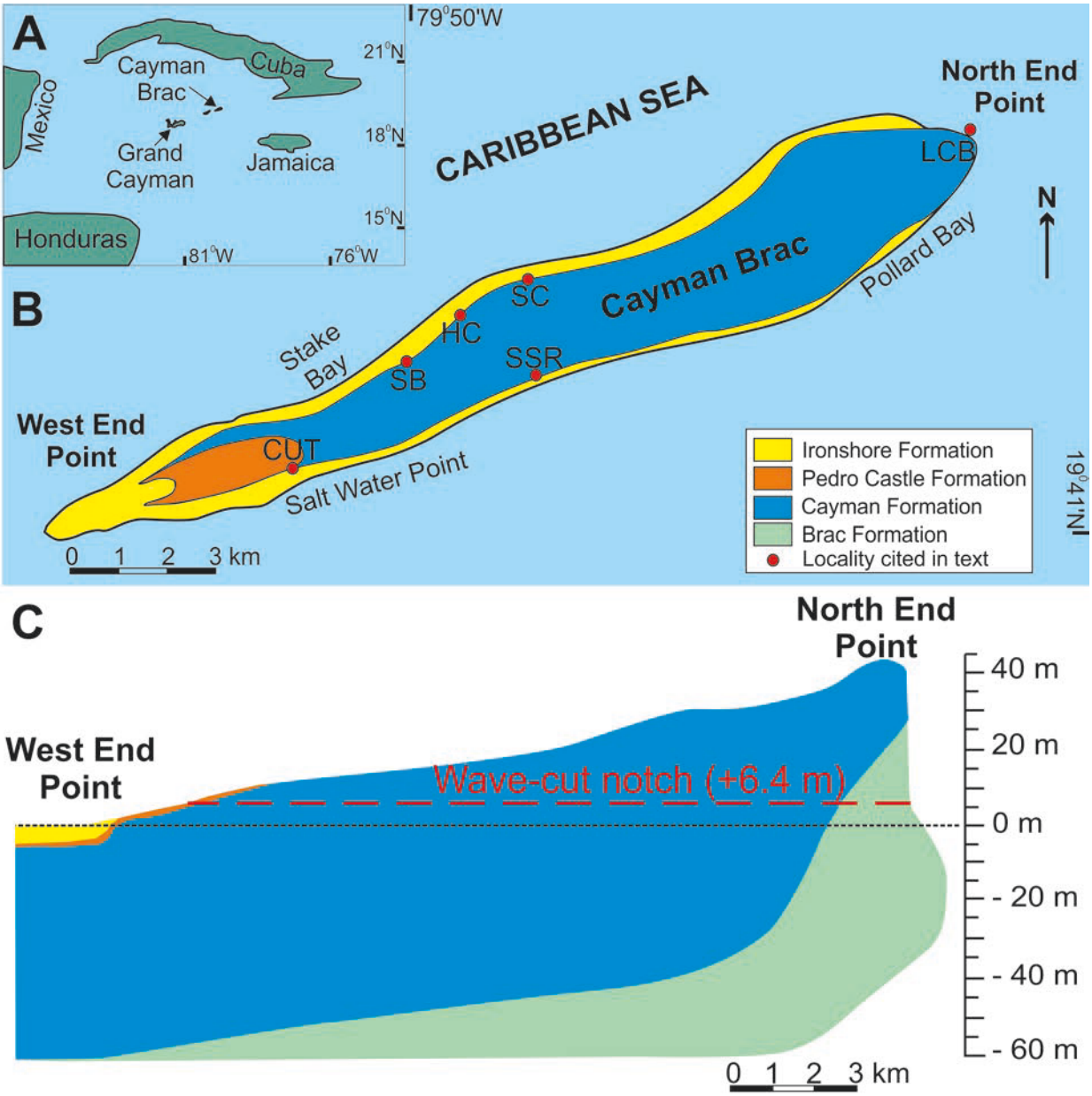

Fig. 1.1 Geographic and geologic map of study area. (A) Location of Cayman Brac. (B) Geological map (modified from Jones, 2010a) showing localities for sample collection and field observations. (C) Geol - ical cross-section from North End Point to West End Point, Cayman Brac (modified from Jones, 1994)

Unlike its two low-lying (typically ≤ 15 m high) sister islands of Grand Cayman and Little Cayman, Cayman Brac rises to 43 m above present sea level at its northeast end (Fig. 1.1C). The uneven topography of Cayman Brac is highly influenced by the tilted bedrock and karstificatio (Liang and Jones, 2015b). The island surface is characterized by phytokarst with small, sharp pinnacles separated by sinkholes (Liang and Jones, 2015a). Terra rossa, derived from weathering of carbonates and/or wind-blown deposits from Sahara or possible North America, is widespread on the islands, and may represent one or more paleosols (Tarhule-Lips, 1993; Liang and Jones, 2015b). The tropical flora on Cayman Brac is dense and continuous despite the fact that soil cover on the island is patchy and thin (Tarhule-Lips, 1993; Jones, 1994). Exposed outcrops are extensively weathered and generally inaccessible. There are no surface freshwater streams or lakes on Cayman Brac (Jones, 1994).

Located to the south of the Tropic of Cancer, Cayman Brac enjoys a tropical oceanic climate, with predominant northeast trade winds and an average annual temperature of 27 °C (Darbyshire et al., 1976). Relative humidity is above 80% throughout the year. The air temperature on Cayman Brac is also affected by the Caribbean current, which brings warm water from the equato . There is a drier season from November to April (25.8 °C) with prevailing northeast to northwest winds, whereas a rainier season from May to October (30 °C) with dominating east winds. Meteoric precipitation on the island varies seasonally and spatially, with western part receiving more rainfall (Jones et al., 1997). The Cayman Islands are situated in the paths of tropical storms and hurricanes, and are commonly affected by destructive storms in September and Octobe .

3. Geological setting

The Cayman Islands are situated on the Cayman Ridge (Fig. 1.2) that extends from Belize to the Sierra Maestra of southeastern Cuba (Fig. 1.1A), rising from sea floor to above sea level

(Perfit and Heezen 1978; Holcombe et al. 1990). Each of the Cayman Islands is probably l - cated on separate fault blocks that have probably experienced independent tectonic movement (Horsfield, 1972; Jones and Hunte , 1990). Studies suggest that the core of the Cayman Ridge is formed of granodiorite overlain by volcanic rocks and capped by Tertiary carbonates (Perfit and Heezen, 1978; Holcombe et al., 1990). Emery and Milliman (1980) suggested that the carbonate successions is more than 401 m thick, based on wells drilled on Grand Cayman.

The Cayman Trough (formerly called the Bartlett Trench), to the south of the Cayman Ridge, is 120 - 180 km wide and over 6000 m deep (Perfit and Heezen, 1978; Macdonald and Ho - combe, 1978). It is the deepest feature in the Caribbean Sea (ten Brink et al., 2002). The Cayman Trough is bisected by the Mid-Cayman Rise, which is a 100 km-long ocean spreading center located off the southwest corner of Grand Cayman. The Swan Island Transform Fault extends westward from the south end of the Mid-Cayman Rise and the Oriente Transform Fault extends eastward from the north end of the rise (Macdonald and Holcombe, 1978). These two left-lateral, strike-slip transform faults form the tectonic boundary between the North American Plate and the Caribbean Plate. The opening of the Cayman Trough was probably initiated during the Late Eocene (Perfit and Heezen, 1978; Rosencrantz et al., 1988). Recent GPS investigates and sei - mic data indicate that this area is still tectonically active (Dixon et al., 1998; DeMets and Wig- gins-Grandison, 2007).

4. Stratigraphic framework

Matley (1926) first named the carbonate successions that formed most of exposed rocks of the islands as the “Bluff Limestone” (Middle Oligocene), and named the Pleistocene limestone that unconformably overlie the Bluff Limestone as the Ironshore Formation. Subsequent studies, however, demonstrated that the Bluff Limestone is formed la gely of dolostone (Pleydell, 1987;

Jones and Hunter, 1989). Thus, Jones and Hunter (1989) proposed the Bluff Formation to remov the associated lithological connotation with Bluff Limestone. They further divided the Bluff Fo - mation into Cayman Member and Pedro Castle Member. Further outcrop investigations (Jones et al., 1994a, 1994b) along the bluff at the east end on Cayman Brac, led to the definition of th Brac Formation. The Brac Formation was separated from the over-lying strata by a southwest-ward-tilting unconformity. Jones et al. (1994b) then elevated the Cayman Member and the Pedro Castle Member to formation status, and elevated the Bluff Formation to the Bluff Group. Hence the Bluff Group now includes the Brac Formation, the Cayman Formation, and the Pedro Castle Formation. Fossils and strontium isotope data indicate that the Brac Formation, and the Pedro Castle Formation were late Oligocene, and Pliocene in age, respectively (Jones et al., 1994a, 1994b; MacNeil and Jones, 2003; Uzelman, 2009). A middle Miocene age was estimated for the Cayman Formation, based on the fossils and its occurrence between the Brac Formation and the Pedro Castle Formation (Zhao and Jones, 2012a, 2012b).

Unconformities that separated each formation in the Bluff Group were initially named after the formation which they capped (Jones and Hunter, 1994). Thus, the unconformity between the Brac Formation and Cayman Formation is call the Brac Unconformity, whereas the unconfor-mity which separates the Cayman Formation and its overlying Pedro Castle Formation is called the Cayman Unconformity. The Pedro Castle Unconformity forms the upper surface of the Pedro Castle Formation. Liang and Jones (2014), however, suggested that they should be named ac-cording to the formations they separated at a particular locality. For example, the Pedro Castle Formation overlies the Cayman Formation in some areas, whereas the Ironshore Formation sits directly above the Cayman Formation in other places. Hence, the unconformities were named Cayman-Pedro Castle Unconformity and Cayman-Ironshore Unconformity, respectively.

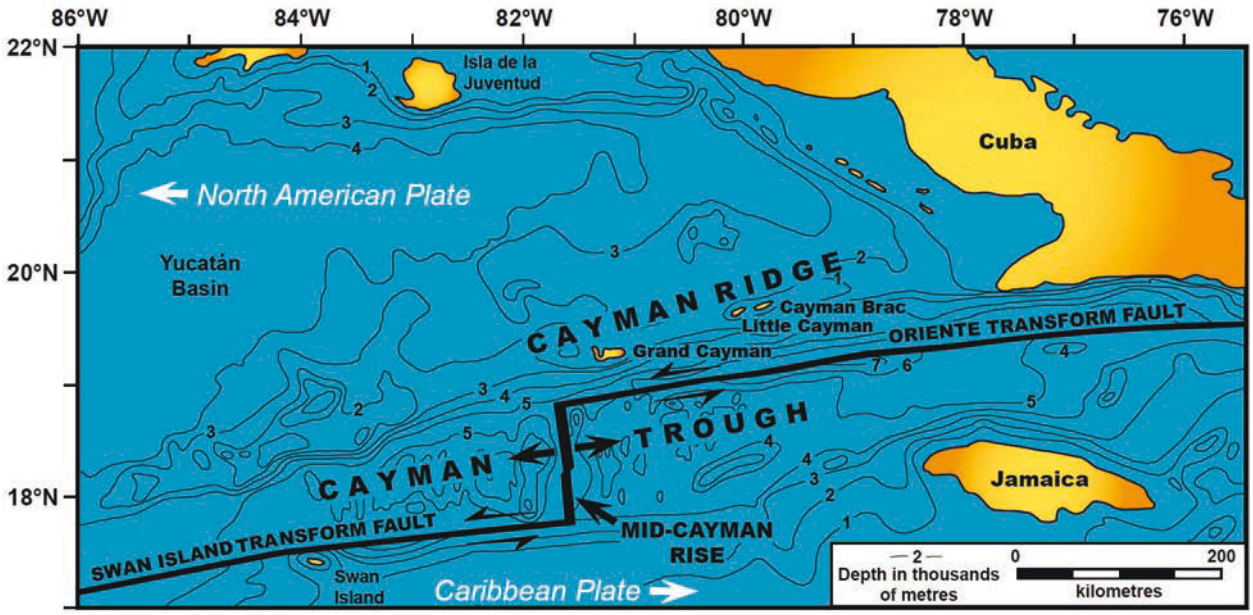

Fig. 1.2 Tectonic setting of Cayman Islands (modified from Uzelman, 2009)

4.1. The Brac Formation

The Brac Formation is exposed in the basal part of the cliffs on the eastern end of Cayman Brac (Fig. 1.1C), where it is up to 33 m thick. The total thickness of the Brac Formation, however, is unknown (Uzelman, 2009; Zhao and Jones, 2012b). The Brac Formation is formed of limestones and dolostones. Along the northeastern coast, it is characterized by bioclastic limestones (wackstones to grainstones) with minor amount of dolostones (Jones et al., 1994b; Uzelman, 2009; Zhao and Jones, 2012b). *Lepidocyclina* is the dominant fossil, along with red algae, and some echinoid fragments. In contrast, on the southeastern coast, the Brac Formation is formed of sucrosic dolostones and dolomitic limestones along with isolated pods of limestone that is like that found on the north coast. On the basis of foraminifera biostratigraphy and strontium isotope (average $^{87}Sr/^{86}Sr$ ratio of 0.70808, indicating 28 Ma old) of the limestone, Jones et al. (1994b) suggested that the Brac Formation was of Late Oligocene age (Fig. 1.3).

4.2. The Cayman Formation

The Cayman Formation, which is widely exposed on Cayman Brac (Fig. 1.1B and C), is probably ~ 100 m thick (Jones et al., 1994b). There, the formation is formed entirely of finely crystalline dolostones (Zhao and Jones, 2012a). These fabric-retentive dolostones contain abundant fossils, including corals, bivalves, gastropods, rhodoliths, *Halimeda*, echinoderm plates, red algae, and foraminifera (Jones and Hunter, 1994; Zhao and Jones, 2012a). There is no evidence of reef development in the Cayman Formation (Jones and Hunter, 1994; Zhao and Jones, 2012a). Fossil-moldic porosity is high because skeletal fragments originally formed of aragonite have been pervasively dissolved (Zhao and Jones, 2012a). Jones et al. (1994) and Zhao and Jones (2012a) suggested that a Middle Miocene age could be inferred on basis of foraminifera fauna assemblage by referring to the established Caribbean biostratigraphy framework (Fig. 1.3).

4.3. The Pedro Castle Formation

The Pedro Castle Formation outcrops on the west end of Cayman Brac (Fig. 1.1B andC), where it is 6 to 20 m thick (Jones et al., 1994b; MacNeil and Jones, 2003; Liang and Jones, 2014). The Pedro Castle Formation is characterized by limestones, dolomitic limestones, and fabric-retentive dolostones (MacNeil and Jones, 2003). There is an overall trend from dolostone at bottom to limestone at the top (MacNeil and Jones, 2003). The Pedro Castle Formation is formed largely of skeletal wackstones with minor amounts of mudstone and packstone (Jones and Hunter, 1994; MacNeil and Jones, 2003). The biota includes bivalves, gastropods, red algae, foraminifera, and scattered corals (MacNeil and Jones, 2003). There is, however, no evidence of reefal development in Pedro Castle Formation. The coral biostratigraphy and $^{87}Sr/^{86}Sr$ isotope ratios of the limestones suggest a Pliocene age for the Pedro Castle Formation (Jones et al., 1994b; MacNeil and Jones, 2003) (Fig. 1.3).

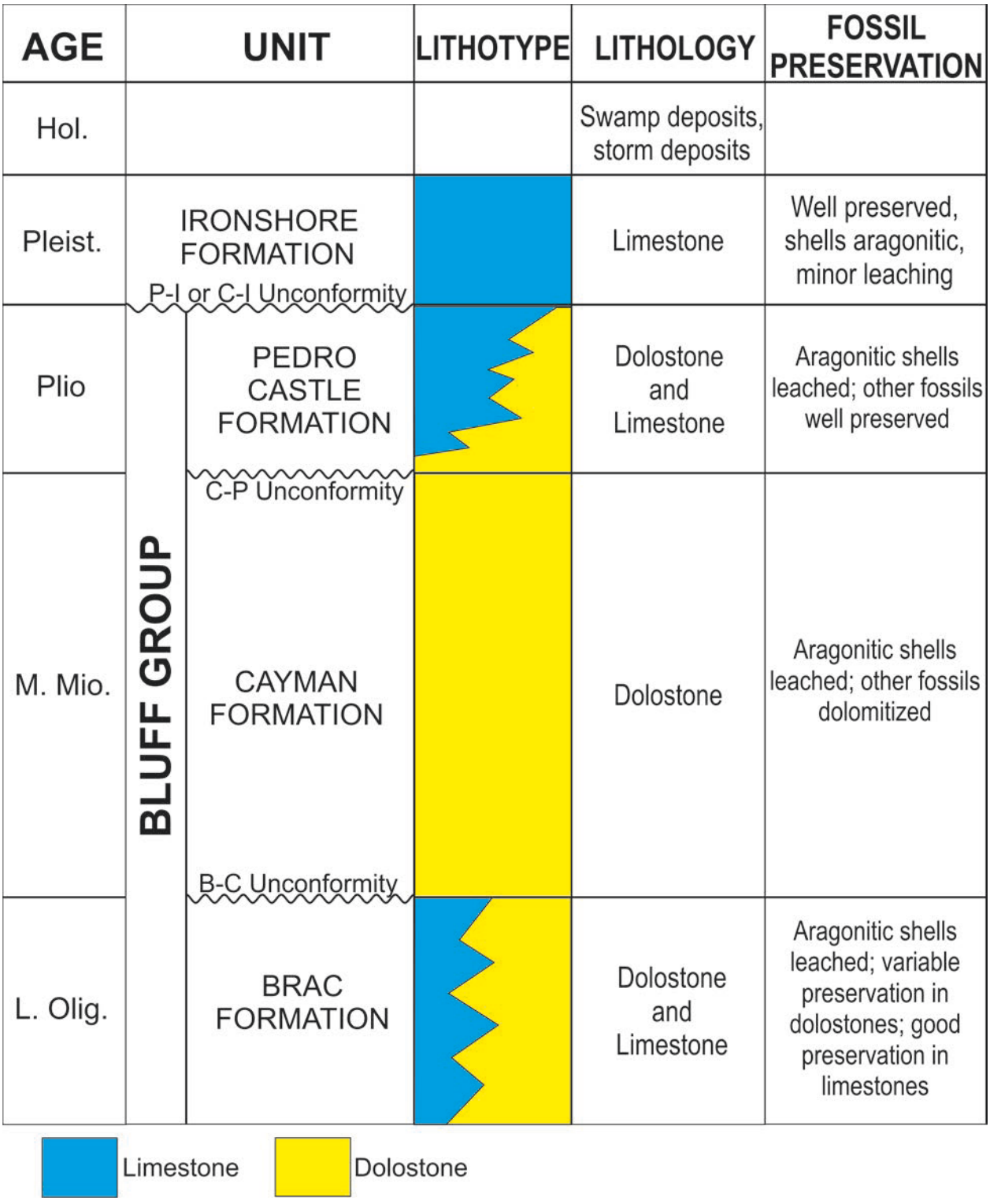

Fig. 1.3 Stratigraphic column on Cayman Brac (modified from Jones, 1994)

4.4. The Ironshore Formation

The Ironshore Formation, which forms a narrow coastal platform around each of the Cayman Islands (Fig. 1.1B and C), is typically less than 9 m thick. On Cayman Brac, this formation is stratigraphically horizontal, which indicates that deposition of those sediments postdated tectonic uplift and tilting of the Bluff Group (Shourie, 1993; Zhao and Jones, 2012b). The Ironshore Formation is characterized by limestones with well-preserved corals, bivalves, gastropods, bivalves, foraminifera, and algae (Zhao and Jones, 2013). The exposed part was deposited ~ 125,000 years ago when the wave-cut notch in the cliff was formed during the ~ 6 m highstand (Coyne and Jones, 2007; Zhao and Jones, 2013) (Fig. 1.3).

5. Methodology

Samples used in this study were collected by Dr. Brian Jones from locality CUT on the south-west coast and locality SB (near Stake Bay) on the north coast of Cayman Brac (Figs. 1.1B). Field examination on the notch-speleothems were also conducted by Dr. Brian Jones at locality SSR.

5.1. Thin section petrography

Twenty-five la ge thin sections (7.5 × 5.0 cm) were made from the notch-speleothems after they had been vacuum impregnated with blue epoxy. Some of the thin sections were parallel to the long growth axis, whereas others were cut transverse to the growth axis. These sections were used to document the mineralogy, crystal morphologies, fabrics, diagenetic processes, and microbes found in the notch-speleothems.

5.2. X-Ray diffractio

X-ray diffraction (XRD) was used to (1) confirm the mineralogy of the speleothems, and (2 calculate the percentages of calcite and aragonite in the samples that were used for oxygen and

carbon isotope analyses. All subsamples (typically 1-2 g) were manually drilled from recognizable laminations from sectioned surfaces and fully ground into powder (75-150 μm) using an agate mortar and pestle to ensure homogeneity and provide a uniform surface area.

For XRD analysis, each sample (~ 1g) was scanned from 5° to 90° 2θ at a speed of 2° θ/min on the Rigaku Ultima IV Powder XRD system that was run at 38 kV and 38 mA using an Ultima IV X-ray generator with a Co tube at the University of Alberta. Mineral identifications were derived using the JADE 9.5 computer program that operates in tandem with the X-ray system. The relative abundance of calcite versus aragonite were calculated according to the empirical equation (1.1):

$$y = 56.2982x^3 - 1.1170x^2 + 45.2572x \quad (1.1)$$

with y = % calcite and $x = d_{104}/(d_{104} + d_{111} + d_{021})$ where d = peak heights.

This empirical equation, was derived by Dr. A. Locock (pers. comm., Electron Microprobe Laboratory, University of Alberta) based on artificial samples created with known percentages of calcite and aragonite. It has also been used by Li and Jones (2014), and Jones and Peng (2016). Replication error of the values acquired by this method is ±2 wt.%.

5.3. Scanning electron microscopy

Scanning electron microscopy (SEM) was used to obtain high resolution and high magnification images of various parts of the speleothems. Small fracture samples (1-3 cm^3) were taken from the parent samples and mounted on SEM stubs using a conductive glue. Each sample was sputter coated with carbon prior to examination on a Zeiss Sigma 300 VP-FESEM using an accelerating voltage of 15 kV operated under high vacuum and variable pressure. In addition to the normal mode, some photomicrographs were taken in backscattered electron (BSE) mode to enhance their quality.

Constituent minerals were identified based on crystal morphology and elemental composition as determined by a Bruker dual detector for energy-dispersive X-ray spectroscopy (EDX) system that is attached to the SEM. Such analyses were done using an accelerating voltage of 15 kV. The average spot size for the EDX analyses was ~1 μm and analyses were replicated in order to confirm the presence of the detected elements. Given that these elemental analyses are standardless and semi-quantitative (estimated accuracy ± 5%), the analytical results are used with caution because only the overall trends and major variations in element constituents are typically reliable. A total of 245 SEM photomicrographs were obtained from three fractured samples of stalactite CUT-Z. Adobe PhotoShop CS © was employed to enhance the contrast and brightness of the thin section and SEM photomicrographs where necessary.

5.4. Stable isotope analysis

Samples for stable isotope analysis were extracted from selected growth bands using a dental-drill with 0.2-0.5 mm drill bits. The same samples were also used for XRD analysis. The composition of these samples ranged from pure calcite to almost pure aragonite. Given that each aragonite lamina is typically < 0.4 mm thick, any attempt to extract pure aragonite (> 99% aragonite) proved impossible. It was, however, relatively easy to obtain pure calcite samples because relatively thick calcite laminations are common.

For all samples, the oxygen and carbon isotopic values were determined at the Department of Earth and Atmospheric Sciences, University of Alberta. Nineteen samples were run in the Stable Isotope Laboratory of Dr. Karlis Muehlenbachs. For these analyses, 15-20 mg of homogeneous powdered samples were reacted with 100% H_3PO_4 at 25 °C for 120 minutes, then extracted gases were analyzed on a Finnigan-MAT 252 isotope mass spectrometer. The precision (standard error) is 0.10‰ for $\delta^{13}C$, and 0.14‰ for $\delta^{18}O$.

Two hundred and five samples were analyzed in the Stable Isotope Geochemistry Laboratory of Dr. Long Li (University of Alberta). Homogeneous powdered samples, each weighing 0.2-0.5 mg, were enclosed in glass reaction vessels and then heated on a thermostat stage to 70 °C for 30 mins, flushed with helium gas for 10 mins, and then acidified with ~1 ml of 100% phosph - ic acid (H_3PO_4). After 1 h of reaction time at 70 °C, the evolved CO_2 gases were injected into a Thermo MAT 253 Stable Isotope Ratio Mass Spectrometer (IRMS) that is coupled with a ConFlo VI system for analysis. In order to ensure the accuracy of measurements, standards were run before and during analyses of the samples. The reproducibility is 0.2‰ for $\delta^{18}O$ and $\delta^{13}C$. The final isotopic values ($\delta^{18}O$ and $\delta^{13}C$) are reported using the δ notation: $\delta_{sample} = (R_{sample}/R_{standard} - 1) \times 1000$, where $R = {}^{18}O/{}^{16}O$ for oxygen isotopes and $R = {}^{13}C/{}^{12}C$ for carbon isotopes. All results are reported relative to the Vienna PeeDee Belemnite (VPDB) standard normalized to NBS-18 ($\delta^{18}O = -2.20‰$, $\delta^{13}C = +1.95‰$) in per mil (‰) notation. The analytical results from two laboratories are comparable.

5.5. Th/U dating

Th/U dating can be used for dating speleothemic samples that are younger than 500 ka (Richards and Dorale, 2003), because they typically behave as closed systems with respect to uranium and its decay products (McDermott et al., 2006). Th/U dating analysis of three samples extracted from notch stalactite CUT-Z were conducted by Dr. Bassam Ghaleb (GEOTOP, Montreal, Quebec) who used an induction-coupled mass spectrometry (ICP-MS). The analytical uncertainties are 2σ of the mean.

6. Objectives

Building on the work of Jones (2010a), the main objectives of this study are as follows.

- To delineate the crystal morphologies and fabrics of the aragonite and calcite, discontinuities, and rhythmic laminations.
- To describe and to interpret stable isotopic values obtained from the aragonite and calcite laminae.
- To determine the paleoclimatic and paleoenvironmental controls on the genesis of the Cayman notch-speleothems.

CHAPTER 2: WAVE-CUT NOTCH AND NOTCH-SPELEOTHEMS

1. Wave-cut notch on Cayman Brac

A distinct wave-cut notch that cuts up to 7 m into the cliff face with its vertical mid-point ~6.4 m above sea level (asl), is one of the most obvious features around the coast of Cayman Brac (Woodroffe et al., 1983; Jones and Hunte , 1990; Tarhule-Lips, 1999). It correlates with the wave-cut notch (~ 6 m asl) that is evident in the dolostones of the Cayman Formation at Rogers Wreck Point (RWP) on Grand Cayman (Fig. 2.1C).

On Cayman Brac, the wave-cut notch is incised into the Brac Formation, the Cayman Formation, and the Pedro Castle Formation on the eastern, middle, and western parts of the island, respectively (Fig. 1.1C). Although well preserved in the central part of the island (Fig. 1.1B), it is rarely evident on the eastern part of the island because of cliff collapse (Jones and Ng, 1988), and it is absent on the western part of the island where the land is below 6 m asl. The wave-cut notch on Cayman Brac is horizontal and its formation clearly postdated tilting of the Tertiary strata (Woodroffe et al., 1983; Coyne et al., 2007; Zhao and Jones, 2012b). The Cayman Islands appear to have been tectonically stable since the incision of the notch (Woodroffe et al., 1983; Jones and Hunter, 1990).

On Little Cayman Brac (LCB on Fig. 1.1B), which is an isolated rock mass on the north-east coast of Cayman Brac that formed from collapse of the cliff face, two notches are evident, namely the +6.4-m notch and the modern notch at present day sea level (Fig. 2.1B). The modern wave-cut notch, about 2 m deep, is also evident on the east end of the Cayman Brac where the cliff is not protected by an offshore fringing reef or a coastal platform arhule-Lips, 1993).

1.1. Age of wave-cut notch

It has been suggested that the +6 m wave-cut notch on Cayman Brac and Cayman Brac formed about 125,000 years ago when sea level was at +6 m (Woodroffe et al., 1983; Jones and Hunter, 1990; Vézina et al., 1999; Coyne et al., 2007). This conclusion is based largely on the position of the wave-cut notch (+6 m) relative to the established Marine Isotope Stage 5e (MIS 5e) highstand (or Sangoman highstand) ~125,000 years ago. Coastal notches at similar elevations and allied with the MIS 5e highstand (Thompson et al., 2011), are found on tectonically stable islands throughout the Caribbean Sea and worldwide (Hearty et al., 2007). These include, for example, the +5.3 ~ +5.9 m notch on the Bahamas (Neumann and Moore, 1975; Mylroie and Carew, 1991; Neumann and Hearty, 1996; Hearty and Neumann, 2001), the +5 ± 1 m notch on Bermuda (Harmon et al., 1983), and the notch at +7.6 ± 2 m on Oahu Island, Hawaii (Ku et al., 1974).

The ~125 ka age of the wave-cut notch and its associated +6 m highstand has been derived from the following lines of evidence.

- Dating of the deposits (especially in-situ corals) associated with the +6 m highstand. In situ corals dated at ~125 ka, found up to 2.5 m asl in Unit D of the Ironshore Formation on Grand Cayman, seem to have grown when the +6 m highstand led to development of the wave-cut notch (Vézina et al., 1999; Coyne et al., 2007; Li and Jones, 2014). Similar conclusions have also been derived from corals on the Bahamas (Neumann and Moore, 1975; Chen et al., 1991; Thompson et al., 2011), Bermuda (Harmon et al., 1983), and Hawaii (Ku et al., 1974). All of these corals typically grow in water that is less than 5 m deep, a depth that is consistent with the notch elevation.

- The well-established sea-level curve for the Cenozoic suggests that the mean sea level during MIS 5e (~125 ka ago) was about 6 to 9 m higher than it is today (Labeyrie et al, 1987; Lea et al., 2002; Waelbroeck et al., 2002; Siddall et al., 2003; Lisiecki and Raymo, 2005; Elderfield et al., 2012; Shakun et al., 2015; Spratt and Lisiecki, 2016).
- Evidence for the ~ 125 ka highstand also comes from cave speleothems. Stalactites, +2 to +4 m asl in Crystal Cave on Bermuda, contain an interior layer of marine aragonite with Serpulid worm tubes that was deposited between 130 ± 11 ka to 110 ± 14 ka (Harmon et al., 1978; Harmon et al., 1981; Harmon et al., 1983). The marine aragonite layer shows that the Sangoman highstand was at least +4 m asl between ~130 ka and 110 ka, which is consistent with the elevations derived from corals and the wave-cut notch on Bermuda (Harmon et al., 1983).
- Coral terraces on Barbados also supports the +6 m asl position of the ~125 ka highstand. There, the position is based on calculations that take into account the current elevation of the dated corals and uplift rates over the last 125,000 years (Schellmann and Radtke, 2004). Th/U dating of the in-situ reef corals found on terrace III indicate a ~125 ka age when there was a highstand at +5 m asl (Broecker et al., 1968; Shackleton and Matthews, 1977; Fairbanks and Matthews, 1978; Bender et al., 1979; Edwards et al., 1987).
- Ages derived from notch-speleothems on Cayman Brac are consistent with the idea that the wave-cut notch formed ~125 ka ago. Tarhule-Lips (1993, 1999) reported an age of ~10 ka for the outer part of one notch-speleothems that came from Cayman Brac. A notch-speleothem collected from locality CUT (sample CUT-Z) during this study yielded three Th/U ages that spanned the period of 49.2 ± 0.6 ka to 46.1 ± 0.4 ka (Table 4.1). It follows that the notch must be older than the maximum age obtained. Hence, the wave-

cut notch has a minimum age of 49.2 ± 0.6 ka. The sea-level curve for the Cenozoic suggests, however, that the sea level was about 70-80 m below present-day sea level (bsl) for the time interval of 49.2 ± 0.6 ka to 46.1 ± 0.4 ka (Spratt and Lisiecki, 2016).

Collectively, the available evidence clearly indicates that the +6 m wave cut notch formed ~ 125,000 years ago when sea level reached a highstand at +6 m.

1.2. Distribution and external morphology of notch-speleothems

Speleothems are irregularly distributed in the wave-cut notch on Cayman Brac (Fig. 1.1B). Thus, notch-speleothems are very common at some localities (CUT, SST, and SB) (Fig. 2.1) but absent at other localities. At CUT, a spring vent is present at the back of the wave-cut notch (Jones, 2010a).

Where present, the notch-speleothems include flowstone, stalactites, stalagmites, and co - umns (Jones, 2010a). Today, none of the notch-speleothems are active, and the stained and weathered surfaces indicate that there has been little precipitation in recent years. The surfaces of the speleothems exhibit a variety of colors ranging from light brown to tan and/or green. Jones (2010a) suggested that those color patterns reflected the different microbial colonies that hav colonized the surfaces of the speleothems.

Flowstones (with rimstone dams and terrace pools), which are uneven, laminated carbonate deposits (up to ~10 cm thick), are developed on the floor of the notch in some areas (Fig. 2.1F).

The stalactites in the wave-cut notch are irregularly conical, cylindrical, or bulbous in shape, and commonly characterized by contorted, irregular surfaces (Fig. 2.1E and F). They are typically 10 ~ 40 cm in diameter and 10 ~ 60 cm long. Most stalactites are characterized by a central ‘soda straw’. When cut (both transverse and longitudinal), stalactites display laminated structures and asymmetrical growth patterns.

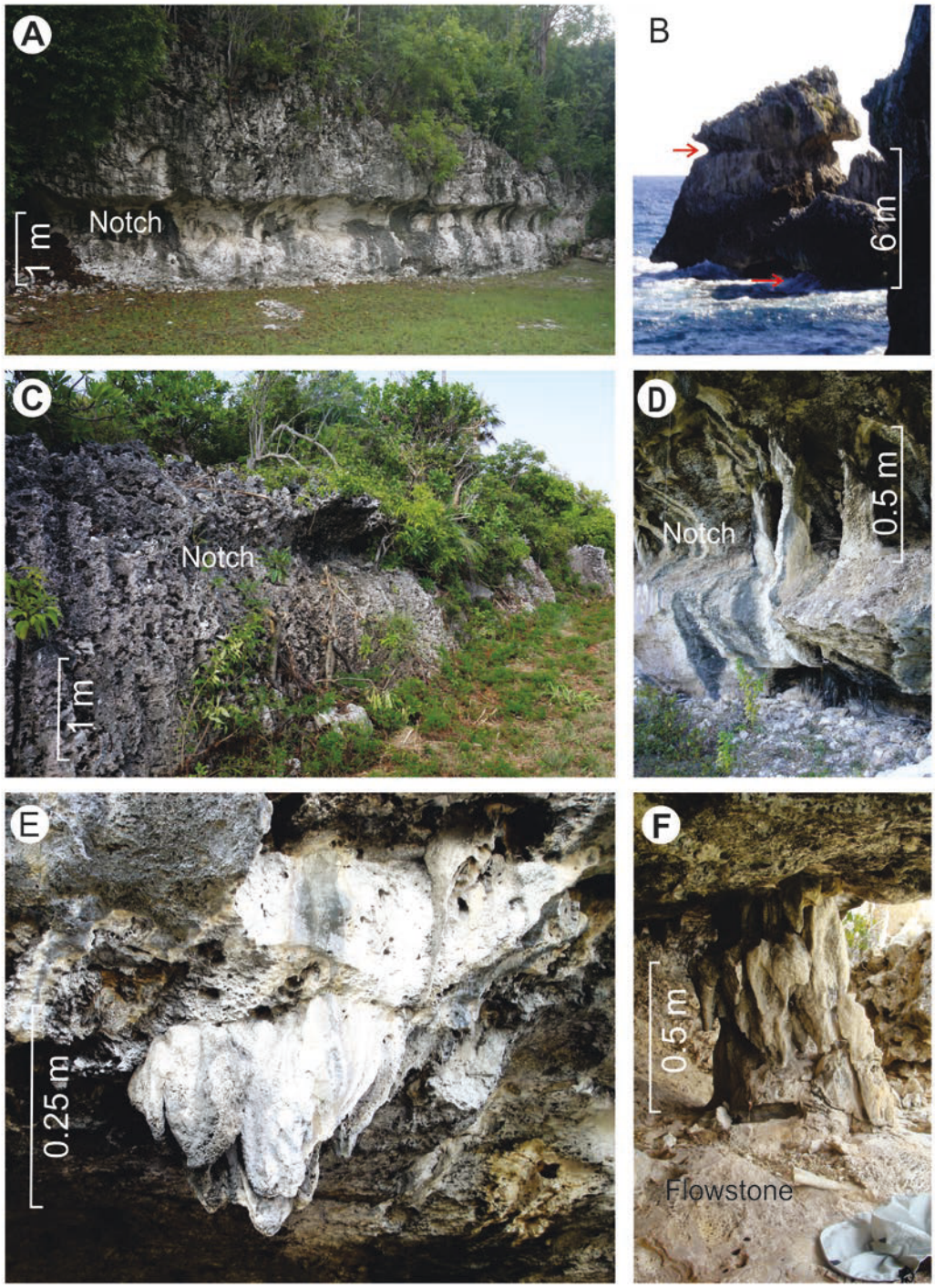

Fig. 2.1 Field photographs of Cayman wave-cut notch and notch-speleothems. Locations shown on Fig. 1.1B. (A) and (D) Wave-cut notch at locality HC, Cayman Brac. (B) 6.4 m notch and modern notch at locality LCB, Cayman Brac. (C) Wave-cut notch at Rogers Wreck Point, Grand Cayman. (E) Notch stalactites at locality SSR, Cayman Brac. (F) Stalactites, stalagmites, columns, and flowstones at locality CU , Cayman Brac.

Stalagmites in the notch (Fig. 2.1D-F), which are cylindrical to conical in shape, are characterized by well-developed internal laminations. They are 10 ~ 40 cm in diameter and 10 ~ 50 cm long. The stalagmites do not have a central 'soda straw'.

Columns, which are present in some parts of the wave-cut notch, developed as stalagmites and stalactites merged together. Some columns are very narrow (point contact) in their middle parts, whereas have almost uniform diameters. Columns are commonly 30 ~ 40 cm in diameter and 50 ~ 80 cm long. Some columns are a combination of several stalactites and stalagmites are up to 1 m high and 1 m wide (Fig. 2.1F).

2. Internal structures

2.1. Terminology

Herein, the term equant describes equidimensional crystals that have a length:width (L/W) ratio < 1.5:1 (Folk, 1965). The term bladed refers to elongate crystals that have a L/W ratio between 1.5:1 and 6:1 (Folk, 1965). Fibrous is used to describe crystals that have a L/W ratio of > 6:1 (Folk, 1965; Frisia et al., 2000; Flügel, 2010) and are typically > 10 μm wide (Flügel, 2010). Acicular is used to describe needle-like crystals that are <10 μm wide, have a L/W ratio of > 6:1, and have pointed terminations (Kendall and Broughton, 1978; Perrin et al., 2014). Following Milliman et al. (1985), Jones et al. (1995), and Martín-García et al. (2009), the term micrite is used in a non-genetic sense for carbonate grains that are < 4 μm long.

The term fabric (or texture) refers to the geometry and spatial arrangement of the constituent crystals (Self and Hill, 2003; Fairchild et al., 2007) and follows the classification of Frisia and Borsato (2010) and Frisia (2015):

- "Fans" are composed of elongate crystals (typically acicular aragonite) radiating from a common center.

- Columnar fabric is composed of crystals elongated perpendicular to the growing surface (Frisia and Borsato, 2010). The columnar calcite was further divided into seven types (Frisia, 2015). Only the following columnar types are present in the Cayman notch-speleothems:
    - Columnar compact consists of calcite crystals with unit extinction and L/W ratio < 6:1. Constituent crystals form a compact aggregate, with welded intercrystalline boundaries and negligible intercrystalline porosity (Frisia, 2015);
    - Columnar open is composed of calcite crystals with unit extinction and L/W ratio < 6:1. These calcite crystals, however, are loosely packed, and have flat to irregular intercrystalline boundaries that are highlighted by linear porosity and/or inclusions (Frisia, 2015);
    - Elongated columnar type is composed of calcite crystals with L/W ratio ≥ 6:1 that typically have flat intercrystalline boundaries, and uniform to sweeping extinction (Frisia and Borsato, 2010; Frisia, 2015).

The mosaic fabric consists of euhedral to subhedral calcite crystals that are > 30 μm and < 1 cm long, and with L/W ratio ~1:1(Frisia, 2015). Mosaic calcite is divided into those that encompass aragonite needles and those that do not (Frisia, 2015). Microsparite consists of anhedral to sub-euhedral calcite crystals that are > 4 μm and < 30 μm long, with L/W ratio ~1:1(Frisia, 2015).

2.2. Laminations

The notch-speleothems are characterized by well-developed internal laminations that are formed of crystalline calcite, aragonite, and micrite (Figs. 2.2 and 2.3A and B). Laminations formed primarily of calcite are translucent white to grey with low intercrystalline porosity, or

milky with high porosity. In contrast, the aragonite laminae are typically thin and porous with an opaque white appearance. Given that the aragonite laminae and milky calcite laminae commonly look alike, their identifications were confirmed by XRD analyses and optical microsco . The variable thicknesses of the growth laminae reflect the irregular growth patterns of the notch-sp - leothems (Figs. 2.2 and 2.3A-D). Although some laminae are characterized by uniform thickness, others thicken and thin laterally and commonly pinch out and disappear (Fig. 2.2). Differences between growth laminae reflect variations in their thickness, mineralog , crystal fabrics, and porosity.

Calcite laminae, which are up to 2 mm thick, are more abundant than the aragonite laminae. The thickness of most calcite laminae is equal to the length of the constituent crystals. There are no systematic relationships between the milky-porous calcite and the grey-translucent calcite laminae. They two may alternate, or may be present in the same lamina (Fig. 2.4A, B).

Aragonite laminations are generally < 0.25 mm thick and are commonly sandwiched between calcite laminae (Figs. 2.2C, 2.3B, and 2.5A and C). In some aragonite-rich speleothems, howev- er, there are packages of aragonite laminae (Fig. 2.3), and/or frequently alternating aragonite and calcite laminae (Fig. 2.5C).

Rare laminae are composed of aragonite and calcite. The spatial relationship between ara- gonite and calcite is highly variable within one single lamina (Fig. 2.2C). These laminae are up 0.40 mm thick.

Dark colored micrite laminae, up to 1 cm thick, are present in some speleothems. Many of the thin (< 50 μm thick) laminae are laterally discontinuous (Figs. 2.2C and 2.3A and B). The thicker laminae vary from continuous, poorly laminated to discontinuous and patchy (Fig. 2.2).

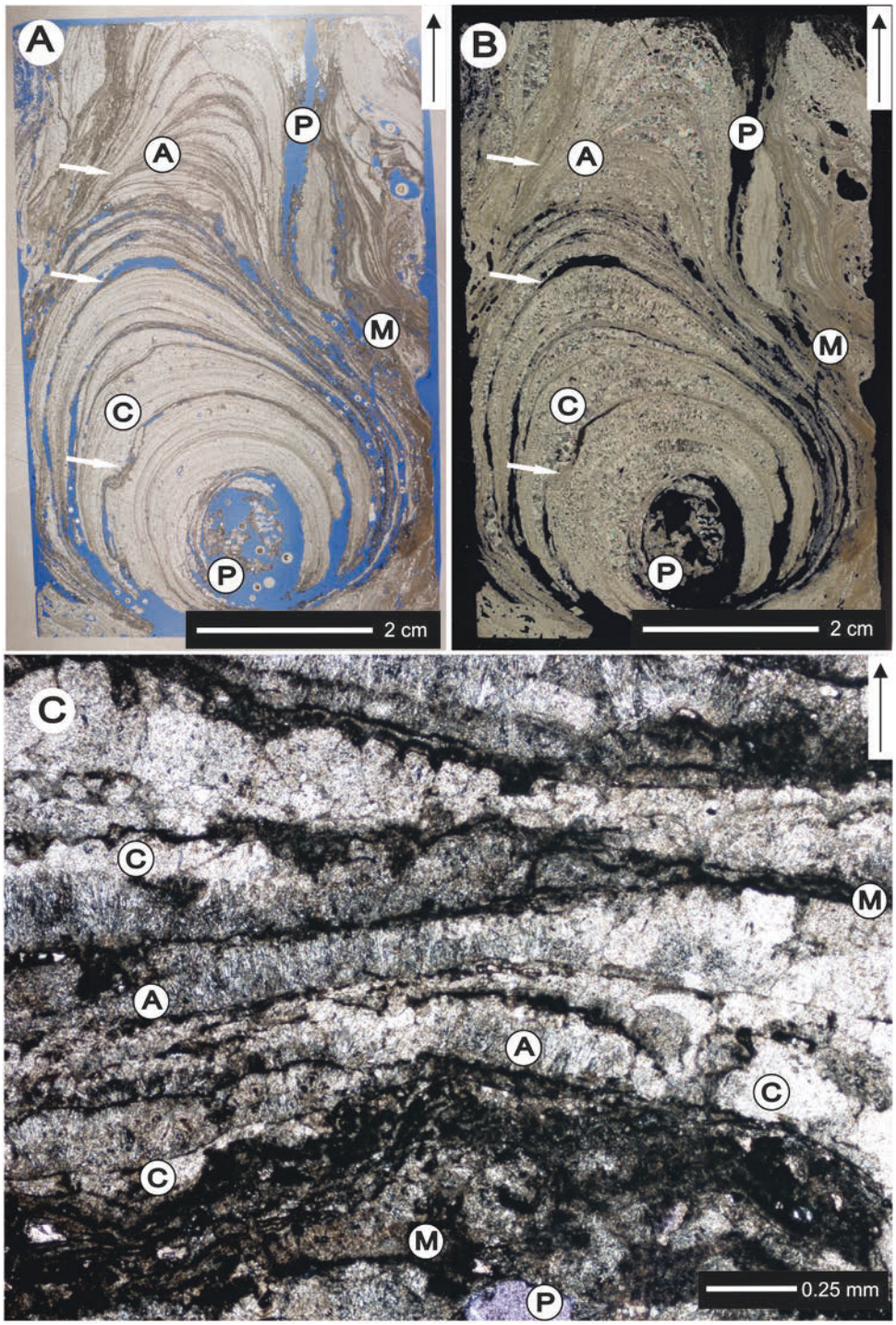

Fig. 2.2. Photomicrographs from Notch Stalactite CUT-3. A=Aragonite, C=Calcite, M=Micrite, P=Pore. Panel A with plane polarized light, panels B and C with crossed polarized light. (A, B) Transverse cross-section showing calcite, aragonite, aragonite-calcite laminae, and micrite laminae and unconformities (white arrows). (C) Complex relations among growth laminae and laminae boundaries. Black arrow indicates growth direction.

2.3. Boundaries between laminations

Boundaries between the laminae, which range from poorly- to well-defined (Figs. 2.2, 2.3, and 2.4A and B), are highlighted by (1) changes in the mineralogy, (2) changes in the crystal fabrics, and/or (3) truncation of underlying laminae. Many boundaries are highlighted by dark-colored micrite and/or microbial mats. Although most boundaries are subparallel to each other (Figs. 2.2 and 2.3), others crosscut older boundaries and the underlying laminations (Figs. 2.2A and B and 2.3C).

Both conformable boundaries and unconformable boundaries are present in notch-speleothems. A conformable boundary separates two laminae that are parallel to each other. Most conformable boundaries are distinct with their morphology being controlled by the underlying lamina (Figs. 2.2 and 2.3). Although most boundaries are continuous and laterally traceable, they can become diffuse locally (Fig. 2.4B). In contrast, unconformable boundaries are characterized by (1) truncation of the underlying laminae and, in some cases, older boundaries (Fig. 2.3C), (2) microbial borings, and/or (3) micrite/microbial mats (Figs. 2.2C and 2.3E). The term unconformity is used for large-scale unconformable boundary that is typically visible on section surfaces (e.g., Figs. 2.2A and B and 2.3C).

2.4. Fractures

Fractures, generally centimeter-scale in length and up to up to 1 mm wide, cut through several laminations, and are typically (sub)perpendicular to lamination boundaries (Fig. 2.3F). The fractures are either filled by aragonite and/or calcite crystals cements (Fig. 2.3F), or remain empty.

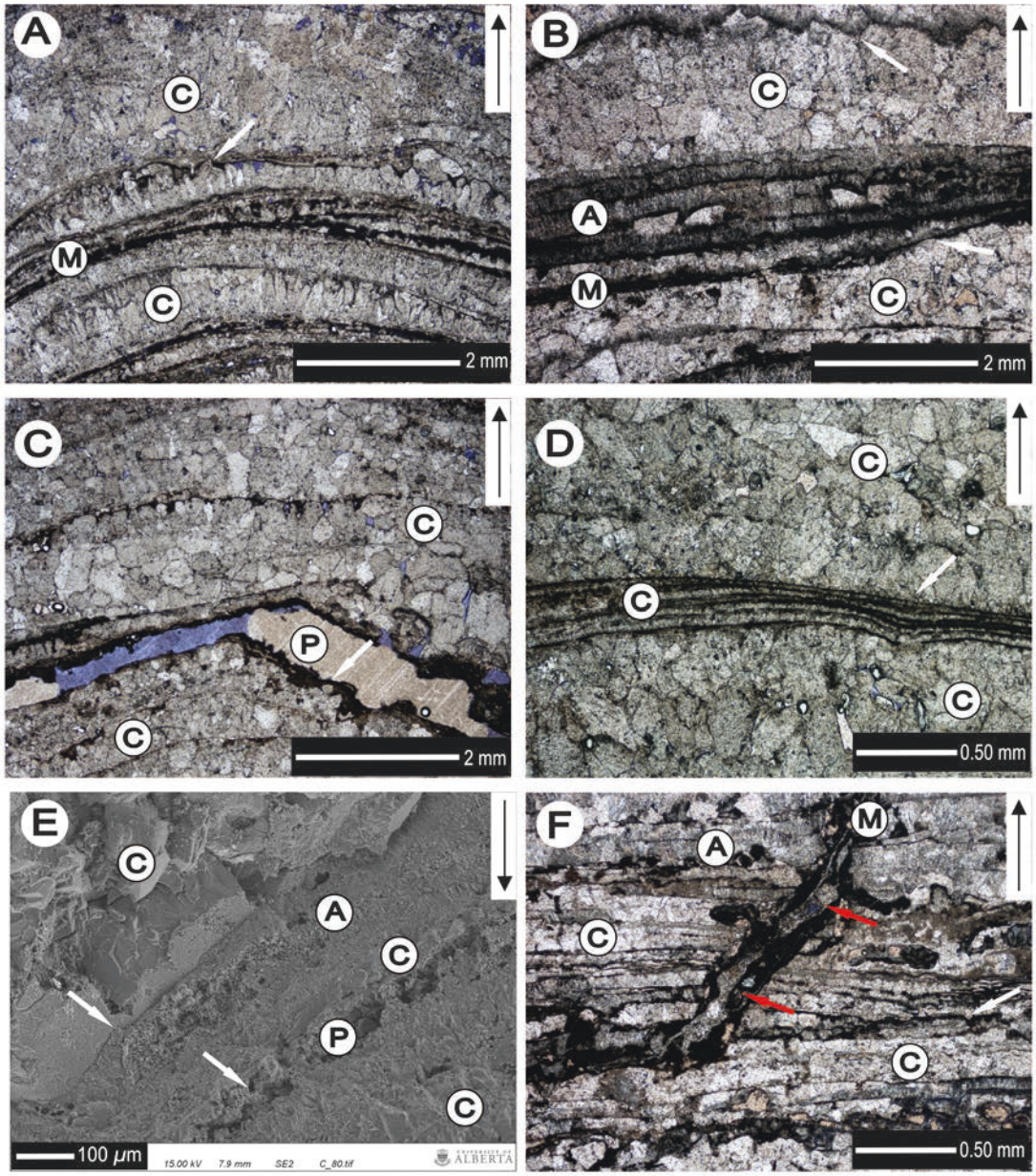

Fig. 2.3. Thin section and SEM photomicrographs showing growth laminae and boundaries between laminae in Cayman notch-speleothems. Black arrow indicates growth direction. A=Aragonite, C=Calcite, M=Micrite, P=Pore. (A) Calcite laminae of variable thinness. Note micrite laminae and their relationship with lamination boundary (white arrow). (B) Aragonite laminae sandwiched between calcite laminae. Note unconformity overlaid by micrite. (C) Unconformity with truncation of underlying calcite laminae. (D) Unconformity without erosive features. (E) Complex spatial relations among calcite laminae, aragonite laminae and boundaries. (F) Calcite and aragonite laminae cut by fracture (red arrows) lined with micrite and calcite cements.

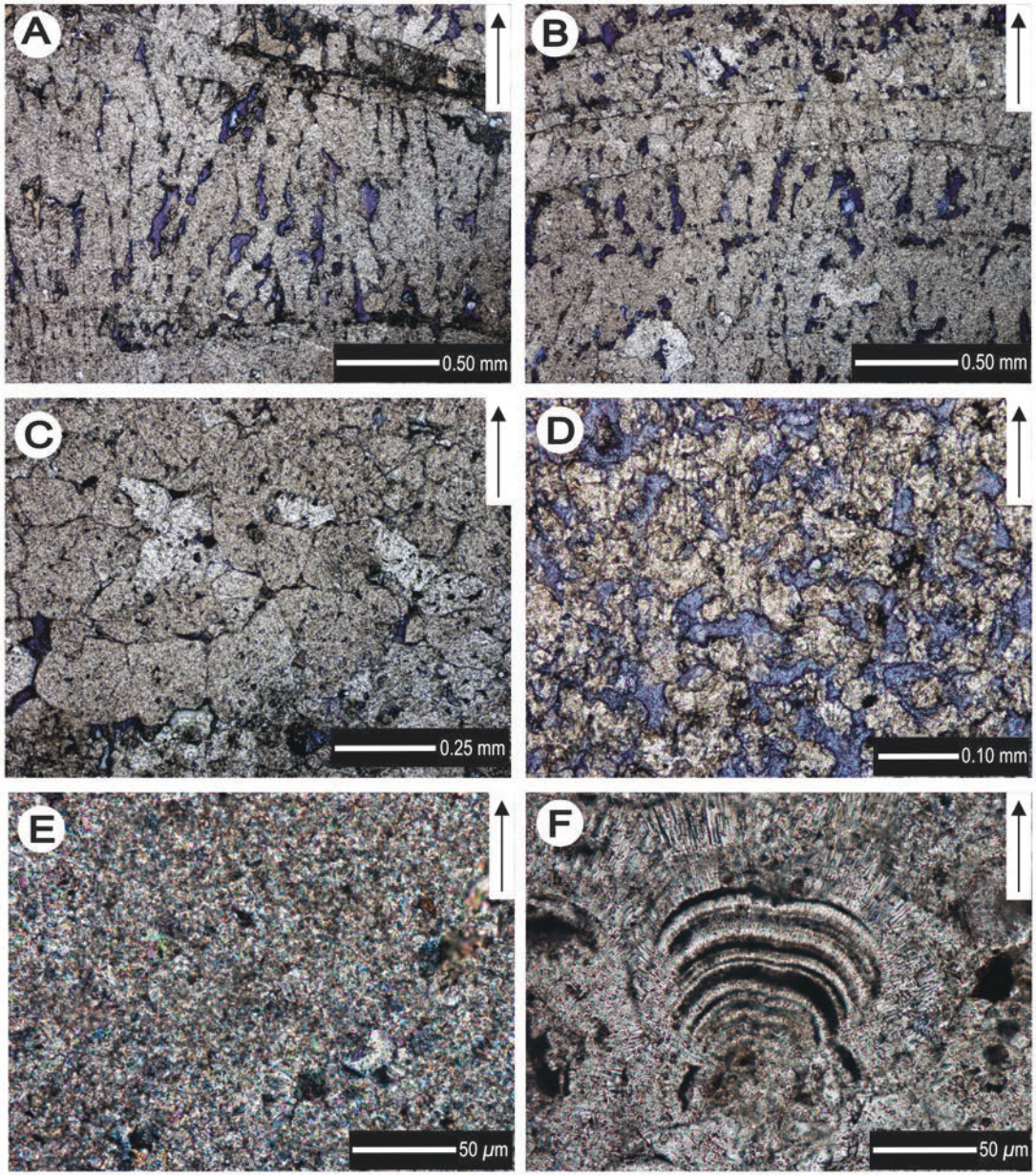

Fig. 2.4. Thin section and SEM photomicrographs showing fabrics in Cayman notch-speleothems. Black arrow indicates growth direction. (A) Elongated columnar calcite. (B) Columnar compact calcite and columnar open calcite. (C) Mosaic calcite. (D) Microspar to mosaic calcite. (E) Micrite. (F) Aragonite fans with growth banding.

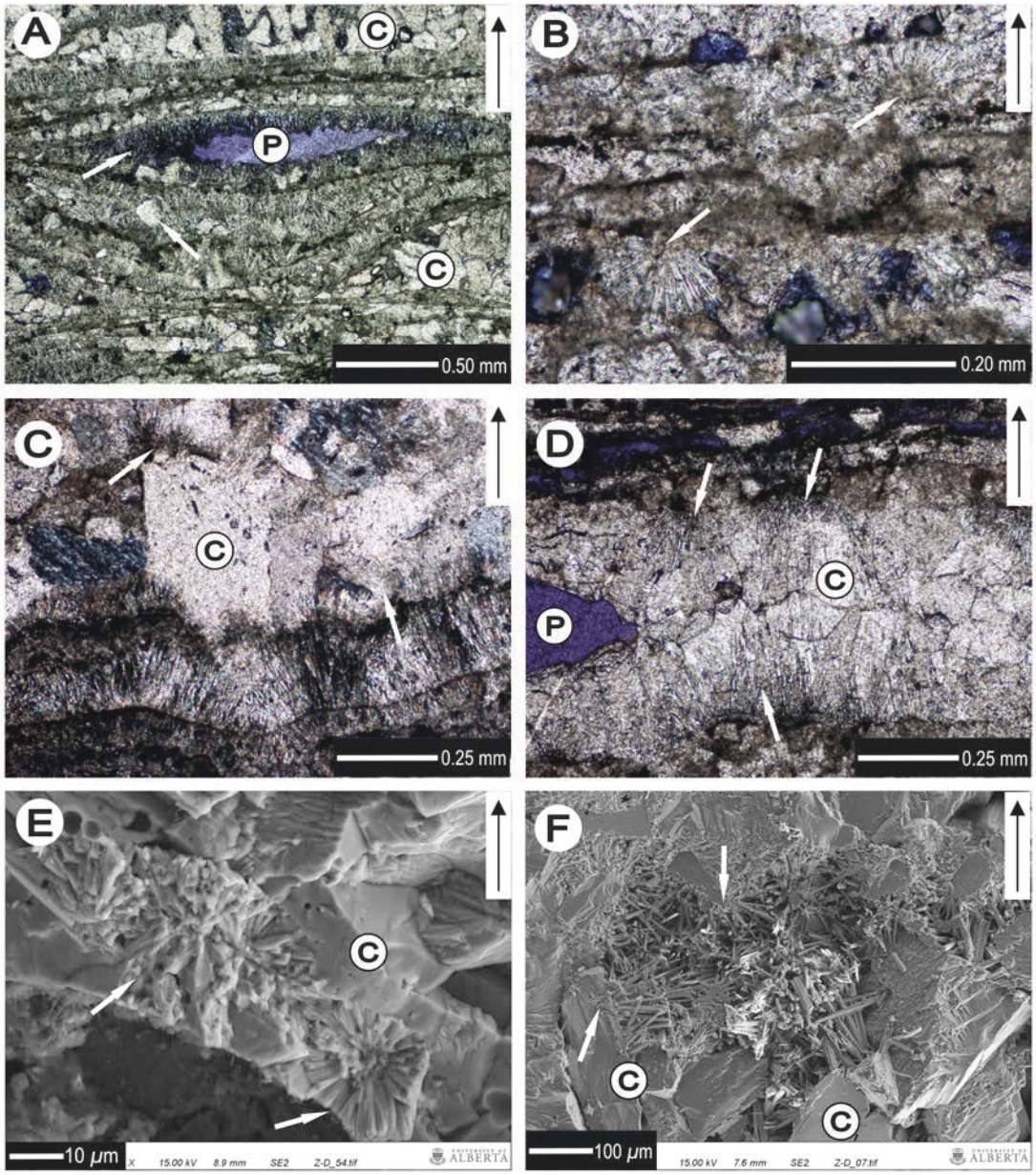

Fig. 2.5. Thin section (A-D) and SEM (E, F) photomicrographs showing temporal and spatial relationships between aragonite and calcite in Cayman notch-speleothems. Black arrow indicates growth direction. C=Calcite, P=Pore. (A) Alternating aragonite and calcite laminae. Note aragonite cement (upper white arrow) lining pore, and the mosaic calcite crystals (lower white arrow) between aragonite fans. (B) Aragonite fans (white arrows) in calcite laminae. Lower left aragonite fan is a cement as with its growth opposite to growth trend of speleothem. (C) Alternating calcite and aragonite laminae (crossed polarized light). Aragonite crystals nucleated on calcite crystal faces (upper white arrow) vs aragonite crystals encased by calcite crystals (lower white arrow). (D, E) Mosaic calcite crystals with encased some aragonite needles or whole aragonite bundles. (F) Aragonite crystals nucleated on calcite crystal faces.

2.5. Mineralogy, crystal morphology, and fabrics

XRD and thin section examination show that the notch-speleothems are formed largely of calcite and aragonite, with minor amounts of halite, Mg-calcite, and dolomite. Minor gypsum and kerolite (?) had also been documented by Jones (2010a).

The thin aragonite laminae are typically composed of aragonite fans that are nucleated on basal boundary (Figs. 2.2C, 2.3B and 2.5A), older aragonite crystals (Figs. 2.3B and 2.5A), or calcite crystals (Fig. 2.3B). The aragonite fans are three-dimensional radiating clusters that consist of groups of acicular crystals of varying lengths and widths (Figs. 2.4F, 2.5E and F, and 2.6E and F). The fans, up to 300 μm wide and high, generally have their median symmetry axes perpendicular to the substrate. Growth banding is a common feature of most aragonite fans (Fig. 2.4F). The boundaries between neighboring fans are typically irregular (Figs. 2.4F and 2.5C). Individual aragonite crystals, up to 300 μm long, but generally < 100 μm long and 3–8 μm wide, typically have flat crystal faces and a hexagonal cross-section with interfacial angles of ~120° (Fig. 2.6E).

Calcite laminae are mostly composed of columnar fabric (Figs. 2.3A and 2.4A and B), and mosaic and microsparite fabric locally (Fig. 2.4C, D). Although an individual calcite lamina is typically composed of one fabric, there may be lateral changes from mosaic to columnar, or columnar open to columnar compact within an individual lamina (Fig. 2.4A, B).

Columnar compact. Calcite crystals generally have bladed morphology, and similar crystal sizes that are typically 80 ~ 100 μm wide and 200 ~ 300 μm long (Figs. 2.3A and 2.4B). Growth banding are visible in some crystals locally.

Columnar open. The bladed calcite crystals that form this fabric are generally ~120 μm wide and 200 ~ 300 μm long (Fig. 2.4B).

Elongated columnar. Calcite crystals are typically 100 ~ 150 μm wide, and 600 μm to 1.5 mm long (Fig. 2.4A). Individual fibrous crystals have pointed to blunt terminations, with few growth defects on flank faces. Intercrystalline boundaries are locally highlighted by linear inclusions and/or pores (Fig. 2.4A).

The mosaic fabric in Cayman notch-speleothems consists of equant calcite crystals that are typically of 200-300 μm long (Figs. 2.4C and 2.5D). The crystals are compactly packed together, with welded intercrystalline boundaries, low porosity, and low inclusion abundance (Figs. 2.4C and 2.5D). Most mosaic calcites are characterized by the presence of numerous aragonite relicts encased by calcite crystals (Fig. 2.5D, E). The high relief of encased aragonite needles differentiates them from their host calcite under microscopy (Fig. 2.5D). Aragonite needles may extend from one host calcite into its neighbors (Fig. 2.5D). The aragonite relicts are locally fuzzy, with only needle-like ghosts preserved in the host calcites. Clear dissolution features are, however, absent between the encased aragonite needles and the host calcite crystals (Fig. 2.5D, E). Whereas, in some mosaic calcites, there are no aragonite needles or aragonite needle-like ghosts preserved within the calcite crystals (Fig. 2.5C). The calcite crystals display unit to sweeping extinction. SEM observation indicates that equant rhombohedra are the predominant crystals forms for mosaic fabric (Fig. 2.5E).

Calcite laminae that are composed of microsparite fabric in Cayman notch-speleothems usually contain some mosaic crystals that are larger than 30 μm (Fig. 2.4D). All microsparite laminae are characterized by high intercrystalline porosity (Fig. 2.4D).

2.6. Relationships between calcite and aragonite

The relationship between aragonite and calcite in the notch-speleothems is complex and variable at all scales. Some speleothems are formed almost entirely of calcite, whereas other contain

significant amounts of aragonite (Figs. 2.2 and B and 2.3B). In some lamina, aragonite crystals may be scattered between the calcite crystals (Fig. 2.5B), whereas in others, calcite crystals may be scattered between the dominant aragonite crystals (Figs. 2.3B and 2.5A). In mixed aragonite-calcite laminae, the spatial relations between the aragonite and calcite include (1) lateral changes from aragonite to calcite (Fig. 2.2C), (2) laterally alternating aragonite and calcite crystals (Fig. 2.5A), and (3) aragonite crystals forming the inner part and calcite forming the outer part (Fig. 2.5C). At the microscale, calcite crystals (1) are found within and/or between aragonite fans (Fig. 2.5F), (2) may encase a bundle of aragonite crystals (Fig. 2.5E), and/or (3) may grow on the top of aragonite fans with the upper parts of the aragonite needles partially encased by the calcite (Fig. 2.5C). Aragonite crystals are commonly nucleated on the surfaces of the calcite crystal (Fig. 2.5A, C, and F).

2.7. Microbes

The microbiota in Cayman notch-speleothems include diverse types of filamentous microbes, coccoid microbes, and actinomycetes (Jones, 2010a, his Figs. 8, 9, 10, and 11), that are up 500 μm long (Fig. 2.6A, B). Preservation of the microbes, which is variable, ranges from distorted, desiccated forms to calcified bodies (Jones, 2010a, his Figs. 8, 9, 10, and 1). Jones (2010a) suggested that the coccoid microbes and actinomycetes dominated the biota found.

These microbes, which are commonly associated with the micrite, are evident as (1) dark lines (Figs. 2.2C, 2.3A, B and F, and 2.6A) or dark-colored opaque patches (Figs. 2.2C and 2.3F) along lamination boundaries, and (2) vaguely laminated microstromatolites (Jones, 2010a, his Fig. 4F). The microbes are found as isolated individuals (Fig. 2.6C, D) or in concentrated groups (Figs. 2.6A and B and 2.7C). Some of the calcified filamentous microbes (up to 10 μm diamet , up to 500 μm long), for example, are locally concentrated in microbial-calcite laminae that are

generally porous and up to 2 cm thick. Similar large filamentous microbes have also been repor - ed in cave speleothems from Grand Cayman (Smith, 1987).

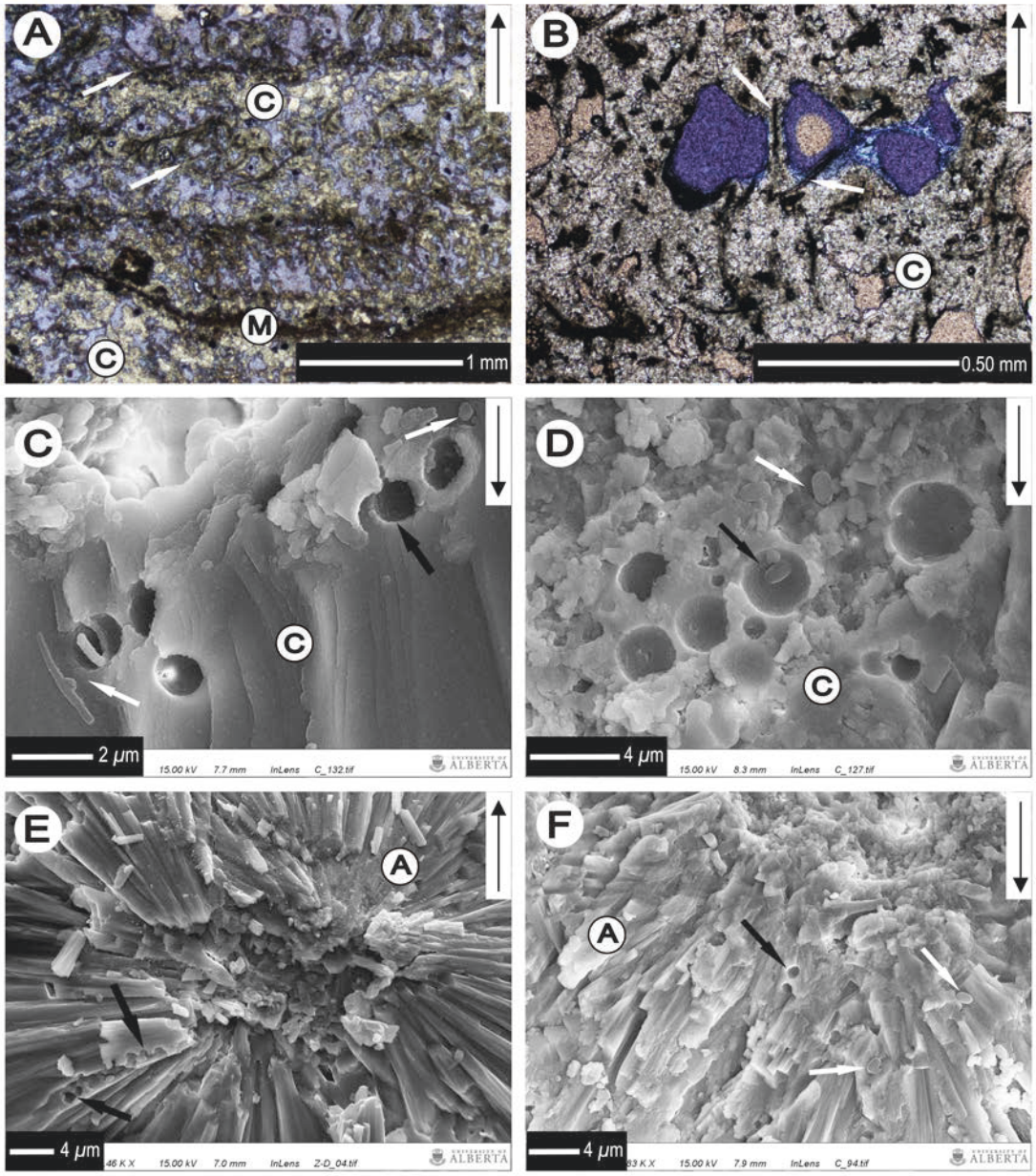

Fig. 2.6. Thin section (A, B) and SEM (C-F) photomicrographs showing microbial structures in Cayman notch-speleothems. A=Aragonite, C=Calcite, M=Micrite. (A) Porous calcite laminae formed of calci- fied filamentous microbes (white arrows) and calcite crystals. (B) Calcified filamentous microbes (wh arrows) surrounded by finely crystalline calcite. (C, D) Microbial holes (black arrow) with some small filamentous microbes and spores (?) (white arrows) in calcite. (E, F) Microbial holes (black arrows) and spores (?) (white arrows) in aragonite fans.

Microboring are evident in some of the calcite or aragonite crystals (Fig. 2.6C, D). The microborings are rounded on their cross-sectional shape, < 10 μm wide and < 10 μm deep (estimated). Microbes are still evident in some of these borings (Fig. 2.6C, D). There is commonly some microcrystalline aragonite and/or calcite around the microbes (Fig. 2.7D).

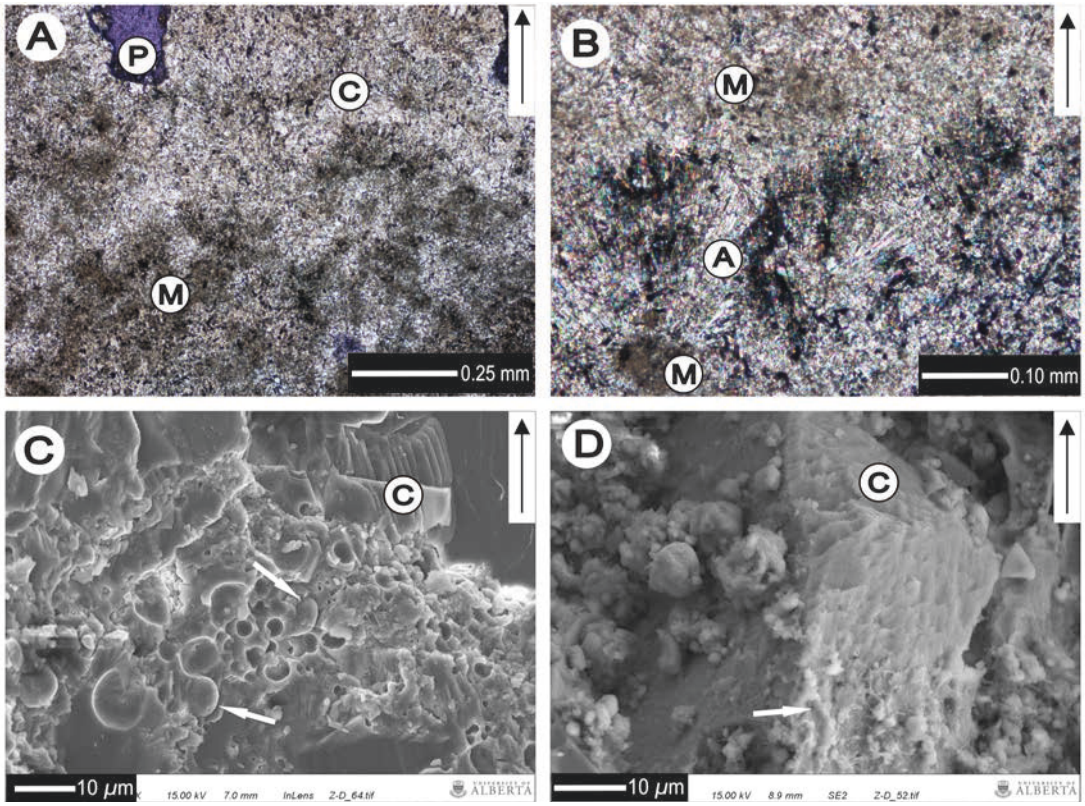

Fig. 2.7. Thin section (A, B) and SEM (C, D) photomicrographs of micrite in Cayman notch-speleothems. A=Aragonite, C=Calcite, M=Micrite, P=Pore. (A) Micrite laminate. (B) Transitions from aragonite crystals to micrite (crossed polarized light). (C) Spores (?) (white arrows) in micrite laminae. (D) Spiky calcite crystal faces with mucus (white arrow) and micrite.

CHAPTER 3: STABLE ISOTOPE GEOCHEMISTRY

1. Introduction

Two hundred and twenty-four samples, collected along transects across the notch stalactites CUT-1, CUT-2, CUT-3, CUT-4, and CUT-Z, were analyzed for stable isotopic compositions. Stalactites CUT-3, CUT-Z, and CUT-1 were the primary focus, given that one hundred and ninety-two samples came from these three stalactites (Fig. 3.1). The 32 samples from CUT-2 and CUT-4 were used primarily for verification of the analyses obtained from the three main samples.

Overall, the $\delta^{18}O$ values vary from -6.5‰ to +0.3‰ (average -3.1‰ VPDB), whereas the $\delta^{13}C$ values range from -11.4‰ to +1.9‰ (average -6.1‰ VPDB) with a strong covariance between the two (Fig. 3.1). There is a strong positive linear correlation between the percentage of aragonite (Arag%) and the $\delta^{18}O$ (Fig. 3.2A) and $\delta^{13}C$ values (Fig. 3.2B). Forty-two pure calcite samples (Arag% = 0) yielded $\delta^{18}O$ values from -6.5‰ to -1.9‰ (Fig. 3.3A), and $\delta^{13}C$ values from -11.4‰ to -4.4‰ (Fig. 3.3B).

2. Stalactite CUT-3

A cross-section through stalactite CUT-3 shows that it is formed of three distinct zones: zone 1 – the dark inner core, zone 2 – the porous white zone, and zone 3 – the outer, compact white zone (Fig. 3.4). Zones 1 and 2 are separated by a well-defined unconformity that is highlighted by (1) truncation of the underlying laminae, (2) a contrast in colors, and (3) overlying laminae that are parallel to the unconformity. Underlying laminae, formed of micrite and/or aragonite, further highlight this unconformity. The unconformity between zones 2 and 3 is characterized by similar features, but with thin aragonite/micrite laminae at the base of zone 3. These two unconformities represent periods of erosion and/or non-deposition of unknown duration. Section X-X' encompasses zones 1, 2, and 3 (56 samples), and section Y-Y' (27 samples) only includes zone 2.

2.1. Zone 1 - dark inner zone

Based on the mineralogy and fabrics, this zone is divided into subzones A to D (Fig. 3.4). They are separated by unconformities that are characterized by local truncation of the underlying laminae and are typically overlain by thin laminae formed of micrite and/or aragonite (Fig. 3.4).

- **Zone 1A**: This central zone, up to 6 mm thick, is characterized by white porous laminae that are formed of aragonite and calcite. Thin-section examination shows that aragonite fans and dark-colored micrite dominate this zone, whereas mosaic calcite is minor.
- **Zone 1B**: This calcite zone, up to 30 mm thick, is formed largely of compact calcite laminae that are separated by three thin (~0.5 mm) aragonite laminae (Fig. 3.4). The compact calcite laminae, which have low porosity, are composed of columnar compact and mosaic fabrics, whereas the aragonite laminae are formed of aragonite fans.
- **Zone 1C**: This zone, ~26 mm thick, is characterized by alternating aragonite and calcite laminae, with aragonite forming ~60% of the total thickness (Fig. 3.4). The calcite laminae, composed of columnar compact and mosaic fabrics, have low porosity. The aragonite laminae, formed of aragonite fans, are more porous than the calcite laminae. Micrite is commonly present in the aragonite and the calcite laminae.
- **Zone 1D**: This calcite zone, ~24 mm thick, is formed of thick, compact calcite laminae that are separated by thin aragonite laminae (~20% of the total thickness). The calcite laminae are formed of columnar compact, columnar elongated, and mosaic fabrics, whereas the aragonite laminae are formed of fans and minor amounts of micrite.

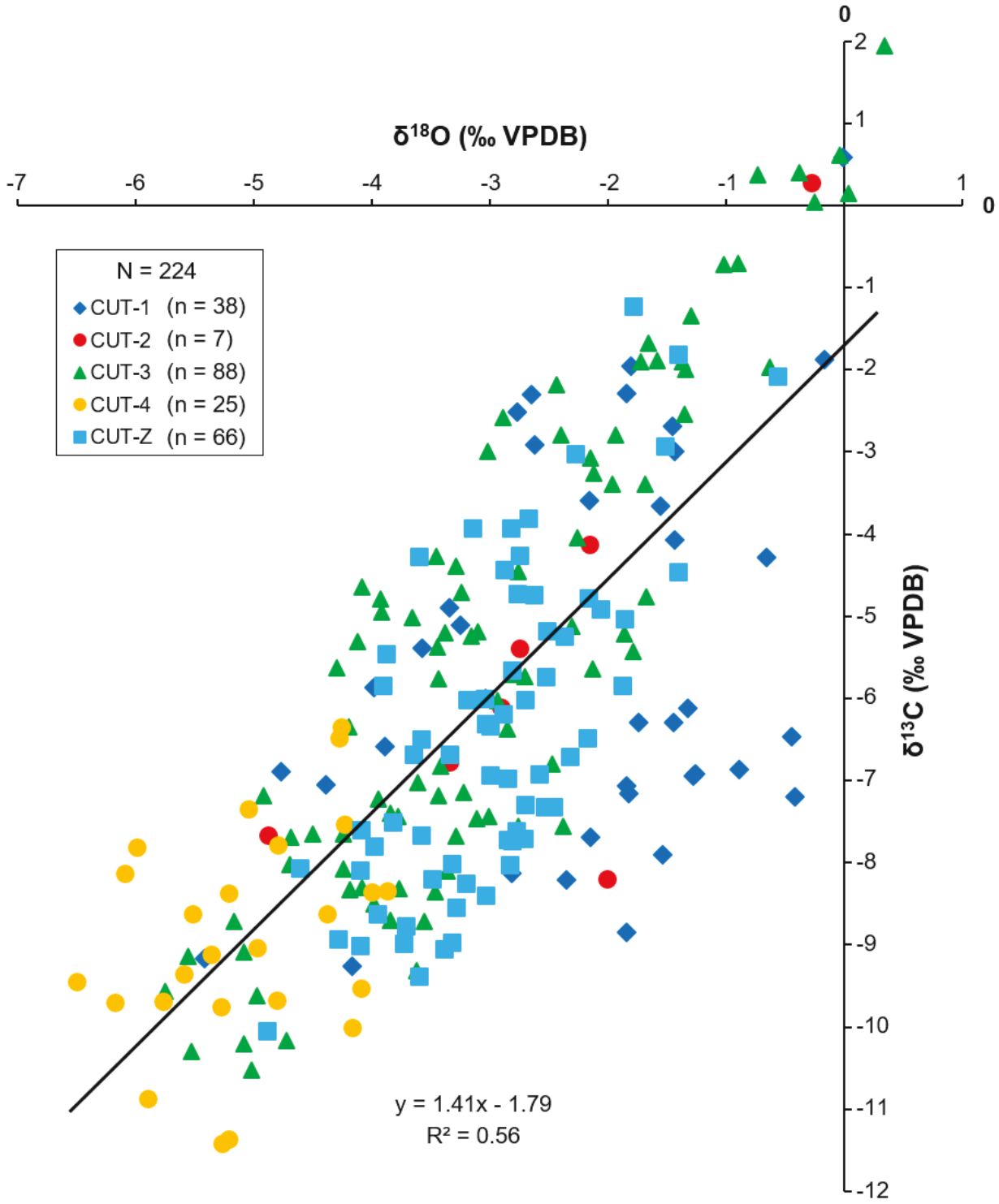

Fig. 3.1. Stable oxygen and carbon isotope compositions of samples from Cayman notch-speleothems.

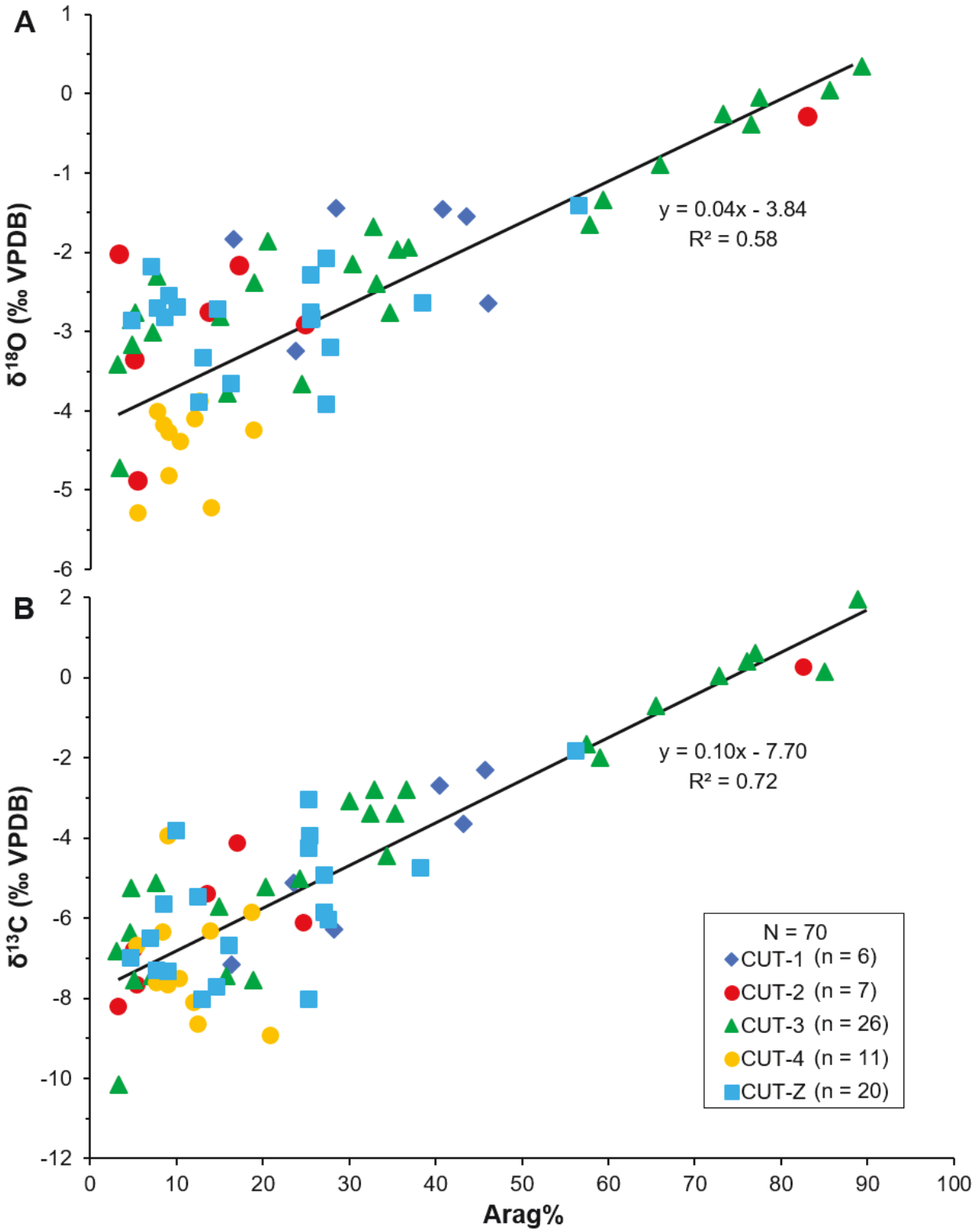

Fig. 3.2. Cross-plots of stable-isotopic compositions versus aragonite abundance (Arag% - determined by XRD analysis) of seventy samples from Cayman notch stalactites. (A) $\delta^{18}O$ versus Arag%. (B) $\delta^{13}C$ versus Arag%. Values from pure calcite laminae (Arag% = 0) are excluded from these cross-plots.

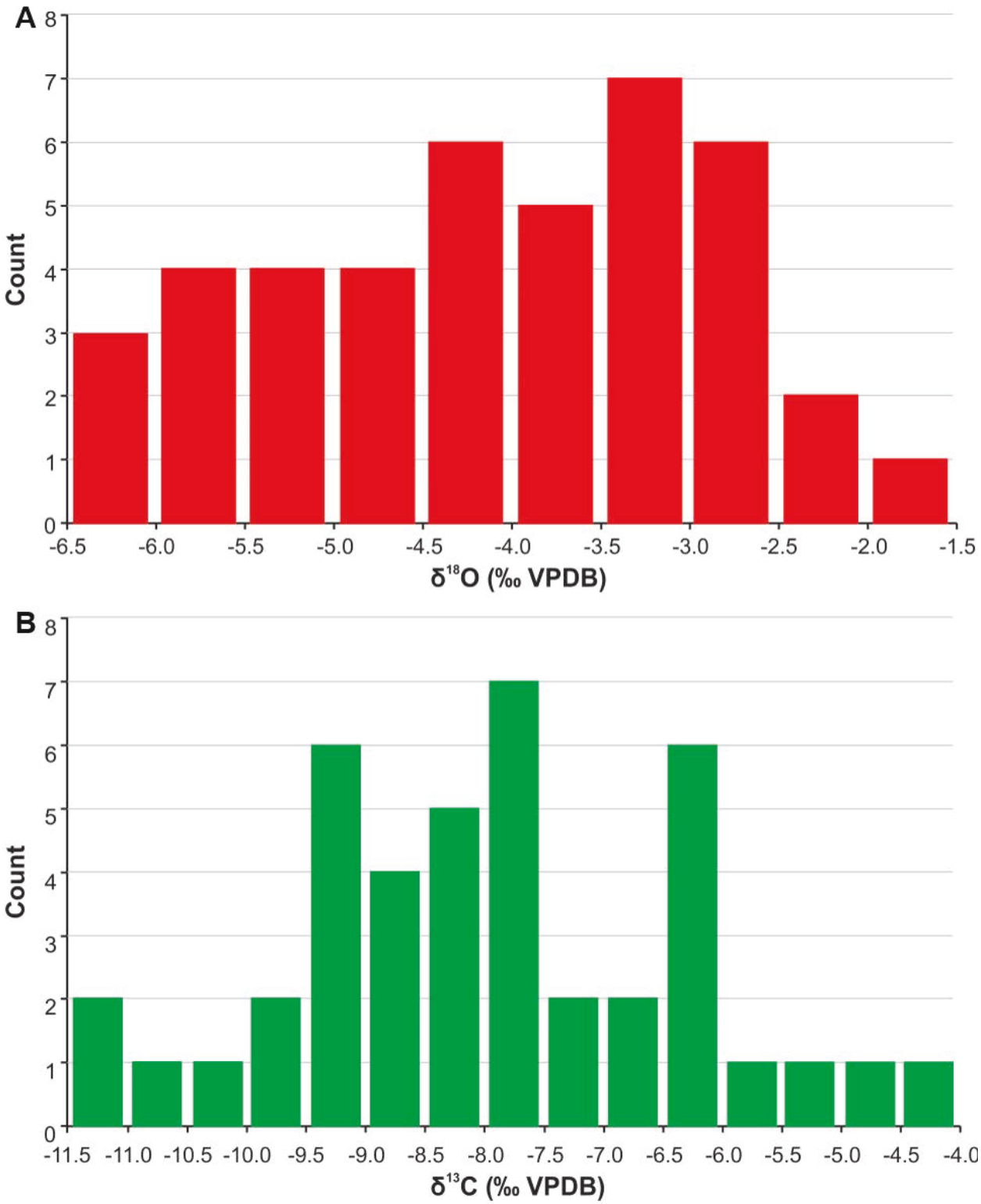

Fig. 3.3. Frequency histograms (based on count) of forty-two $\delta^{18}O$ (A) and $\delta^{13}C$ (B) values from pure calcite laminae (Arag% = 0) in stalactites CUT-3 (n = 2), CUT-4 (n = 14), and CUT-Z (n = 26).

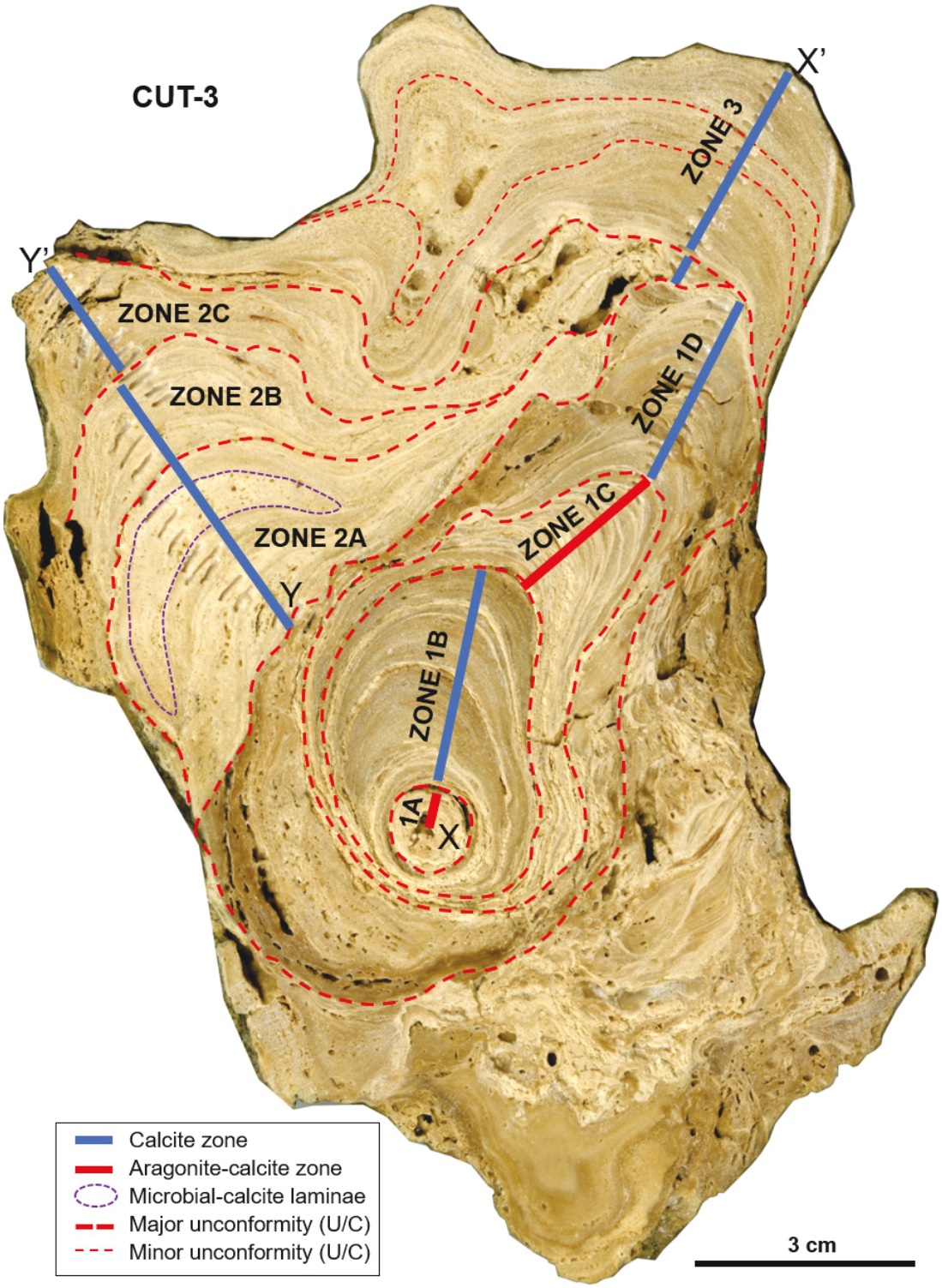

Fig. 3.4. Transverse section of stalactite CUT-3, showing zone 1 – the aragonite-rich dark inner core (divided into zones 1A to 1D) surrounded by outer calcite zones (zones 2 and 3); samples for stable isotopic analysis came from section X-X' and section Y-Y'.

2.2. Zone 2 - porous white zone

Zone 2 (Fig. 3.4), up to 60 mm thick, is formed of porous calcite laminae (zones 2A and 2B) and compact calcite laminae (zone 2C), with the porous calcite laminae being the most common (~70%). Zones 2A, 2B, and 2C are separated from each other by unconformities that are characterized by truncation of the underlying laminae. Section Y-Y' includes 6 mm-thick microbial-calcite laminae that is characterized by numerous calcified filamentous microbes (Fig. 3.4) Thin-section analysis shows that micrite and microsparite with minor amounts of mosaic calcite crystals form the porous calcite laminae, whereas the compact calcite laminae are formed of columnar compact and mosaic fabrics. Thin aragonite laminae are present locally.

2.3. Zone 3 - compact white zone

Zone 3 (~30 mm thick) is formed of porous calcite laminae (~5 mm thick) that are sandwiched between compact calcite laminae (Fig. 3.4). Thin aragonite laminae are present locally. Micrite and mosaic calcite crystals dominate the porous calcite laminae, whereas the compact calcite laminae are typically composed of columnar compact and mosaic fabrics.

2.4. Stable-isotopic variation

Stalactite CUT-3 is characterized by fluctuating ^{18}O and $\delta^{13}C$ values, with $\delta^{18}O$ values from −5.8‰ to +0.3‰ (average -3.0‰) and $\delta^{13}C$ values between -10.5‰ and +1.9‰ (average -5.5‰). There is a high correlation between the $\delta^{18}O$ and the $\delta^{13}C$ values (Figs. 3.5 to 3.8). Overall, zone 1 yielded heavier $\delta^{18}O$ and $\delta^{13}C$ values than zones 2 and 3 (Figs. 3.5, 3.7 and 3.8). The most enriched $\delta^{18}O$ and $\delta^{13}C$ signatures came from the aragonite laminae of zone 1C, with $\delta^{18}O$ and $\delta^{13}C$ values around 0‰ (Figs. 3.6, 3.7, and 3.8). Samples extracted from the laminae overlying the unconformable boundaries show enriched $\delta^{18}O$ and $\delta^{13}C$ values.

Zones 1 to 3 in CUT-3 are characterized by different isotope values

- Zone 1: The four subzones in Zone 1 yielded variable isotope signatures.
    1. Zone 1A: One sample from this zone yielded a $\delta^{18}O$ value of -2.0‰ and a $\delta^{13}C$ value of -3.4‰.
    2. Zone 1B: Eight calcite samples yielded $\delta^{18}O$ values between -4.7‰ and -2.4‰ (average -3.4‰) and $\delta^{13}C$ values between -10.2‰ and -5.2‰ (average -7.2‰), whereas the two aragonite samples gave $\delta^{18}O$ values of -1.9‰ and $\delta^{13}C$ values of -5.2‰, and $\delta^{18}O$ values of -2.8‰ and $\delta^{13}C$ values of -4.5‰, respectively. The $\delta^{18}O$ and $\delta^{13}C$ values fluctuate throughout this zone
    3. Zone 1C: Thirteen aragonite samples yielded $\delta^{18}O$ values from -2.4‰ to +0.3‰ (average -1.0‰), and $\delta^{13}C$ values between -3.4‰ and +1.9‰ (average -1.0‰). Three calcite samples yielded $\delta^{18}O$ values between -3.1‰ and -2.8‰ (average -3.0‰), and $\delta^{13}C$ values between -7.4‰ and -5.2‰ (average -6.1‰). From the base to top of this zone 2C, the $\delta^{18}O$ values increased from -3.4‰ to 0‰, before decreasing to -3.1‰, and then increasing to ~ +0.3‰. Parallel changes in the $\delta^{13}C$ values are also evident. These fluctuating isotope values reflect the alternating aragonite-calcite laminae found in this zone.
    4. Zone 1D: Six calcite samples yielded $\delta^{18}O$ values between -2.9‰ and -2.1‰ (average -2.4‰) and $\delta^{13}C$ values between -6.0‰ and -3.3‰ (average -5.0‰). In contrast, five aragonite samples yielded $\delta^{18}O$ values from -1.7‰ to -1.0‰ (average -1.4‰) and $\delta^{13}C$ values from -4.8‰ to -0.3‰ (average -2.1‰).
- Zone 2: Thirty samples from this zone were analyzed. One sample from the basal laminae in this zone, composed of micrite and aragonite, yielded $\delta^{18}O$ values of -0.2‰ and $\delta^{13}C$ values of -3.4‰. Four aragonite samples yielded $\delta^{18}O$ values from -2.9‰ to -1.6‰

(average -1.8‰) and and $\delta^{13}C$ values between -5.4‰ and -1.9‰ (average -3.6‰). Twenty-five calcite samples yielded ^{18}O values from -5.8‰ and -3.1‰ (average -4.0‰) and $\delta^{13}C$ values of -10.5‰ to -4.3‰ (average -7.6‰). Three samples from the microbial-rich laminae yielded $\delta^{18}O$ values of -4.5‰ to ~ -3.4‰ (average -3.8‰), and $\delta^{13}C$ values of -7.6‰ to ~ -7.0‰ (average -7.3‰). The porous calcite laminae (zone 2A and 2B) are characterized by relatively stable $\delta^{18}O$ values of ~ -3.5‰, and $\delta^{13}C$ values of -9.3‰ to -2.4‰. In contrast, the compact calcite laminae yielded increasing $\delta^{18}O$ values from -5.8‰ to -1.6‰, and increasing $\delta^{13}C$ values from -10.5‰ to -1.9‰ from the base to top of zone 2C.

- Zone 3: Five samples from the porous calcite laminae yielded $\delta^{18}O$ values from -4.3‰ to -3.0‰ (average -3.6‰) and $\delta^{13}C$ values between -5.6‰ and -3.0‰ (average -4.6‰). In contrast, ten samples from the compact calcite laminae yielded lighter $\delta^{18}O$ values of -5.6‰ to -3.8‰ (average -4.6‰) and lighter $\delta^{13}C$ values of -9.1‰ to -4.6‰ (average -7.8‰) than the porous calcite laminae. In zone 3, the $\delta^{18}O$ values fluctuate over a narrow value range, whereas the $\delta^{13}C$ values fluctuate widel .

3. Stalactite CUT-Z

A cross-section through this aragonite-poor stalactite shows that it is formed of zones 1, 2, and 3 that are defined la gely by their colors (Fig. 3.9). These zones are separated from each other by unconformities that are characterized by truncation of the underlying laminae and unconformable overlying laminae. These unconformities are typically overlain by thin micrite and/or aragonite laminae. Stratigraphic relationships showed that Zone 1 is the oldest whereas Zone 3 is the youngest.

Three samples (one sample from each zone) yielded Th/U dates of 49.2 ± 0.6 ka, 46.3 ± 0.4

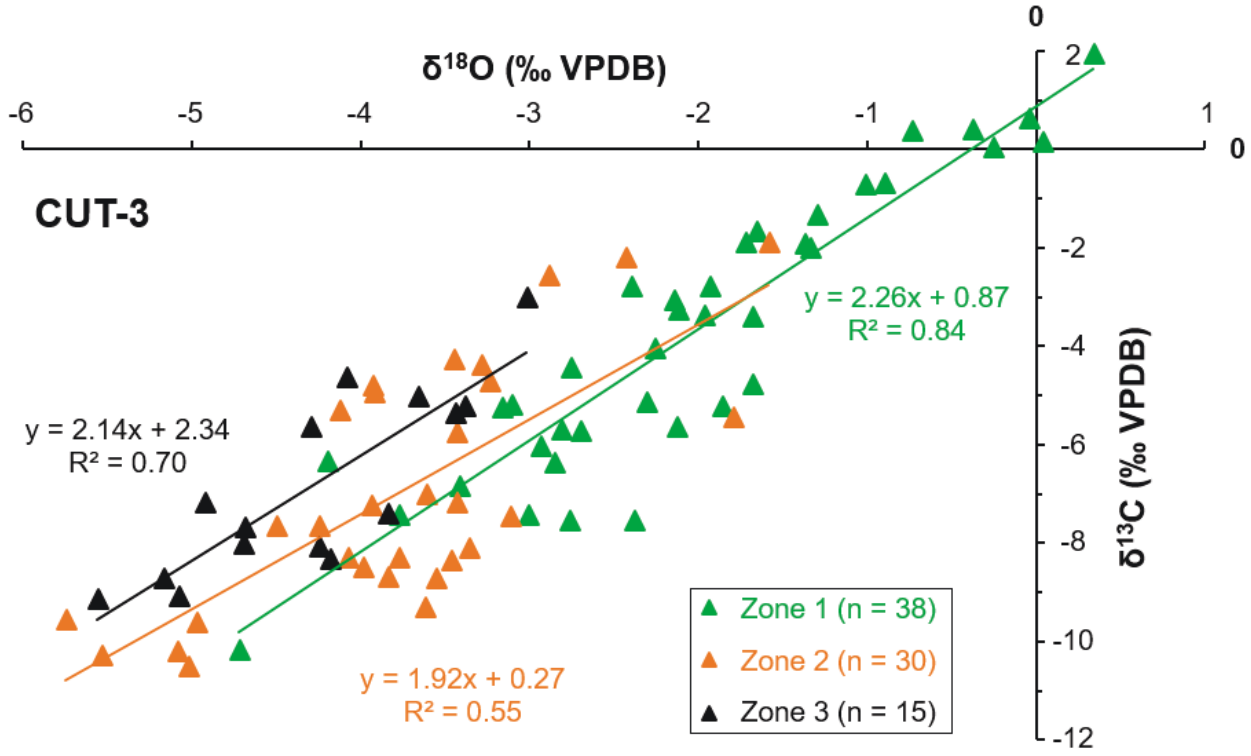

Fig. 3.5. Comparison of $\delta^{18}O$ and $\delta^{13}C$ values from zones 1, 2, and 3 in stalactite CUT-3.

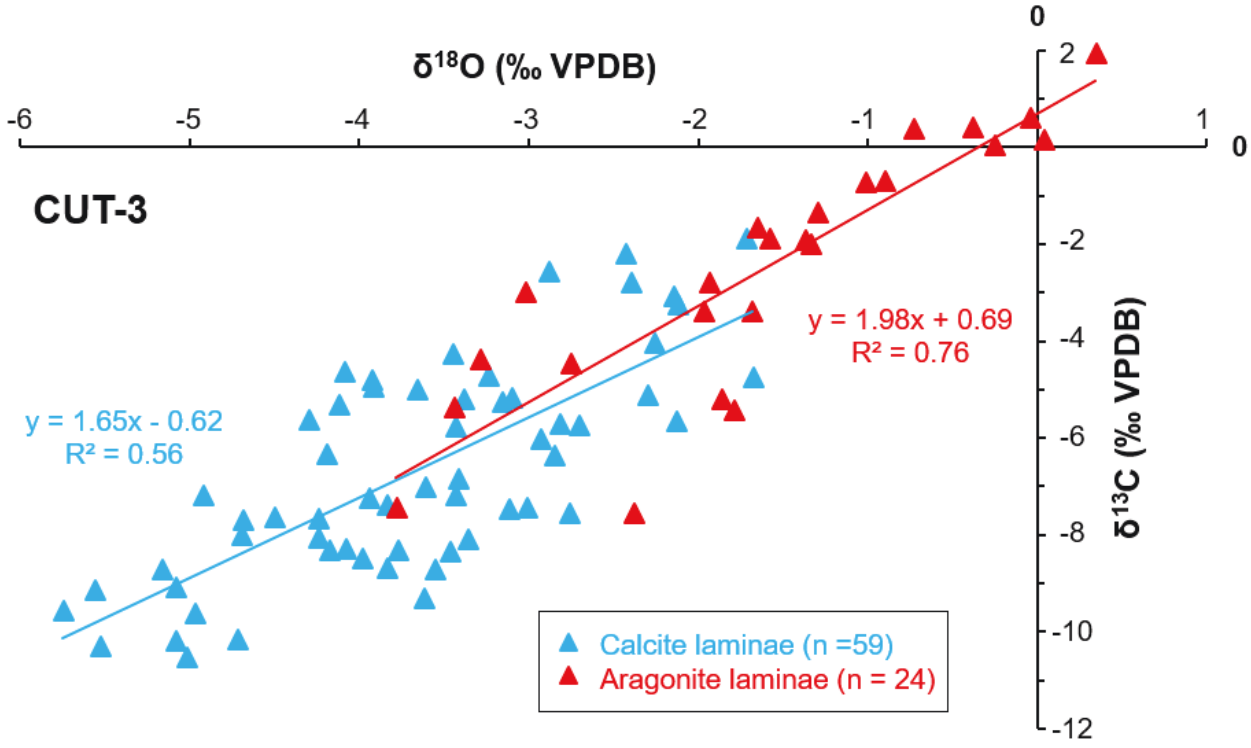

Fig. 3.6. Comparison of $\delta^{18}O$ and $\delta^{13}C$ values for calcite laminae and aragonite laminae from stalactite CUT-3.

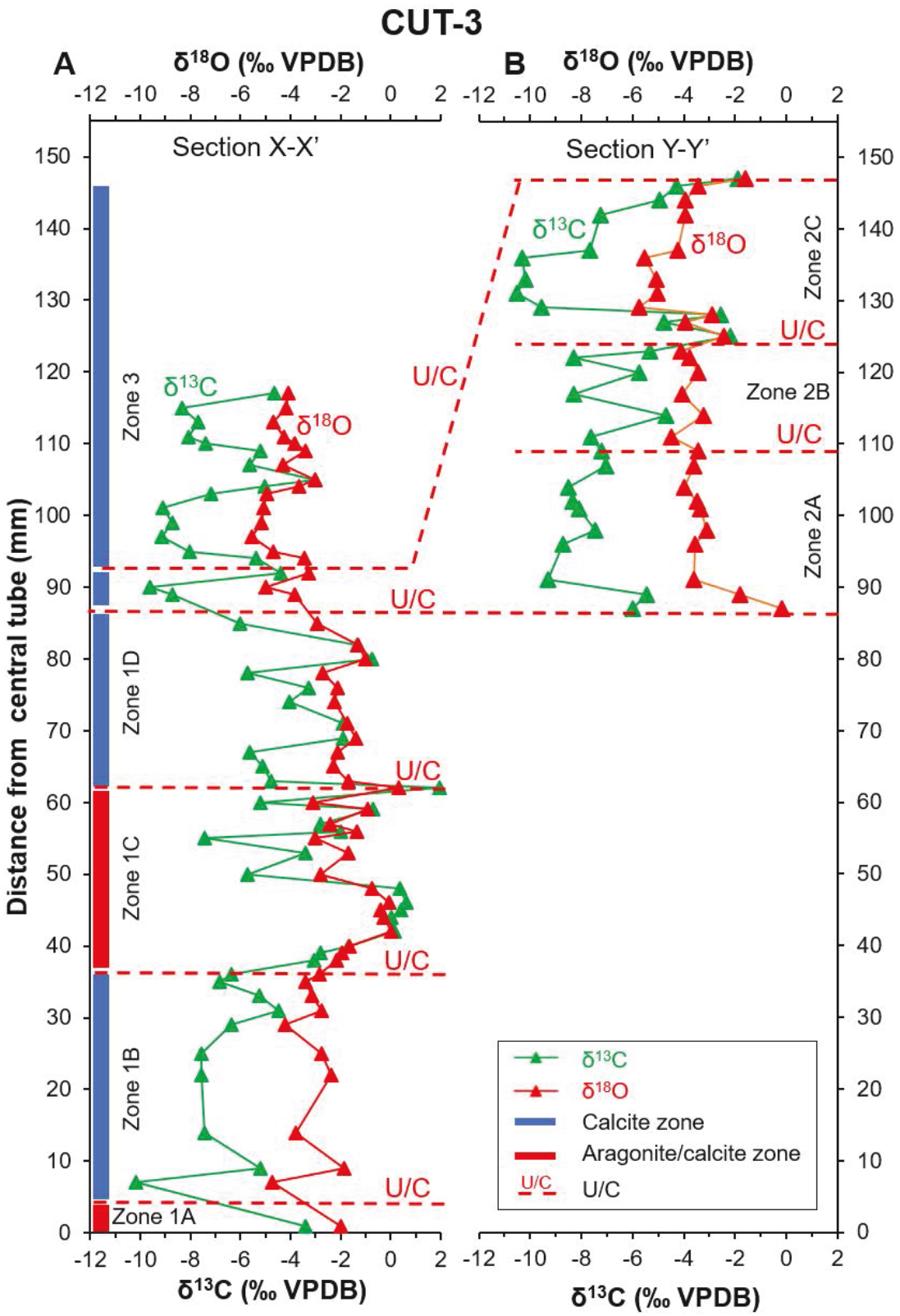

Fig. 3.7. Stable C and O isotope profiles of stalactite CU -3. (A) Stable-isotopic profiles along Section X-X'; (B) Stable-isotopic profiles along Section Y-Y'. See Figure 3.4 for location of zones 1, 2, and 3.

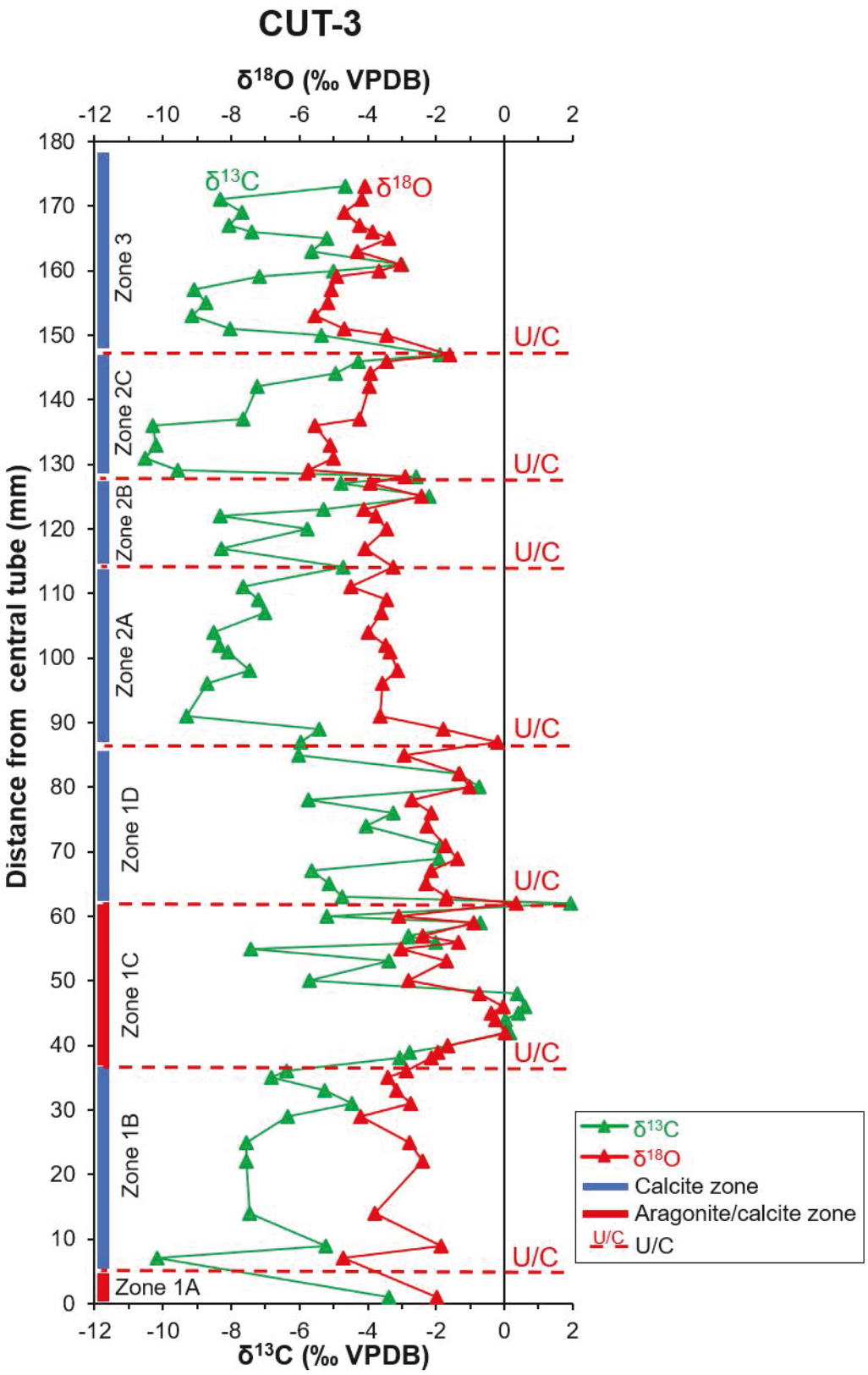

Fig. 3.8. Combined stable isotope profiles of stalactite CU -3. Zones 1 and 3 are from Section X-X', and zone 2 is from Section Y-Y' (Figs. 3.4, 3.7).

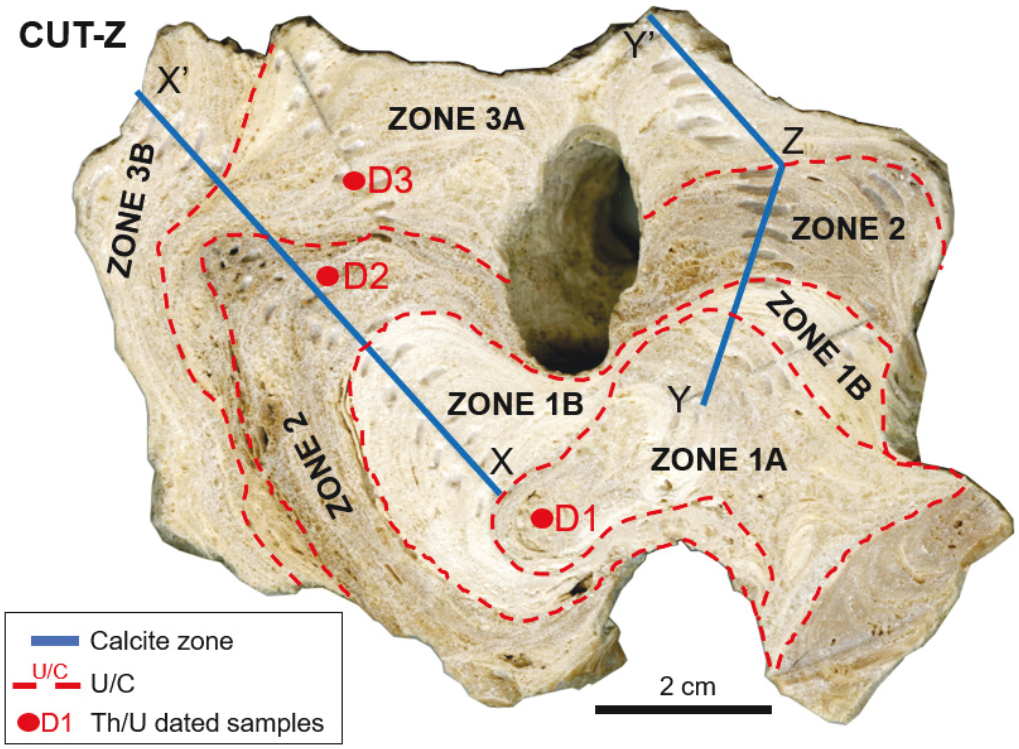

Fig. 3.9. Transverse section of stalactite CUT-Z Showing zones 1 - inner white zone (two sub-zones); 2 - middle brown zone; and 3 - outer white zone. These zones are separated by unconformities (U/C). Stable-isotopic samples came from section X-X' and Y-Z-Y'.

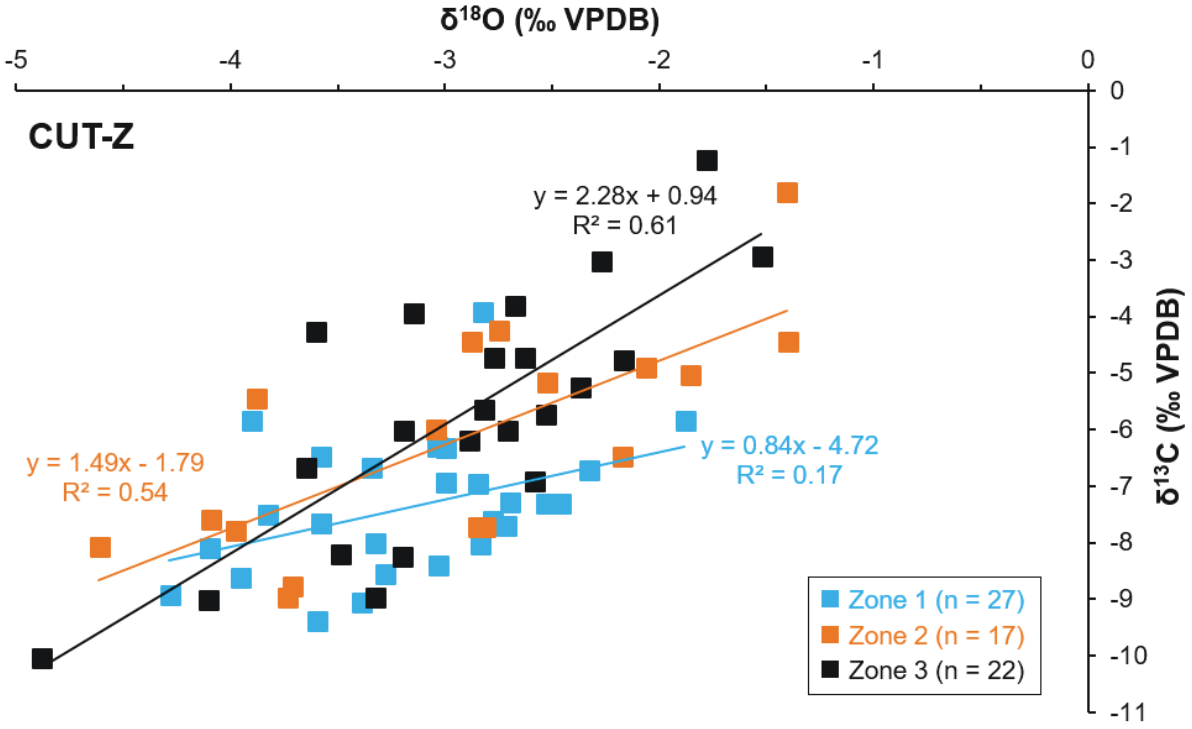

Fig. 3.10. Stable oxygen and carbon isotope compositions from zones 1, 2, and 3 in stalactite CUT-Z (Fig. 3.9). Results obtained from aragonite/micrite laminae above unconformities were excluded in this figure

ka, and 46.1 ± 0.4 ka (Fig. 3.9). Section X-X' (37 samples) and section Y-Z-Y' (29 samples) encompass all of these zones.

3.1. Zone 1 - inner white zone

This zone is formed of zones 1A and 1B that are separated by an unconformity that truncates the underlying laminae (Fig. 3.9). Zone 1A (up to 4 cm thick), which is the core that includes the central tube, is composed of compact calcite laminae (~90%) and fewer porous calcite laminae (~10%). Zone 1B, which surrounds zone 1A, is up to 2 cm thick and formed largely of porous calcite laminae (~95%). Microsparite and minor amounts of micrite and mosaic crystals form the porous calcite laminae. The compact calcite laminae are composed of elongated columnar, columnar compact, columnar open, and mosaic fabrics. Aragonite cements are found locally in the compact calcite laminae, but are absent from the porous calcite laminae. Rare thin aragonite laminae (~2%) are present immediately above the boundaries between zones 1A and 1B, and between zones 1 and 2.

3.2. Zone 2 - middle brown zone

This zone is formed largely of calcite laminae (~95%) with rare thin aragonite laminae (~5%). The calcite laminae are composed of elongated columnar, columnar open, and columnar compact fabrics, and minor mosaic crystals, and micrite. Aragonite fans and minor amounts of micrite form the thin porous aragonite laminae. Minor amounts of aragonite cement are present in some of the pores in the porous calcite laminae.

3.3. Zone 3 - outer white zone

Subzones 3A and 3B are separated by an unconformity that truncates the underlying laminae (Fig. 3.9). Both subzones are composed of calcite laminae with some intercalated thin aragonite laminae (~5%). The calcite laminae are composed of columnar open, columnar compact, micrite,

microsparite, and mosaic fabrics. The thin aragonite laminae are formed of aragonite fans and minor amount of micrite. The calcite and aragonite laminae are porous.

3.4. Stable-isotope variation

The stable-isotopic values obtained along sections X-X' and Y-Z-Y' are comparable in terms of their trends and range of values (Figs. 3.10 to 3.11). The $\delta^{18}O$ values range from -4.9‰ to -0.6‰ (average -3.0‰), and the $\delta^{13}C$ values range from -10.0‰ to -1.2‰ (average -6.4‰) (Figs. 3.10 to 3.12). There is a good correlation between the $\delta^{18}O$ and $\delta^{13}C$ values (Figs. 3.10 to 3.12).

The three zones yielded highly variable $\delta^{13}C$ values, but relatively stable $\delta^{18}O$ values:

- Zone 1: Nine calcite samples from zone 1A yielded $\delta^{18}O$ values of -3.4‰ to -2.5‰ (average -2.9‰) and $\delta^{13}C$ values of -9.0‰ to -7.0‰ (average -7.8‰). Two aragonite samples from this zone yielded $\delta^{18}O$ values of -2.3‰ and $\delta^{13}C$ values of -6.7‰, and $\delta^{18}O$ values of -2.8‰ and $\delta^{13}C$ values of -8.0‰, respectively. Twelve calcite samples from zone 1B yielded $\delta^{18}O$ values of -4.3‰ to -1.9‰ (average -3.4‰) and $\delta^{13}C$ values of -9.4‰ to -5.8‰ (average -7.5‰). Three aragonite samples obtained from laminae close to the zone boundaries yielded $\delta^{18}O$ values between -3.9‰ and -0.6‰ (average -2.4‰) and $\delta^{13}C$ values between -5.8‰ and -2.1‰ (average -4.0‰). It is notable that both the $\delta^{18}O$ and the $\delta^{13}C$ values are stable in zone 1A, whereas both the $\delta^{18}O$ and the $\delta^{13}C$ values decrease from the base to the top of zone 1B.
- Zone 2: Twelve calcite samples from this zone yielded $\delta^{18}O$ values of -4.6‰ to -2.2‰ (average -3.4‰) and $\delta^{13}C$ values of -9.0‰ to -4.4‰ (average -7.0‰). Five aragonite samples yielded $\delta^{18}O$ values between -2.8‰ and –1.4‰ (average -1.9‰), and $\delta^{13}C$ values between -5.0‰ and -1.8‰ (average -4.1‰). When compared with zone 1, zone 2 showed comparable $\delta^{18}O$ values, but enriched $\delta^{13}C$ values.

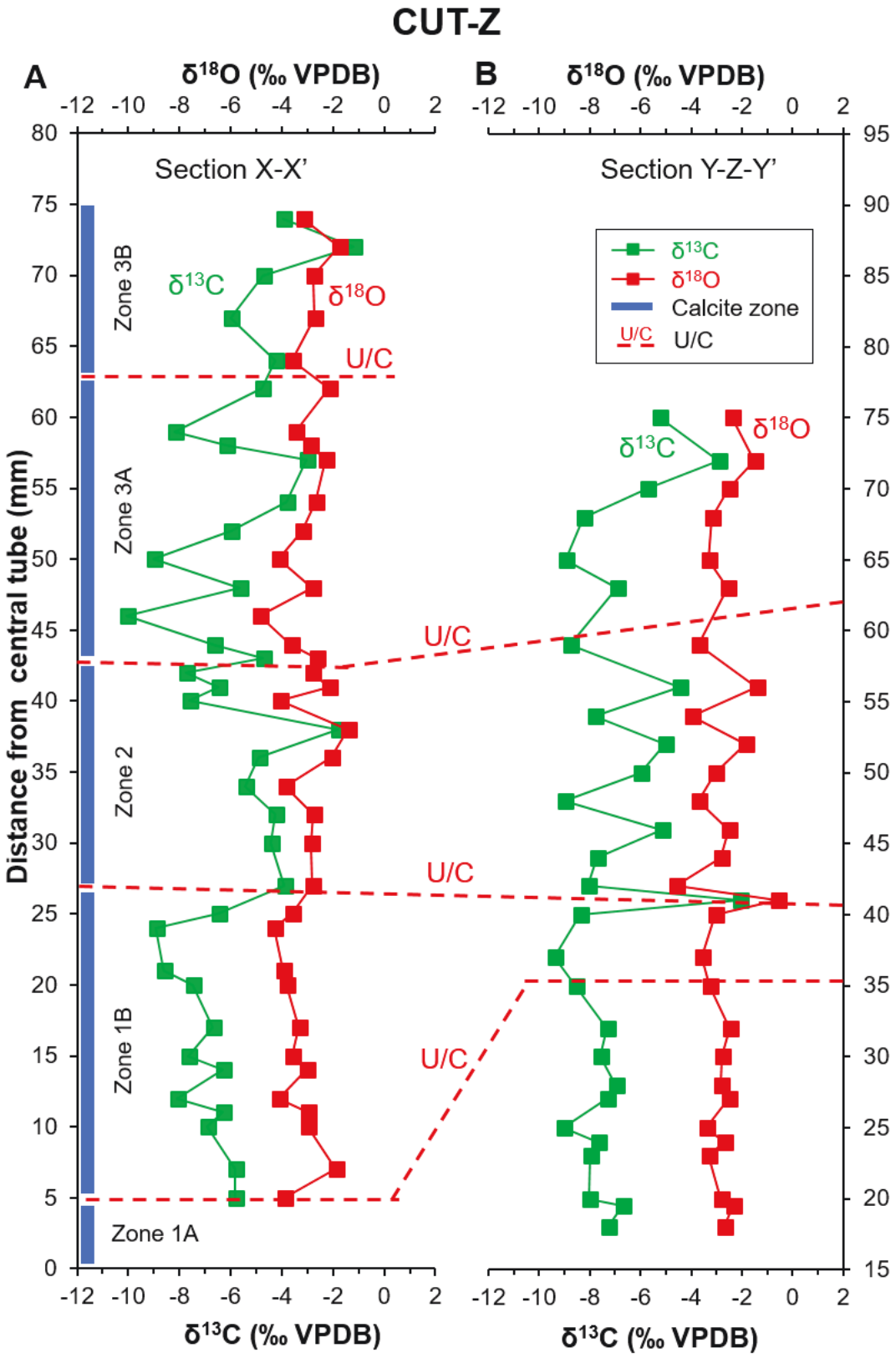

Fig. 3.11. Stable-isotope profiles across stalactite CU -Z. (A) Stable-isotopic profiles along Section X-X', and (B) stable-isotopic profiles along Section Y-Z-Y'.

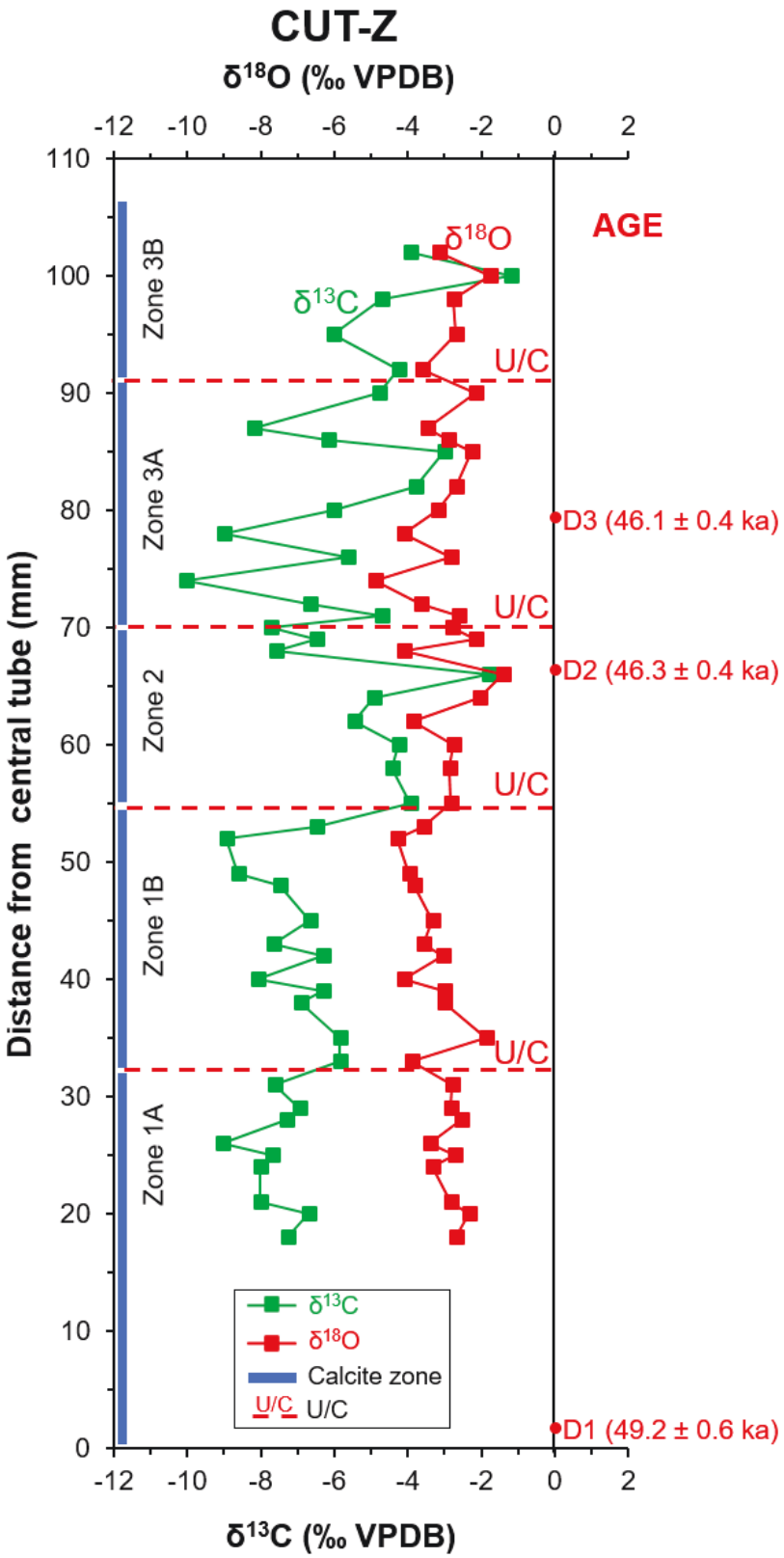

Fig. 3.12. Combined stable-isotopic profiles across stalactite CU -Z. Zone 1A from Section Y-Z-Y', and Zones 1B, 2, and 3 are from Section X-X' (Fig. 3.9, 3.11). Three Th/U dating results are labeled.

- Zone 3: Seventeen calcite samples yielded $\delta^{18}O$ values between -4.9‰ and -2.2‰ (average -3.1‰) and $\delta^{13}C$ values between -10.0‰ and -3.8‰ (average -6.1‰). Five aragonite samples yielded $\delta^{18}O$ values of -3.2‰ to -1.5‰ (average -2.3‰) and $\delta^{13}C$ values of -6.0‰ to -1.2‰ (average -3.6‰). The $\delta^{18}O$ values (fluctuating around -3‰) of zone 3 are comparable with other two zones, whereas the highly unstable $\delta^{13}C$ values of zone 3 are different from those in zones 1 and 2

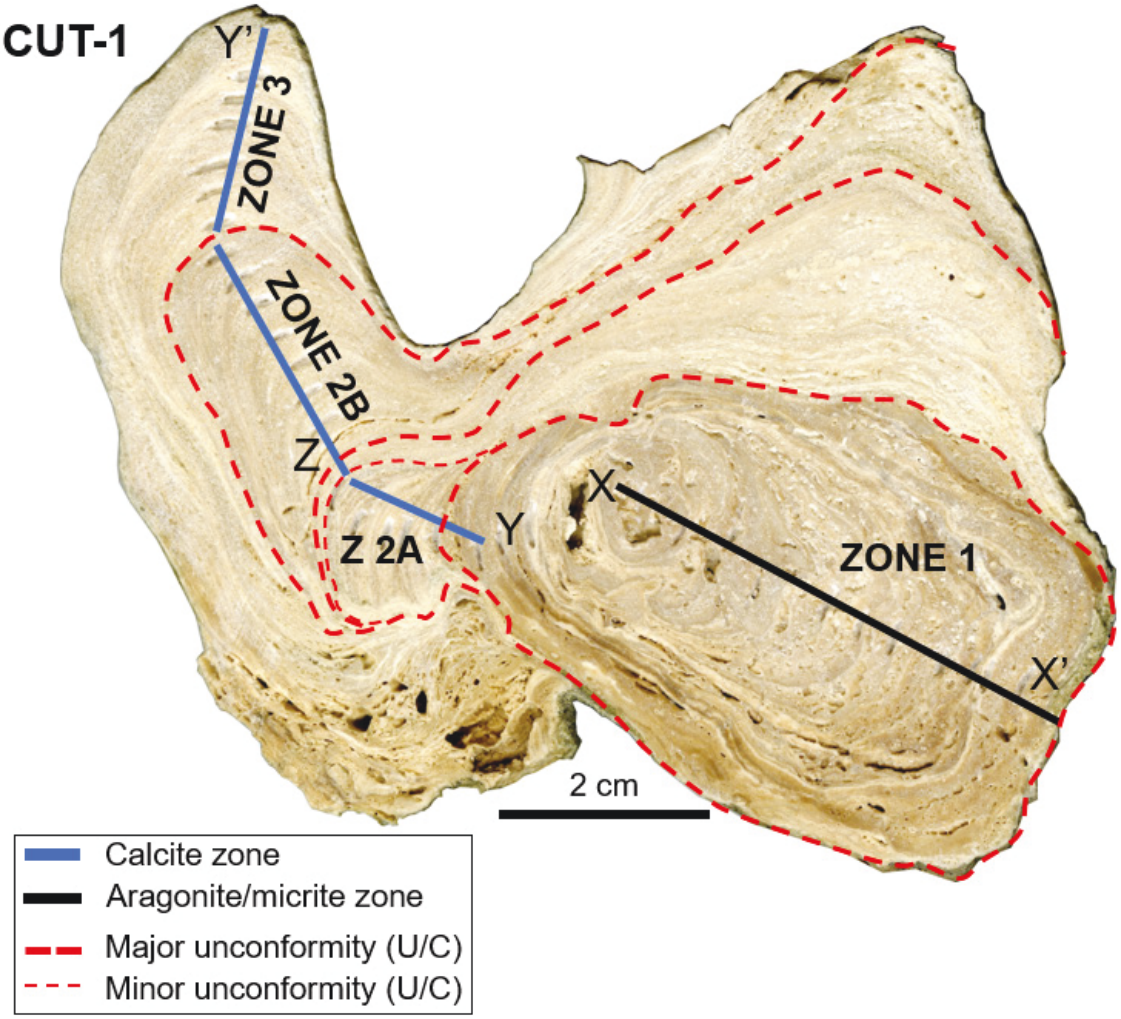

Fig. 3.13. Transverse section of stalactite CUT-1, showing: Zone 1 - dark inner core surrounded by white outer portion of Zones 2A, 2B, and 3. Samples for C and O isotope analysis obtained from sections X-X' and Y-Z-Y'.

4. Stalactite CUT-1

The cross-section through stalactite CUT-1 reveals Zone 1, a dark inner core ~50 mm thick, that is surrounded by zones 2 and 3 (Fig. 3.13). The unconformity between zones 1 and 2 is highlighted by color differences, truncation of the underlying laminae, and the unconformable ove - lying laminae. Zone 2 (up to 40 mm thick) and Zone 3 (up to 20 mm thick) are also separated by an unconformity that truncates the underlying laminations. Section X-X' (14 samples) covered Zone 1, whereas section Y-Z-Y' (24 samples) included four samples from Zone 1, fourteen samples from Zone 2, and six samples from Zone 3 (Fig. 3.13).

4.1. Zone 1 - dark inner zone

The porous dark inner core is dominated by micrite that is composed of calcite and lesser amounts of aragonite. Thin-section analysis indicates that some aragonite fans, columnar compact, and mosaic fabrics are also present.

4.2. Zone 2 - compact white zone

This zone includes two subzones (zone 2A and 2B) that are separated by an unconformity that is characterized by unconformable overlying laminae (Fig. 3.13). Thin (~ 0.3mm) micrite laminae developed directly on the unconformable boundary. Zone 2A consists of compact calcite laminae and intercalated aragonite laminae. The compact calcite laminae are composed largely of columnar compact and mosaic fabrics; whereas thin aragonite laminae, characterized by fans fabric and micrite, are intercalated between the calcite laminae. Zone 2B consists of compact calcite laminae that are typically composed of elongated columnar, columnar compact, and minor mosaic fabrics. Aragonite laminae are rare in zone 2B.

4.3. Zone 3 - porous outer zone

Zone 3, formed of porous calcite laminae, is distinguished from zone 2 by its lighter color. Thin-section analysis indicates that the porous calcite laminae are dominated by microsparite, micrite, and mosaic fabrics, and high intercrystallite porosity. Thin aragonite laminae are locally intercalated between the calcite laminae.

4.4. Stable-isotopic variation

Stalactite CUT-1 yielded $\delta^{18}O$ values from -5.4‰ to 0.0‰ (average -2.2‰) and $\delta^{13}C$ values from -9.3‰ to +0.6‰ (average -5.5‰) (Figs. 3.14 to 3.16). Each zone displays different ^{18}O and $\delta^{13}C$ variations:

- Zone 1: Eighteen samples from this zone yielded $\delta^{18}O$ values between -2.4‰ and 0‰ (average -1.3‰) and $\delta^{13}C$ values between -8.8‰ and +0.6‰ (average -5.8‰). Five aragonite samples yielded $\delta^{18}O$ ranging from -1.6‰ to 0‰ (average -1.0‰) and $\delta^{13}C$ values ranging from -6.3‰ to +0.6‰ (average -3.3‰). In this zone, the $\delta^{18}O$ values are relatively stable, and the $\delta^{13}C$ values are also stable except for a few enriched excursions. The $\delta^{18}O$ and $\delta^{13}C$ values are poorly correlated.
- Zone 2: Four samples from zone 2A yielded $\delta^{18}O$ values from -2.8‰ and -0.2‰ (average -1.5‰) and $\delta^{13}C$ values of -8.1‰ and -1.9‰ (average -5.5‰). In this zone, the $\delta^{18}O$ values are relatively stable whereas the $\delta^{13}C$ values fluctuate widel . Nine samples from zone 2B yielded $\delta^{18}O$ values of -5.4‰ to -1.8‰ (average -3.8‰) and $\delta^{13}C$ values of -9.3‰ to -2.3‰ (average -6.5‰). The intercalated porous calcite laminae yielded the most depleted $\delta^{18}O$ and $\delta^{13}C$ values of Zone 2 (Fig. 3.16). Compared to Zone 1, the $\delta^{18}O$ values in this zone vary more widely and are lighter, and the $\delta^{13}C$ values also fluctuate in a wide range. The $\delta^{18}O$-$\delta^{13}C$ covariation is this zone is high.

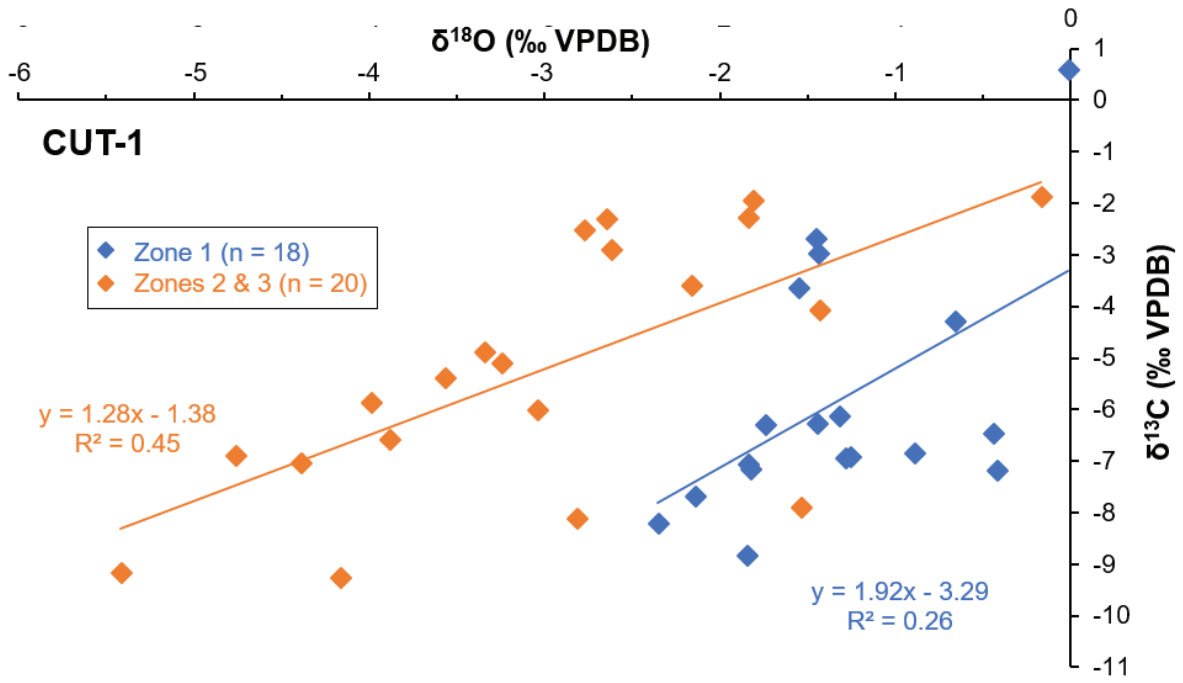

Fig. 3.14. Stable oxygen and carbon isotope compositions in three zones of stalactite CUT-1.

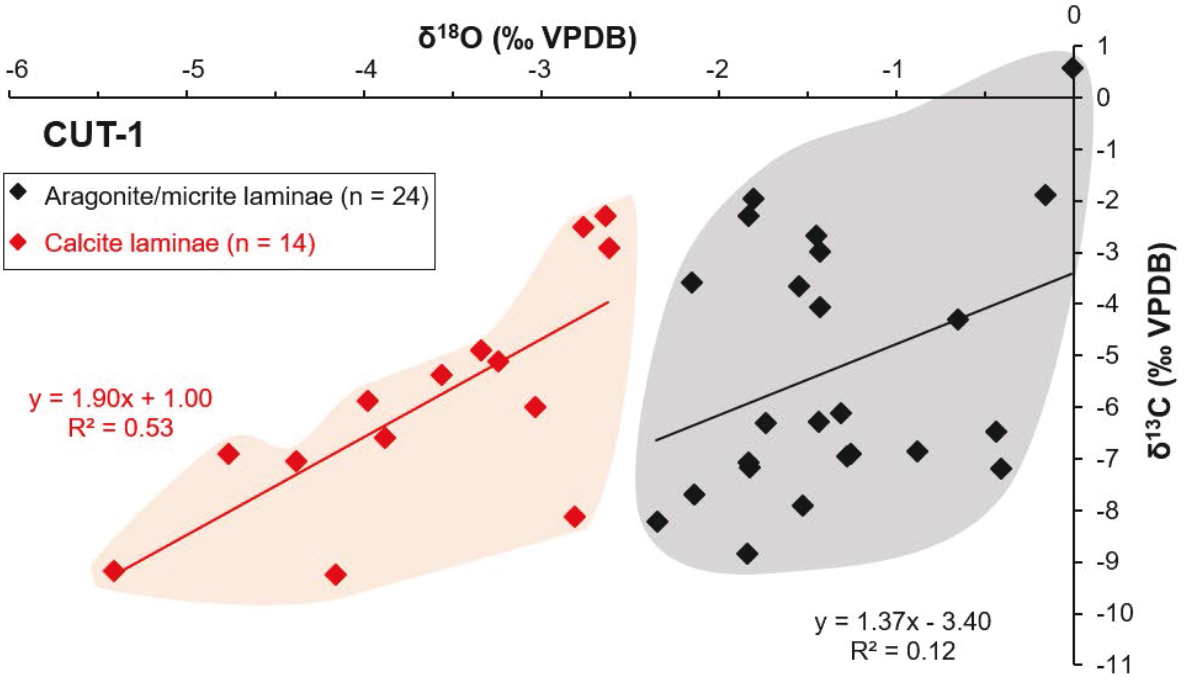

Fig. 3.15. Comparison of stable-isotopic values between calcite, and aragonite and/or micrite laminae from stalactite CUT-1.

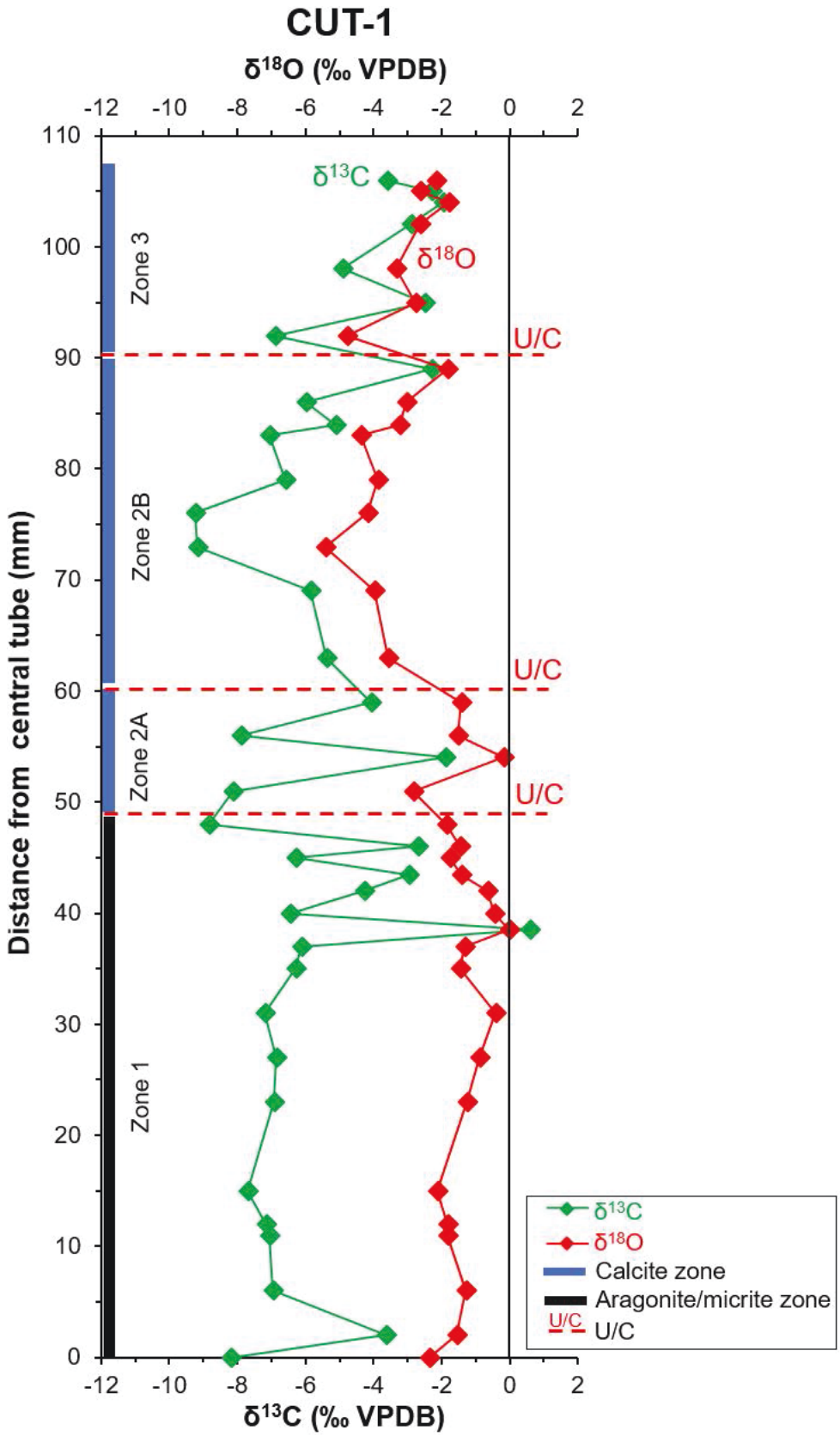

Fig. 3.16. Stable-isotopic variation profiles across stalactite CU -1 (Fig. 3.13).

- Zone 3: Seven samples from this zone yielded $\delta^{18}O$ values from -4.8‰ to -1.8‰ (average -2.9‰) and $\delta^{13}C$ values of -6.9‰ to -2.0‰ (average -3.8‰). The $\delta^{18}O$ values showed an overall increasing trend from the base to the top of zone 3. The $\delta^{13}C$ values similarly parallel the increasing trends in this zone. The $\delta^{18}O$ values vary in the similar range with Zone 2, and are more depleted than Zone 1. While the $\delta^{13}C$ values of this zone are heavier than other two zones. There is a strong correlation between the $\delta^{18}O$ and $\delta^{13}C$ values in this zone.

5. Correlation

Given that the three notch stalactites were collected from a small area at locality CUT, it is reasonable to expect some similarity between them. Correlations between stalactites CUT-1, CUT-3, and CUT-Z are evaluated based on comparisons of unconformities and minerology, $\delta^{18}O$ profiles, and ^{13}C profiles (Figs. 3.17 to 3.19)

5.1. Correlation based on unconformities and mineralogy

Each of the three notch stalactites are characterized by distinct zones that are separated by unconformities, which represent periods of erosion and/or non-deposition (Figs. 3.4, 3.9, and 3.13). Correlation between these stalactites can be based on these unconformities as well as the zones.

Stalactites CUT-3 and CUT-1 are both characterized by dark inner cores that are separated from their white outer portions by well-defined unconformities that are similar to each ot - er (Figs. 3.4, and 3.13). The calcite laminae and unconformities of the white outer portions of stalactites CUT-3 and CUT-1 are also similar. It is difficult, howev , to correlate the cores of the two stalactites, because the inner core of CUT-1 is dominated by dark-colored micrite whereas the inner core of CUT-3 is formed of calcite and aragonite/calcite zones. Stalactite CUT-Z does

not display the well-defined unconformity that separates the inner core and outer zones, as in the other two stalactites. Mineralogically, stalactite CUT-Z is comparable with the white outer portion of stalactite CUT-1, and with the outer portions (zones 2 and 3) and possible zone 1D of stalactite CUT-3 (Fig. 3.17).

5.2. Correlation based on $\delta^{18}O$ profile

The $\delta^{18}O$ values of the notch stalactites basically reflect the ^{18}O signatures of the formative fluids, which were controlled la gely by the temperature and rainfall. Comparisons of the trends in the $\delta^{18}O$ profiles of CU -1, CUT-3, and CUT-Z was facilitated by comparing the fluctuations relative to a $\delta^{18}O$ value of -2.8‰, which is the average for all samples analyzed from these three stalactites (Fig. 4.18). For this purpose, the $\delta^{18}O$ values obtained from the aragonite were transformed into "calcite" values using a calcite-aragonite fractionation value of 0.75‰ (Kim et al., 2007).

The $\delta^{18}O$ profile of Stalactite CU -3, which is the longest, is divided into zones O-I to O-IV (Fig. 3.18). Zones O-I, O-III, and O-IV have $\delta^{18}O$ values that are mostly less than -2.8‰, whereas zone OII has $\delta^{18}O$ values that are generally greater than -2.8‰.

The $\delta^{18}O$ profile of Stalactite CU -1 is divided into three zones that correspond to zones O-II, O-III, and O-IV of CUT-3 (Fig. 3.18). The three zones evident in stalactite CUT-Z are equivalent to zones O-II and O-IV of CUT-3 (Fig. 3.18).

The fact that each $\delta^{18}O$ zone can include several petrographic zones and unconformities (compare Figs. 3.17 and 3.18), indicates that the petrographic and isotopic parameters were not necessarily correlated.

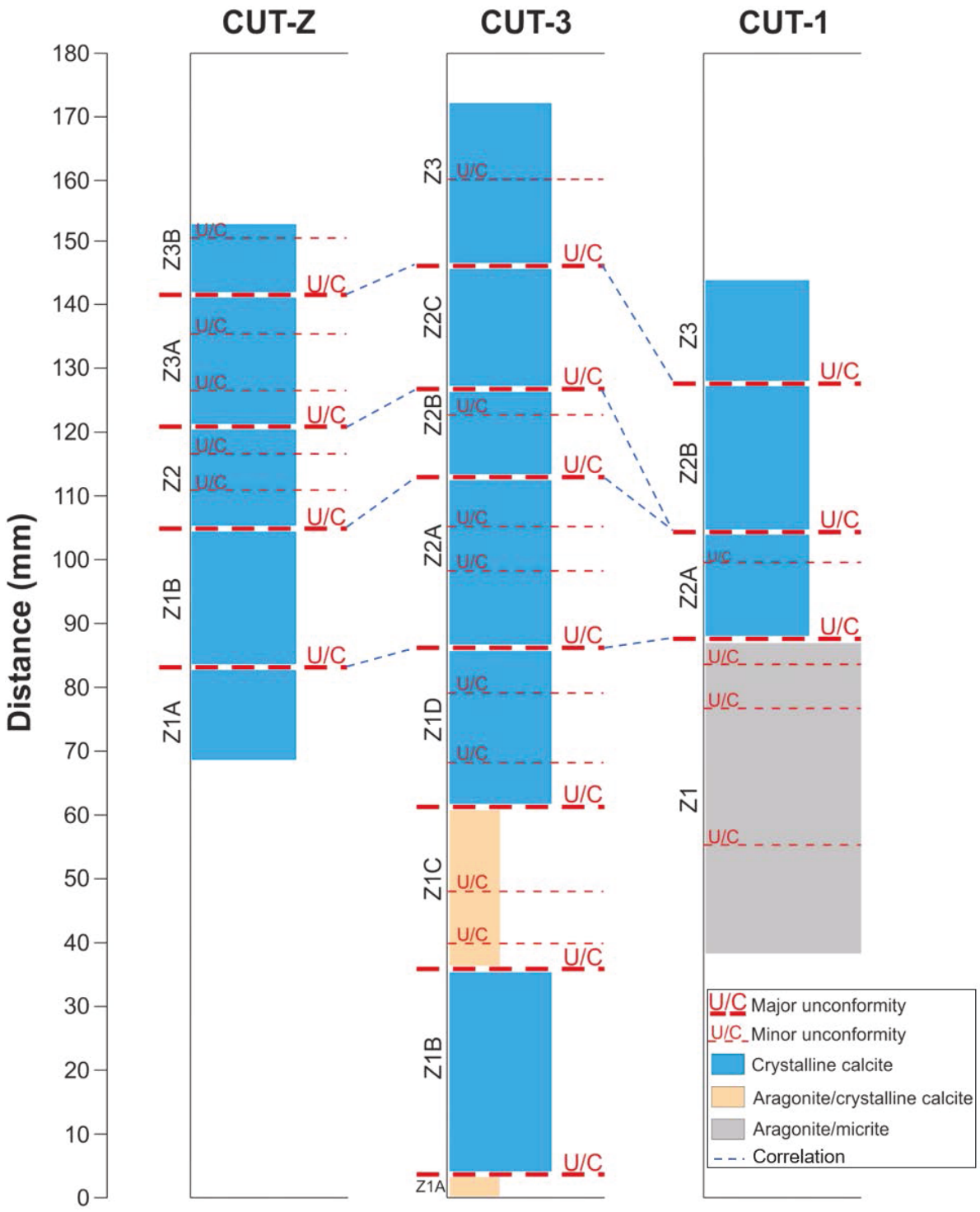

Fig. 3.17. Correlation of stalactites CUT-Z, CUT-3, and CUT-1 based on unconformities and mineralogy.

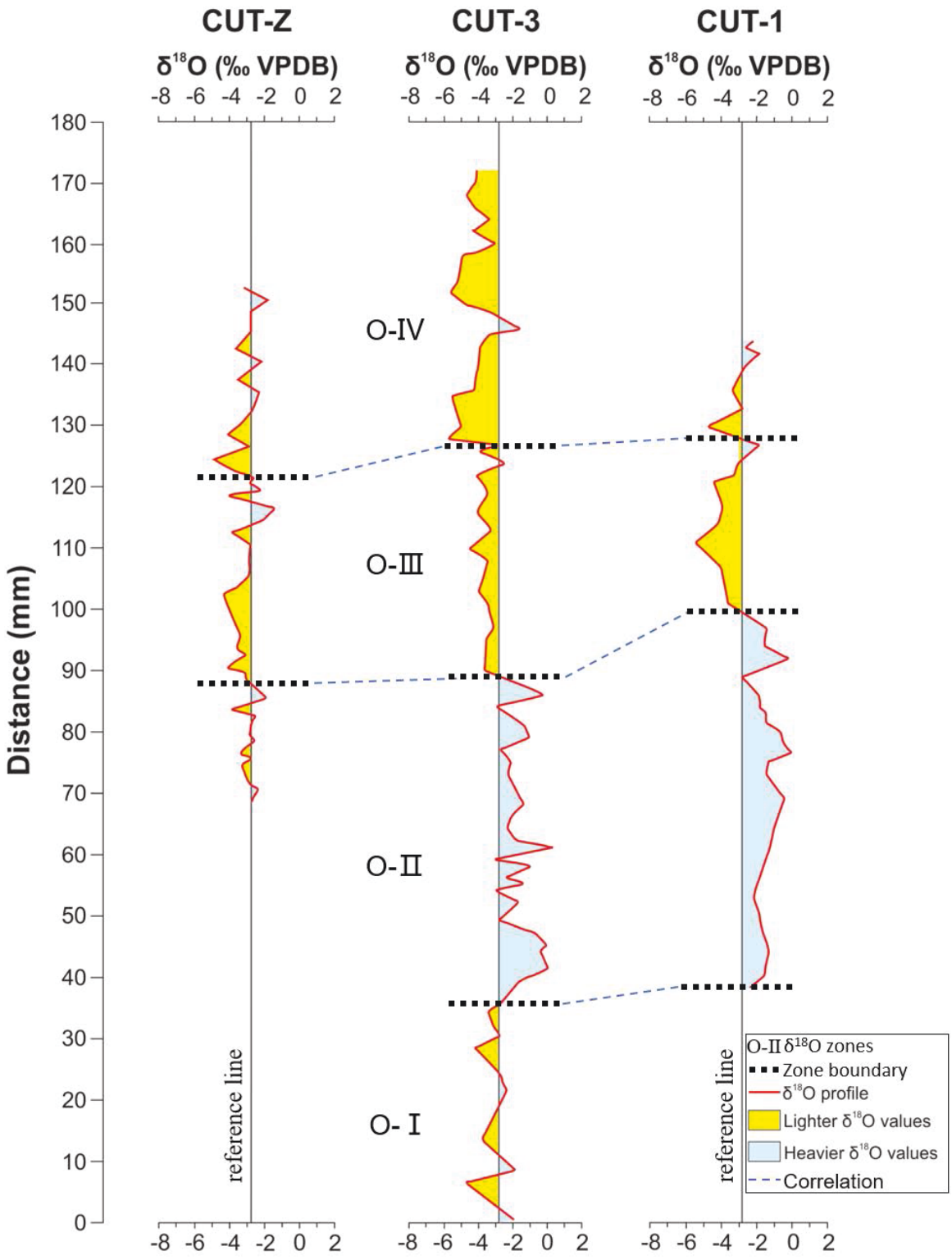

Fig. 3.18. Correlation of stalactites CUT-Z, CUT-3, and CUT-1 based on $\delta^{18}O$ values. Note the $\delta^{18}O$ curves are 'calcite' values corrected by calcite-aragonite fractionation factor (0.75‰, Kim et al., 2007). The reference line ($\delta^{18}O$ = -2.8‰) is the average $\delta^{18}O$ value of the three stalactites. O-I, O-II, O-III, and O-IV stand for four $\delta^{18}O$ zones.

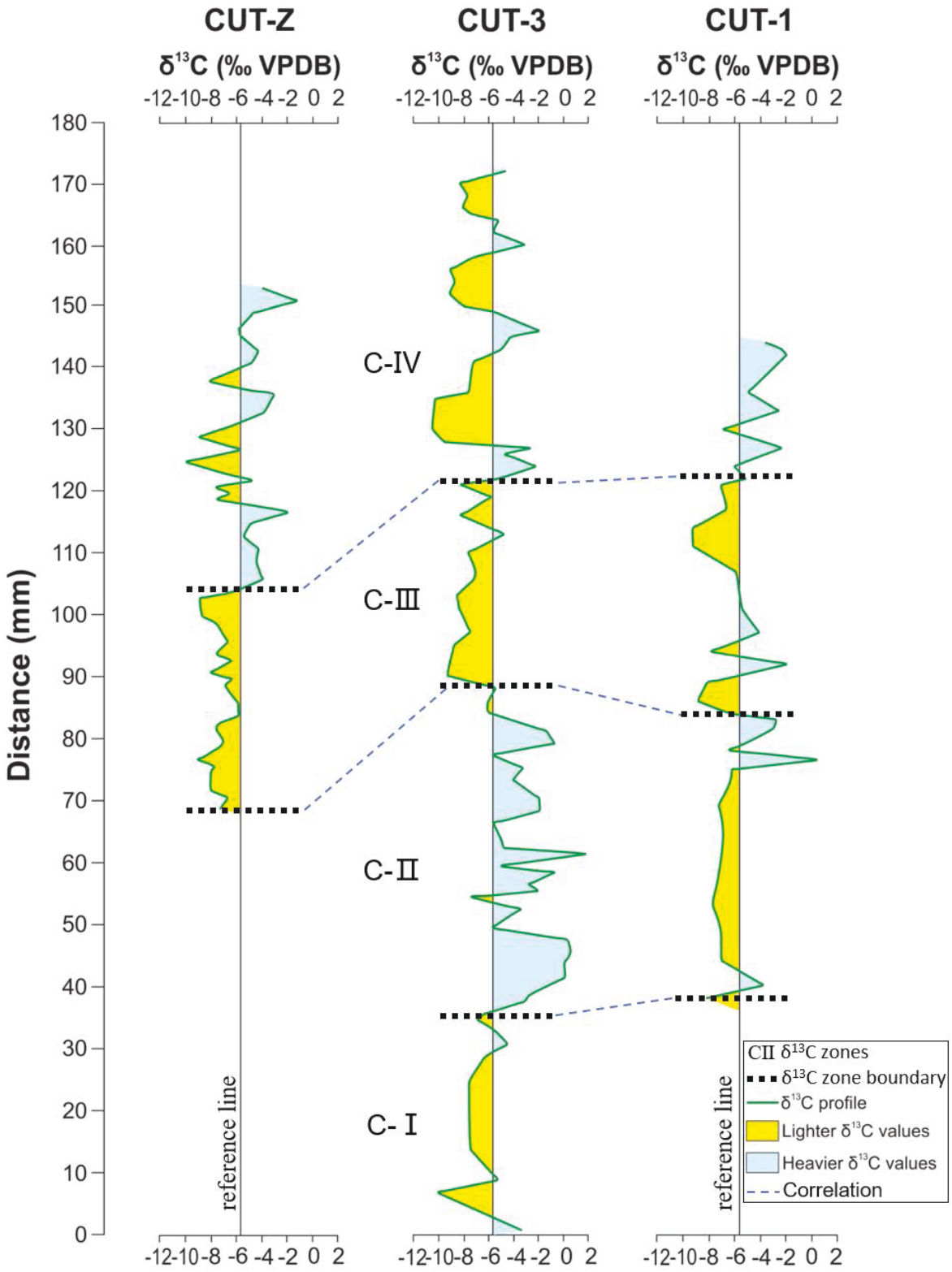

Fig. 3.19. Correlation of stalactites CUT-Z, CUT-3, and CUT-1 based on $\delta^{13}C$ values. The reference line ($\delta^{13}C$ = -5.8‰) is the average $\delta^{13}C$ value of the three stalactites. C-I, C-II, C-III, and C-IV stand for four $\delta^{13}C$ zones.

5.3. Correlation based on $\delta^{13}C$ profile

The $\delta^{13}C$ values of the notch stalactites reflect the ^{13}C properties of percolating fluids, which was controlled largely by the overlying vegetation (C3 versus C4 plants, as defined by Farquhar et al., 1980; Sage, 2004). Comparison of the $\delta^{13}C$ profiles of the three notch stalactites was faci - itated by comparing the $\delta^{13}C$ values relative to a $\delta^{13}C$ value of -5.8‰, which is the average value for these three stalactites (Fig. 3.19).

The $\delta^{13}C$ profile of Stalactite CU -3 is divided into zones C-I to C-IV. Zones C-I and C-III have $\delta^{13}C$ less than -5.8‰, zone C-II is mostly greater than -5.8‰, and C-IV is less than -5.8‰ apart from a few excursions to values greater than -5.8‰ (Fig. 3.19).

Stalactite CUT-Z includes two zones that correlate to zones C-III and C-IV of CUT-3. The $\delta^{13}C$ curve of Stalactite CUT-1 is divided into three zones that are equivalent to zones C-II, C-III, and C-IV of CUT-3 (Fig. 3.19). Zone C-II of CUT-1 is, however, dominated by $\delta^{13}C$ values less than -5.8‰, which is due to the high micrite content.

Like the $\delta^{18}O$ defined zones, each ^{13}C zone typically includes several petrographic zones and many unconformities (compare Figs. 3.17 and 3.19), suggesting that the $\delta^{13}C$ values do not always parallel to the petrographic changes.

5.4. Suggested correlation

There exist both agreements and disagreements among the correlations based on unconformi- ties and minerology, the $\delta^{18}O$ profiles, and the ^{13}C profiles. Based on petrographic and isotopic features, it is evident that:

- The unconformity between zones 1D and 2A of stalactite CUT-3 (Fig. 3.4) correlates to the unconformity between zones 1 and 2A of CUT-1 (Fig. 3.13);
- Stalactite CUT-Z correlates to the outer portions of CUT-3 and that of CUT-1;

- The dark inner core of CUT-3 correlates to dark inner core of CUT-1, despite their difference in mineralogy and $\delta^{13}C$ values.

Overall, the three notch stalactites are petrographically and isotopically comparable. Therefore, the stable-isotopic profiles from three notch stalactites record the paleoenvironmental information at least between 49.2 ± 0.6 ka and 46.1 ± 0.4 ka (Table 4.1).

6. Paleotemperature based on $\delta^{18}O$

The temperature of the water from which the speleothems were formed can be calculated if the (1) $\delta^{18}O$ values of the formative waters are assumed to have had the same value as the present day shallow groundwater of -4.5‰ SMOW, and (2) precipitation of Cayman notch-speleothem calcite was in isotopic equilibrium with the formative waters. Herein, the paleotemperature profiles for these speleothems were calculated using the equations developed by Epstein et al. (1953), O'Neil et al. (1969), Hays and Grossman (1991), Kim and O'Neil (1997), Sharp (2007), and Grossman (2012). For this purpose, all the aragonite $\delta^{18}O$ values determined from the notch-speleothem were first converted into "calcite" values based on the percentage of aragonite in the sample and an average aragonite-calcite fractionation factor of 0.75‰ (valid between 20 °C and 30 °C – Kim et al., 2007). The six equations yielded temperature (T) curves that included temperatures from -5.7 to 21.1 °C. These T curves can be divided into two groups by their systematic temperature difference of 2-4 °C between them two (Fig. 4.20):

- Group 1: This group, which included the curves generated from the equations of Kim and O'Neil (1997) and Grossman (2012) and overlap each other, yielded calculated temperatures (CTs) of -5.7 to 19.3 °C (average 6.5 °C);
- Group 2: This group, which included the four curves generated from the equations of Epstein et al. (1953), O'Neil et al. (1969), Hays and Grossman (1991), and Sharp (2007)

overlap each other and yielded calculated temperatures of -3.2 to 21.1 °C (average 8.9 °C).

Herein, the temperature results obtained from the Sharp (2007) equation are used because: (1) CTs of Group 2 have less unreasonable values (< 0 °C), (2) four CT curves in Group 2 overlap each other, and (3) the Sharp (2007) equation in Group 2 has commonly been used for speleothem $\delta^{18}O$-based paleotemperature calculations (e.g., Lachniet, 2009; Jiménez de Cisneros et al., 2015).

Using the equation established by Sharp (2007), the $\delta^{18}O$ values from stalactite CUT-3, CUT-Z, and CUT-1 yielded paleotemperatures of -0.2 to 21.3 °C (average 10.1 °C), 5.1 to 17.4 °C (average 10.1 °C), and -0.7 to 19.8 °C (average 7.0 °C), respectively. The three temperature profiles for these speleothems are compatible (Fig. 3.21).

The temperature profile for Stalactite CU -3, which provides the longest temporal record, is divided into three periods (Figs. 3.20 to 3.21):

- **Warm Period I (W-I)**: The calculated temperature of this period (consisting of $\delta^{18}O$ Zone OI, see Fig. 3.20) are 5.9 to 16.8 °C with an average ~ 10.4 °C.
- **Cold Period I (C-I)**: This period, consisting of $\delta^{18}O$ Zone O-II (Fig. 3.20) is characterized by calculated temperatures of -0.2 to 10.0 °C with an average of 5.2 °C.
- **Warm Period II (W-II)**: The calculated temperature of this period (including $\delta^{18}O$ Zones O-III and O-IV, Fig. 3.20) are 4.4 to 21.3 °C with an average of 13.4 °C.

The CTs for the speleothems yielded large temperature variations (up to 25 °C), and values that seem unreasonable (e.g., < 0 °C) given the tropical setting of Cayman Brac and present-day water temperatures. Errors in the CT may have arisen because of the following issues.

- The formative fluids did not have a constant $\delta^{18}O$ value of -4.5‰ SMOW. This is supported by the modern water isotopic results (Table 4.2), which have $\delta^{18}O$ values that range from -7.3 to -1.6‰ for rainwaters, -7.7 to -2.7‰ for dripwaters, and -5.5 to -3.5‰ for the shallow fresh groundwaters on the Cayman Islands. Hence, the $\delta^{18}O$ values of formative water for the notch-speleothems were likewise variable.
- The oxygen isotopes in the notch-speleothems and their formative waters was not in equilibrium. It is not surprising to have disequilibrium isotopic fractionations in the notch-speleothems, given that the wave-cut notch was and is still open to the atmosphere. If the shallow groundwater values ($\delta^{18}O_{water}$ of -4.5‰ VSMOW, T of 28 °C) are used in the paleotemperature equation of Sharp (2007), the calcite precipitated in equilibrium with the groundwater should have an average $\delta^{18}O$ value of -7.1‰ VPDB. In contrast, measured Cayman notch-speleothems $\delta^{18}O$ values, from -6.5‰ to +0.3‰ (average -3.1‰ VPDB), are enriched relative to the calculated -7.1‰, indicating that the disequilibrium fractionation was probably due to evaporation. Tarhule-Lips (1999) reported $\delta^{18}O_{calcite}$ values of ~ -7 to -5.5‰ (average -6.3‰ VPDB) during the interval of ~ 50 to 45 ka in cave speleothem from Cayman Brac (Tarhule-Lips, 1999, her Fig. 3.16). If a value of -3‰ VPDB (roughly the $\delta^{18}O$ average value difference between Cayman notch-speleothems and Cayman cave speleothems) is used to correct the notch-speleothems $\delta^{18}O_{calcite}$ results, Stalactite CUT-3 then yields temperature values of 10.4 to 36.6 °C (average 23.0 °C) that are systematically ~ 13 °C warmer than the temperature profile based on uncorrected notch-speleothem $\delta^{18}O_{calcite}$ values (Fig. 3.21).
- The “calcite” $\delta^{18}O$ values used in the calculation may have inherited some errors during the conversion procedure, due to a presumed calcite-aragonite fractionation factor of

0.75‰ under equilibrium conditions. The fractionation factors may be much different under disequilibrium conditions from under equilibrium conditions.

7. Paleovegetation and bedrock contribution based on $\delta^{13}C$

Variations in the $\delta^{13}C$ values of speleothems are influenced by the (1) proportion of C3 versus C4 vegetation on the overlying surface, and (2) variable amounts of $\delta^{13}C$ that are derived from the bedrock (McDermott et al., 2004; Fairchild et al., 2006). Both are ultimately linked to climatic conditions and specifically to arid versus wet climates

The percentage of C3 vegetation can be calculated by equation 3.1 (modified from Tarhule-Lips, 1999; Gillson et al., 2004):

$$\delta^{13}C_{calcite} = x\delta^{13}C_{C3} + (1-x)\,\delta^{13}C_{C4} \qquad \text{(Equation 3.1)}$$

where $x = (\delta^{13}C_{calcite} - \delta^{13}C_{C4}) / (\delta^{13}C_{C3} - \delta^{13}C_{C4})$.

The contribution of bedrock to the speleothem $\delta^{13}C$ compositions can be calculated by equation 3.2, which was proposed by Shopov et al. (1997):

$$P_{bedrcok} = 100\% * (\delta^{13}C_{soil} - \delta^{13}C_{calcite}) / (\delta^{13}C_{soil} - \delta^{13}C_{bedrock}) \qquad \text{(Equation 3.2)}$$

All aragonite $\delta^{13}C$ results were first converted into "calcite" $^{13}C_{calcite}$ values using their relative abundance and the calcite-aragonite carbon isotope fractionation factor of ~2‰ between 25 to 30 °C (Tucker and Wright, 1990, their Fig. 6.23). There are no available data of soil CO_2 $\delta^{13}C_{C3}$ and soil CO_2 $\delta^{13}C_{C4}$ values in Cayman Islands. Based on published studies, McDermott (2004) summarized that: (1) soil CO_2 $\delta^{13}C$ values typically range from -26 to -20‰ VPDB under C3 plants, whereas soil CO_2 $\delta^{13}C$ values range from -16 to -10‰ VPDB under C4 plants, and (2) carbonate deposits in equilibrium with soil CO_2 respired from C3 plants typically have a $\delta^{13}C_{C3}$ range of -14 to -6‰ (average -10‰ VPDB), and a $\delta^{13}C_{C4}$ range of -6 to +2‰ (average -2‰ VPDB) under C4 plants cover. Herein, the calculation of proportions of C3 versus C4 vegetation

(equation 3.1) were based on average value of -10‰ for $\delta^{13}C_{C3}$ and -2‰ for $\delta^{13}C_{C4}$, respectively.

In Equation 3.2, the calcite-CO_2 carbon isotope fractionation factor is ~9‰ between 25 to 30 °C (Tucker and Wright, 1990, their Fig. 6.23). At locality CUT, the wave-cut notch is overlain by dolostones with $\delta^{13}C$ average of +2.5‰ VPDB for the Cayman Formation (Zhao and Jones, 2012a), and dolostones with $\delta^{13}C$ average of +0.3‰ and limestones with $\delta^{13}C$ average of -5.5‰ for the Pedro Castle Formation (MacNeil and Jones, 2003). All of these $\delta^{13}C$ compositions have the potential of influencing the ^{13}C signatures of Cayman notch-speleothems. Therefore, each value was used in the equation 3.2 to calculate the variable amounts of $\delta^{13}C$ that were derived from the bedrocks.

Calculations yielded (1) unreasonable negative percentages (< 0%) of C3 vegetation (equation 3.1), and (2) unreasonable percentages (> 100%) of bedrock contributions (equation 3.2) that are all "impossible situations". Like the $\delta^{13}C$ profiles, the percentage of C3 vegetation and the bedrock contribution profiles are comparable and divisible into three periods (Fig. 3.22)

- **Wet Period I (WP-I)**: This period, including $\delta^{13}C$ zone C-I (Fig. 3.20), is characterized by higher C3 plant percentage but lower bedrock contributions, indicating that evaporation was less important, possibly due to the climate being wetter.
- **Dry Period I (DP-I)**: This period, consisting of $\delta^{13}C$ zone C-II (Fig. 3.20), is characterized by lower C3 plant percentage but higher bedrock contributions, suggesting that evaporation was more important, possibly due to a drier climate.
- **Wet Period II (WP-II)**: This period, including $\delta^{13}C$ zones C-III and C-IV (Fig. 3.20), is characterized by higher C3 plant percentage but lower bedrock contributions, suggesting wetter climatic conditions with less evaporation.

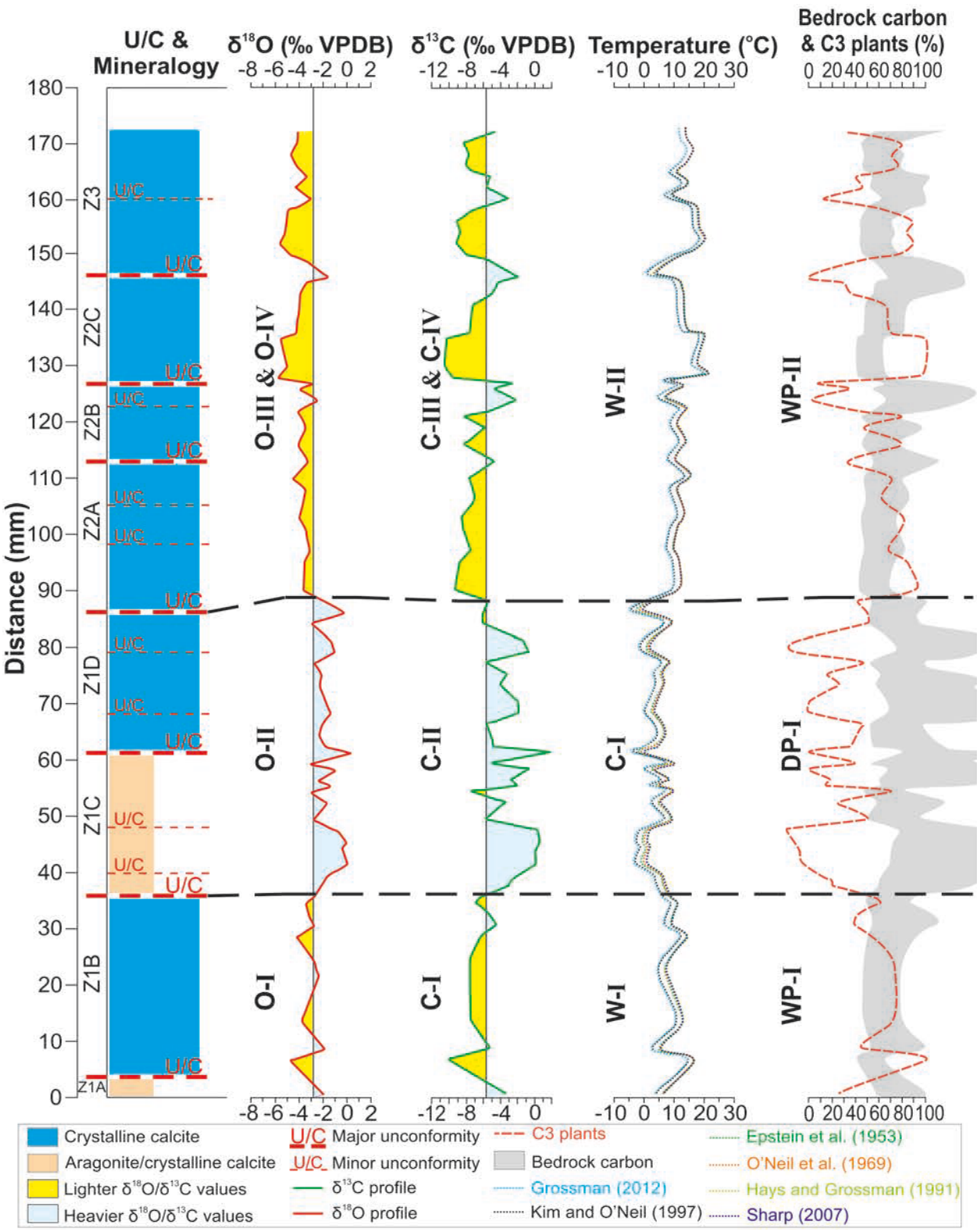

Fig. 3.20. Comparison of unconformities and mineralogy, $\delta^{18}O$ zones (O-I to O-IV), $\delta^{13}C$ zones (C-I to C-IV), temperature periods (warm W-I and W-II, and cold C-I), and proportion of C3 plants and bedrock carbon (WP-I and WP-II - wet periods, and DP-I - dry period) for stalactite CUT-3.

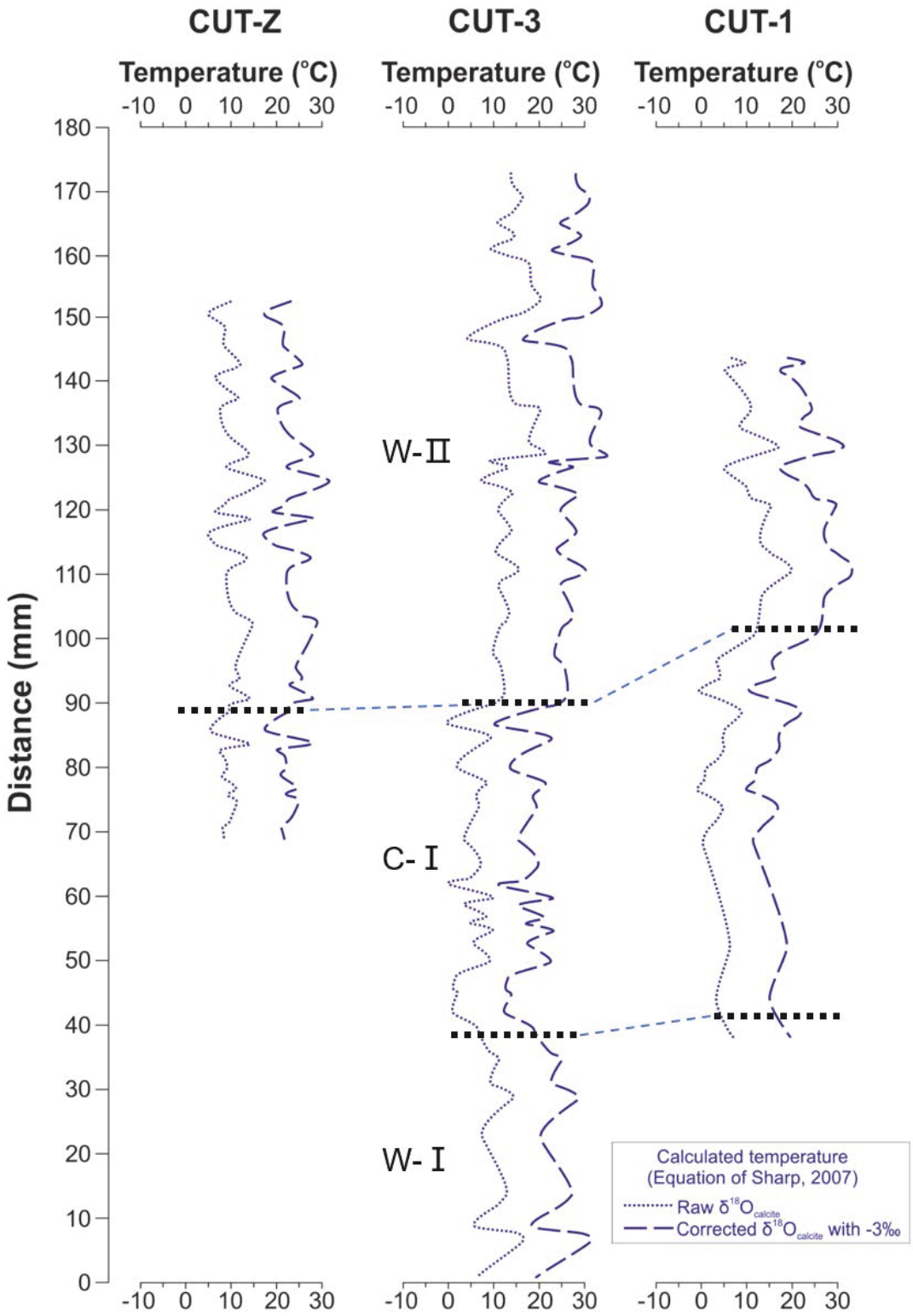

Fig. 3.21. Paleotemperature curves of three notch stalactites (based on equation from Sharp, 2007). Each notch stalactite yields two temperature curves, with one curve using raw calcite $\delta^{18}O$ values while another curve using corrected calcite $\delta^{18}O$ values for evaporation. W-I = warm period I, C-I = cold period I, and W-II = warm period II.

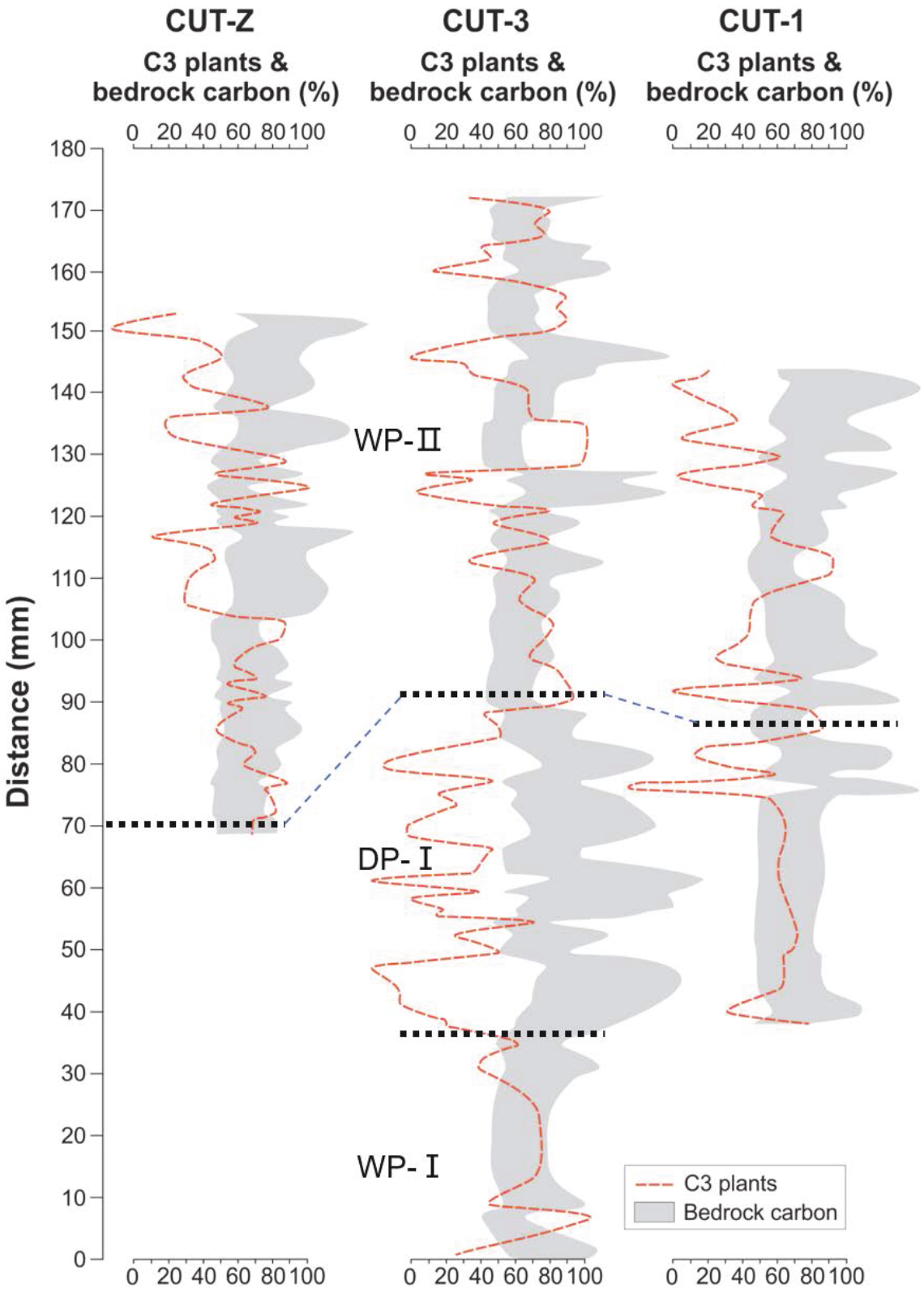

Fig. 3.22. Percentage of C3 plants and bedrock carbon. A decrease in C3 plants and an increase in bedrock indicates a trend to a drier and cooler climate. WP-I = wet period I, DP-I = dry period I, and WP-II = wet period II.

CHAPTER 4: DISCUSSION

1. Growth period

Th/U dating shows that stalactite CUT-Z grew between 49.2 ± 0.6 ka and 46.1 ± 0.4 ka ago (Table 4.1). Analyses of the stable isotopes show that this period of growth included a warm and wet period, a cooler and drier period, and finally another warm and wet period (Figs. 3.20 to 3.22). This period of growth corresponds to the time of the Dansgaard/Oeschger interstadial 13 (D/O-13), the Heinrich stadial 5 (HS-5), and the Dansgaard/Oeschger interstadial 12 (D/O-12) (Fig. 4.2), which are millennial-scale climate events that dramatically influenced climatic fl - tuations during the Last Glacial period (Dansgaard et al., 1984; Heinrich, 1988; Johnsen et al., 1992). Comparison of the stable isotopic values from stalactite CUT-3 (Fig. 3.17 to 3.19), which provides the longest record among the Cayman speleothems, with other paleoenvironmental records worldwide shows that its growth responded to these global, millennial-scale climate changes. The transitions from the D/O-13 (~ 49.3-48.3 ka, relative to NGRIP chronology, Svensson et al., 2008) to HS-5 (~ 48.3-47 ka), and from HS-5 (~ 48.3-47 ka) to D/O-12 (~ 47-44.8 ka) are characterized by sharp shifts in the $\delta^{18}O$ and $\delta^{13}C$ values of the Cayman notch-speleothems (Fig. 4.2).

1.1. D/O-13 period (~ 49.3-48.3 ka)

For this period, the Cayman notch-speleothems yielded negative $\delta^{18}O$ and $\delta^{13}C$ values that are consistent with those seen in the Greenland ice cores (Svensson et al., 2008), Omani speleothems (Burns et al., 2003), Chinese speleothems (Wang et al., 2001), and Costa Rican speleothems (Lachniet et al., 2009). Schmidt et al. (2006) documented warm temperatures for the D/O-13 period in Western Caribbean ocean sediments, which also corresponds to the warm D/O-13 event that has been reported in Greenland ice cores (Svensson et al., 2008). Lachniet et al. (2009),

Wang et al. (2001), and Burns et al. (2003) attributed the more negative $\delta^{18}O$ values derived from tropical/subtropical speleothems to increased monsoon rainfalls. This is also consistent with proxy data from ocean sediments in the Cariaco Basin that have been attributed to wetter climatic conditions caused by the northerly shift of the Intertropical Convergence Zone (ITCZ) during the warmer D/O-13 period (Deplazes et al., 2013).

1.2. HS-5 period (~ 48.3-47 ka)

The Cayman notch-speleothems are characterized by more positive $\delta^{18}O$ and $\delta^{13}C$ values for the HS-5 period, which correspond to data derived from the Greenland ice cores (Svensson et al., 2008), tropical/subtropical speleothems (Burns et al., 2003; Wang et al., 2001; Lachniet et al., 2009; Arienzo et al., 2017), and ocean sediments (Schmidt et al., 2006; Deplazes et al., 2013) (Fig. 4.2). For this period, Schmidt et al. (2006) documented a slight cooling of ~ 2-3 °C for the surface seawater temperatures (SST) for the Western Caribbean Sea, and Henry et al. (2016) reported a similar temperature decrease in the paleo SSTs for Bermuda. The cooling evident in the tropical/subtropical regions probably corresponds to the cold Heinrich events that are recorded in the Greenland ice cores (Svensson et al., 2008). Cooling during the HS-5 period led to dry conditions in the tropical areas, including the Caribbean. Lachniet et al. (2009) attributed the more positive $\delta^{18}O$ values of Costa Rican speleothems in the HS-5 period to reduced rainfall because of weaker summer monsoons in the Caribbean. Arienzo et al. (2017) also reported enrichments in stable isotopes (especially $\delta^{13}C$ results) and suggested a drier climate during for the HS-5 period. All these results are in agreement with Chinese (Wang et al., 2001) and Omani speleothems (Burns et al., 2003). It is notable that Costa Rican speleothems display a depleted $\delta^{18}O$ interval (Fig. 4.2F) amid the generally more positive $\delta^{18}O$ signature of the HS-5 period, suggesting that some wet intervals occurred during this period. Such features are not, however, evident in the

Cayman notch-speleothems or in the Bahamian speleothems documented by Arienzo et al. (2017). Nevertheless, the fluctuating ^{18}O and $\delta^{13}C$ values, alternating aragonite and calcite laminae, and unconformities in the Cayman notch-speleothems may be indicative of some wetter (and possibly warmer) intervals on the Cayman Islands during the HS-5 period.

1.3. D/O-12 period (~ 47-44.8 ka)

The $\delta^{18}O$ and $\delta^{13}C$ values of Cayman notch-speleothems shift back to more negative values for the D/O-12 period. These are consistent with other paleoenvironmental proxies recorded for this period (Svensson et al., 2008; Burns et al., 2003; Wang et al., 2001; Lachniet et al., 2009; Deplazes et al., 2013; Arienzo et al., 2017). Henry et al. (2016) detected this D/O-12 warming event in ocean sediments around Bermuda and Svensson et al. (2008) detected it in the Greenland ice core. The depletion in $\delta^{18}O$ values in tropical/subtropical speleothems across the world had been attributed to increasing monsoon rainfalls in response to the warming of the D/O-12 event. Examples include the Omani speleothems (Burns et al., 2003), Chinese speleothems (Wang et al., 2001), Costa Rican speleothems (Lachniet et al., 2009), and Bahamian speleothems (Arienzo et al., 2017).

Table 4.1 Th/U dating results from Stalactite CUT-Z.

Sample ID	Distance from central tube (mm)	^{238}U (ppb)	Error (2σ, ppb)	^{232}Th (ppb)	Error (2σ, ppb)	$^{234}U/^{238}U$	Error (2σ)
CUT-Z (D1)	1~4	418.5765	1.1229	7.0972	0.0191	1.0236	0.0049
CUT-Z (D2)	29~32	563.9730	1.5020	1.3952	0.0049	1.0404	0.0041
CUT-Z (D3)	36~38	602.183	1.642	2.174	0.008	1.014	0.004

Table 4.1 (continued)

Sample ID	$^{230}Th/^{238}U$	Error (2σ)	$^{230}Th/^{232}Th$	Error (2σ)	Calculated Age (ka)	Error (2σ, ka)
CUT-Z (D1)	0.3730	0.0027	67.2287	0.5043	49.1809	0.5507
CUT-Z (D2)	0.3617	0.0018	446.8077	2.6078	46.3088	0.3757
CUT-Z (D3)	0.350	0.002	296.590	1.966	46.076	0.416

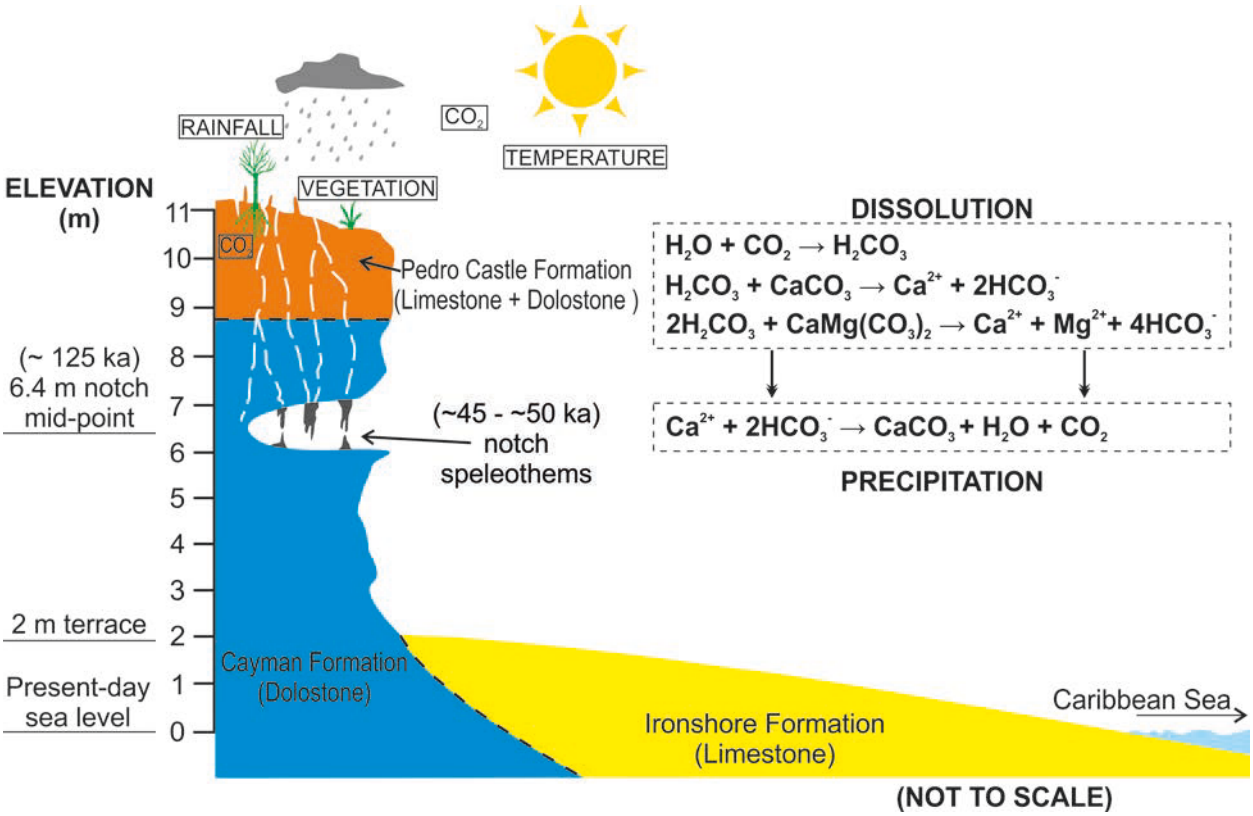

Fig. 4.1. Schematic diagram showing setting in which the notch-speleothems developed at locality CUT (Fig. 1.1B).

2. Environmental controls over the formation of aragonite versus calcite

The cooler and drier HS-5 period was the time interval when most of the aragonite laminae in the Cayman speleothems were precipitated (Fig. 4.2). This suggests that a drier climate with higher rates of evaporation may have favored the precipitation of aragonite. Enriched $\delta^{18}O$ and $\delta^{13}C$ values (Fig. 3.2), significant positive ^{18}O-$\delta^{13}C$ covariations (Fig. 3.2, 3.6), and halite and Mg-calcite found in some of the aragonite laminae also supports this notion. The formation of aragonite in these speleothems agrees with the conclusions of recent studies that high Mg/Ca ratio may be the primary control of aragonite precipitation in cave speleothems (Railsback et al., 1994; Frisia et al., 2002; Zhang et al., 2014). During dry periods, slow water percolation favors the dissolution of dolostones due to longer periods of rock-water interaction, and thereby increases the Mg^{2+} concentrations in the fluids (cf., Singurin y and Berkowitz, 2003). A dry climate

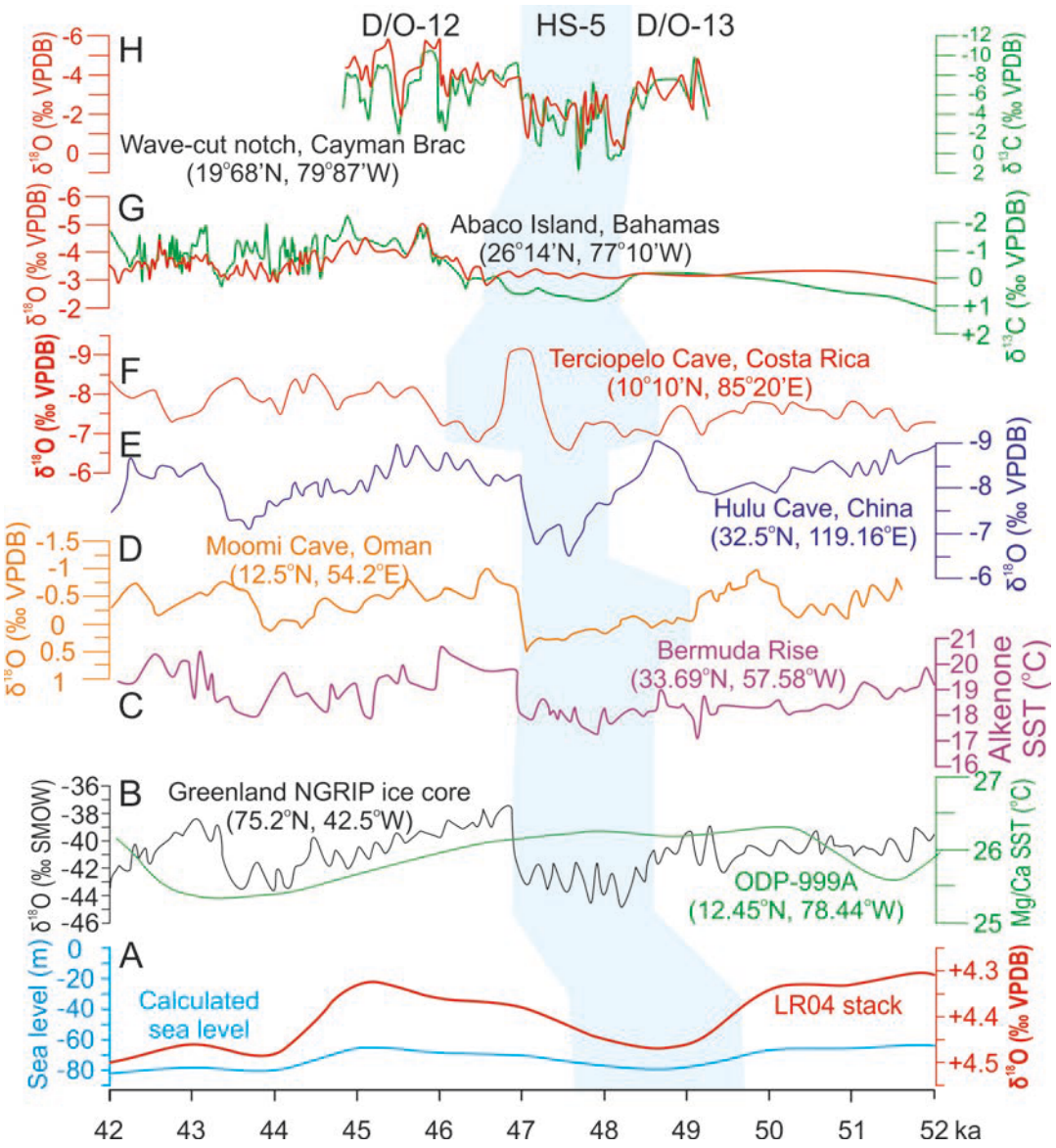

Fig. 4.2. Comparison of stable isotopic values from Cayman notch-speleothems with other paleoenvironmental records. (A) Benthic foraminiferal $\delta^{18}O$ in red (Lisiecki and Raymo, 2005) and paleo sea level in green (Spratt and Lisiecki, 2016). (B) The North GRIP (Greenland) ice core $\delta^{18}O$ record in black (Svensson et al., 2008), and Mg/Ca-derived sea surface temperatures (SSTs) in western Caribbean in green (Schmidt et al., 2006). (C) The alkenone-based SSTs from Bermuda Rise in purple (Henry et al., 2016). (D) Omani speleothem $\delta^{18}O$ records in gold (Burns et al., 2003). (E) Chinese speleothem $\delta^{18}O$ records in blue (Wang et al., 2001). (F) Costa Rican speleothem $\delta^{18}O$ records in red (Lachniet et al., 2009). (G) Bahamian speleothem $\delta^{18}O$ records in red and $\delta^{13}C$ records in green (Arienzo et al., 2017). (H) The notch stalactite $\delta^{18}O$ records in red and $\delta^{13}C$ records in green from Cayman Brac (this study). D/O-13 = Dansgaard/Oeschger interstadial 13, D/O-12 = Dansgaard/Oeschger interstadial 12, and HS-5 = Heinrich stadial 5 (light-blue shading).

with enhanced evaporation also promotes the calcite precipitation (Fairchild et al., 2006; Fairchild and Baker, 2012) along the flow paths, that also elevate the Mg/Ca ratios in the fluids tha favor the precipitation of aragonite.

The cooler temperatures during the HS-5 period challenges the conclusion that aragonite precipitation is favored by high temperatures, as has been suggested by Burton and Walter, (1987), Chen and Xiang (2009), and Rosa and Madsen (2011). The temperature control on the precipitation of aragonite has been widely debated in view of data obtained from cave speleothems (e.g., Hill and Forti, 1997; Rowling, 2004). Spötl et al. (2016), for example, documented active aragonite precipitation at near-freezing conditions (~ 0 °C) in an Austrian alpine cave. All studies seem to support the notion that temperature is not the only factor that controls the precipitation of $CaCO_3$ polymorphs in carbonate deposits, including Cayman notch-speleothems.

Taboroši and Stafford (2003) and Taboroši et al. (2003), based on the active growth of notch-speleothems from Tinian (Mariana Islands), argued that aragonite may have been precipitated from the seawater. Given that the Quaternary was a time of "aragonite seas" (Hardie, 1996; Balthasar and Cusack, 2015), seawater, with high Mg/Ca ratio and enriched $\delta^{18}O$ and $\delta^{13}C$ signatures, seems be to a possible source for aragonite precipitation. This notion, however, is difficul to apply to the Cayman notch speleothems if it is accepted that the sea-level was ~ 65 to 80 m below the present sea level as proposed by Lisiecki and Stern (2016). Drip waters from modern caves and shallow ground waters that are derived from meteoric rainfalls on Cayman Brac can precipitate aragonite and/or calcite, because analysis (Table 5.2) indicate that the waters vary from unsaturated to saturated with respect to aragonite, calcite and dolomite, and contain variable concentration so different ions (e.g. C^{2+}, Mg^{2+}, HCO_3^-).

Alternating aragonite and calcite laminae are one of the most characteristic feature in Cayman notch-speleothems. Transitions from aragonite into calcite laminae in cave speleothems typically reflect the increasing water supply due to wetter conditions (Railsback et al., 1994; Spötl et al, 2002). In the Cayman notch-speleothems (e.g., Fig. 2.2), some laminae are characterized by lateral changes from calcite and aragonite, suggesting that subtle differences in environmental conditions may have controlled their precipitation. This may, for example, reflect local variations in evaporation (cf., Railsback et al., 1994) or the simultaneous precipitation of both minerals from the same fluid (Spötl et al, 2002).

Collectively, meteoric waters were responsible for the formation of aragonite and calcite in the notch-speleothems. Temperature did not control which polymorph was precipitated. Seemingly, a drier climate with enhanced evaporation was the primary control over aragonite precipitation, whereas wet climate favored the precipitation of calcite in Cayman notch-speleothems.

3. Growth patterns of Cayman notch-speleothems

3.1. Unconformities

The unconformities that are common in the Cayman notch-speleothems show that development of these speleothems involved numerous cycles of precipitation and non-precipitation. These cycles may have been controlled by climate conditions (Fig. 4.1).

Each unconformity represents an interval of non-deposition and/or erosion of older laminae because of exceptionally wet or exceptionally dry conditions. Petrographic examination suggests that most unconformities in Cayman notch-speleothems involved the development of dissolution features, including the truncation of previously formed laminae. Unsaturated waters probably controlled their formation. Jones (2010a) also concluded that unconformities may have been caused by corrosion that was mediated by unsaturated water that flowed down the surfaces of

the notch speleothem. Erosive unconformities that are caused by unsaturated waters associated with wetter conditions are also widespread in cave speleothems (e.g., Cabrol and Coudray, 1982; Railsback et al., 2013). Tarhule-Lips (1999), however, concluded that dissolution in cave speleothems on Cayman Brac was primarily the result of condensation corrosion rather than dripwaters. Nevertheless, features evident in the Cayman notch-speleothems support the notion that development of these unconformities was associated with unsaturated waters, especially during periods when the climate was wetter. Although rare, there are some unconformities that are devoid of dissolution features. The laminae below such unconformities are thin, and composed of fine calcite crystals and in some cases, aragonite needles (Fig. 2.3D). Railsback et al. (2013) suggested unconformities with such features in cave speleothems were formed due to diminished water flows under drier climatic conditions

3.2. Diagenesis

Despite the complex temporal and spatial relationships between aragonite and calcite (Figs. 2.2, 2.3, and 2.5), there is no evidence indicative of calcitization of the aragonite. Evidence that cementation contributed to the fabrics in the Cayman notch-speleothems includes (1) calcite crystals fully or partially lining fractures that cross-cut the growth laminae (Fig. 2.3F), (2) aragonite fans that grew in the direction opposite to the outward accretion of the growth laminae (Fig. 2.5B), and (3) aragonite crystals that line cavities (Fig. 2.5A). There are examples showing gradual transitions from aragonite fans to micrite with obscure boundary (Fig. 2.5E), possibly suggesting micritization (?). Cayman notch-speleothems are formed largely of primary precipitates, that have undergone only minor diagenetic change.

3.3. Microbial influence

The influence of microbes in the development of the Cayman notch-speleothems seems to have been restricted to the laminae that developed around calcified filamentous microbes (Jones 2010a, 2010b) (Fig. 2.6A, B). Three samples from microbial-calcite laminae in stalactite CUT-3 (Fig. 3.4) yielded $\delta^{18}O$ and $\delta^{13}C$ values that are similar and comparable with surrounding abiogenic calcite laminae.

The presence of micrite around the microbes and/or the microborings (Fig. 2.6) suggests that the microbes may have played a role in micrite formation. There is also evidence that microbes may have etched the calcite crystals (Fig. 2.6H), in the manner suggested by Jones and Pemberton (1987). Available evidence supports the conclusion of Jones (2010a) that microbes played limited roles in the development of Cayman notch-speleothems.

The microbes and microbial mats in the Cayman notch-speleothems may have developed primarily under drier environmental conditions. Frisia et al. (2012) suggested that some micrite laminae with dissolution features may have been mediated by microbial mats during prolonged dry periods.

Table 4.2 Hydrochemistry and stable isotope data of water samples from Cayman Islands.

Water type	pH	T (°C)	Mg/Ca ratio	$SI_{limestone}$ (mm/L)	$SId_{olostone}$ (mm/L)	pCO_2 (10^{-3} atm)	δD (‰ SMOW)	$\delta^{18}O$ (‰ SMOW)
Cayman Brac: data from Tarhule-Lips (1993, 1999)								
Rain	6.29 ~ 6.70	23.9 ~ 27.6	Average: 3.57	Average: -3.69	Average: -6.69	Average: 0.26	Average: -49.3	Average: -7.4
Dripwater	8.29 ~ 8.99	25.5 ~ 26.7	0.90 ~ 2.10	0.84 ~ 1.42	1.93 ~ 3.15	0.30 ~ 0.39	-51.8 ~ -11.2 (aver: -28.5)	-7.7 ~ -2.7 (aver: -4.8)
Groundwater (lightly brackish)	7.27 ~ 7.43	28.6 ~ 29.7	0.47 ~ 0.82	0.04 ~ 0.18	-0.07 ~ 0.45	0.20 ~ 0.22		
Seawater	8.08 ~ 8.50	27.8 ~ 29.5	5.59 ~ 5.91	0.46 ~ 0.73	1.81 ~ 2.39	0.33 ~ 0.40		
Cayman Islands: data from Ng (1990)								
Rain (Grand Cayman)	7.3 ~ 7.8		0 ~ 0.31	-1.79 ~ -0.51	-2.08 ~ -1.14	0.28 ~ 0.36	-53.8 ~ -8.4 (aver: -27.3)	-7.3 ~ -1.6 (aver: -4.2)
Perched water	7.9	27 ~ 30	1.24 ~ 1.42	0.54 ~ 0.55	0.46 ~ 0.50	0.90 ~ 0.96	-35.3 ~ -35.0 (aver: -35.2)	-5.5 ~ -5.2 (aver: -5.4)
Groundwater (fresh)	7.5 ~ 8.1	27 ~ 30	0.73 ~ 2.76	0.41 ~ 0.81	0.31 ~ 0.77	0.80 ~ 3.00	-31.3 ~ -29.6 (aver: -30.5)	-4.8 ~ -4.4 (aver: -4.5)
Groundwater (lightly brackish)	7.6 ~ 8.0	25 ~ 27	0.80 ~ 2.62	0.48 ~ 0.78	0.44 ~ 0.76	0.61 ~ 2.14	-30.9 ~ -26.3 (aver: -28.7)	-4.5 ~ -3.9 (aver: -4.2)
Seawater (Grand Cayman)	8.2		5.17	0.8006	1.0621		+4.2 ~ +9.1 (aver: +6.4)	+1.2 ~ +1.9 (aver: +1.3)

Table 4.3 Key features and environmental interpretation of the fabrics of Cayman notch-speleothems (modified after Frisia and Borsato, 2010; Frisia et al., 2012; Fairchild and Baker, 2012; Frisia, 2015; Munoz-García et al., 2016).

Notch speleothem fabrics	**Elongated columnar (Ce)**	**Columnar open (Co)**	**Columnar compact (Cc)**	**Mosaic fabric (Mc)**	**Microspirite (Ms)**	**Micrite (M)**	**Aragonite Fans (Af)**
Main petrographic features	L/W ratio ≥ 6:1; appreciable or inappreciable porosity	1.5:1 < L/W ratio < 6:1; intercrystalline boundaries are marked by fluid inclusions or pores	1.5:1 < L/W ratio < 6:1; porosity is not appreciable	1:1 < L/W ratio ≤ 1.5:1; crystal size ≥ 30 μm; with or without aragonite relicts	L/W ratio ~ 1:1; 2 μm < crystal size < 30 μm	Crystal size <2 μm, opaque, patchy extinction, commonly below or above unconformities	Typically, L/W ratio ≥ 6:1; crystal arranger in radiating 'fans'
Conditions of formation	Constant drip rate; relatively fast flow; possible foreign ion	Relative slow drip rate, but faster than Cc; low and constant degree of supersaturation, and low impurity consent	Relative slow and constant drip rate; low and constant degree of supersaturation, and low impurity consent	Diagenesis(?); calcite precursor if without aragonite relicts; aragonite precursor if without aragonite relicts	Diagenesis(?); aggrading neomorphism (micrite to microsparite)?	Low flow/dry; bio-influenced(?); condensation corrosion?	Regular but relatively low discharge; low supersaturation; periods of dryness
Deviation from equilibrium	Quasi-equilibrium	Some degree of disequilibrium, possibly infl - enced by kinetics	Quasi-equilibrium	Quasi-equilibrium to non-equilibrium relied on its precursor	unknown	unknown	Quasi-equilibrium to non-equilibrium; variable influence of kinetics and/or evaporation

CHAPTER 5: CONCLUSIONS

The main conclusions of this study are:

- The notch-speleothems formed in the wave-cut notch on Cayman Brac that developed ~125,000 years ago when sea level was ~ 6 m above the present-day sea level.
- The Cayman notch-speleothems, including stalactites, stalagmites, columns, and flo - stones, are formed largely of calcite and aragonite, with minor amounts of halite, Mg-calcite, and dolomite.
- Aragonite laminae are characterized by radiating aragonite fans, whereas the calcite laminae are formed largely of columnar calcite and lesser amounts of mosaic and microspar calcite.
- The growth of Cayman notch-speleothems was interrupted periodically, as recorded by unconformities that formed during periods of erosion.
- Despite the complex temporal and spatial relationships between the aragonite and calcite in the Cayman notch-speleothems, there is no evidence that any of the calcite resulted from the inversion of aragonite.
- The microbes only influenced the growth of the notch-speleothems in a minor way by calcification, microboring, and etching of the host crystals
- The $\delta^{18}O$ and $\delta^{13}C$ values obtained from the notch-speleothems range from -6.5‰ to +0.3‰ (average -3.1‰ VPDB) and -11.4‰ to +1.9‰ (average -6.1‰ VPDB) respectively, with strong positive covariations between the $\delta^{18}O$ and $\delta^{13}C$ values.
- The temperatures derived from the $\delta^{18}O$ isotopes range from -0.2 to 21.3 °C (average 10.1 °C). Although not in isotopic equilibrium with the parent water, the calculated paleotemperatures indicate that speleothem growth spanned two warm periods that were

interrupted by a cooler period. Interpretation of the $\delta^{13}C$ values suggest that the two warm periods were dominated by C3 plants, whereas the cooler period was characterized by a higher proportion of C4 plants.

- Th/U dating of CUT-Z indicates that it grew ~ 50-45 ka, a time period that included the warm and wet D/O-13 period, the cooler and drier HS-5 period, and the warm and wet D/O-12 period.
- The petrographic and isotopic features of Cayman notch-speleothems are closely linked to the climatic variations that took place when the speleothems formed. The cooler and drier HS-5 period with enhanced evaporation potentially led to the elevated Mg/Ca and elevated saturation states that may have been the main control over aragonite precipitation. Precipitation of the calcite took place during the warm and wet periods (D/O-13 and D/O-12) when there was less evaporation.

REFERENCES

Andrews, J.E., 2006. Palaeoclimatic records from stable isotopes in riverine tufas: synthesis and review. Earth-Science Reviews 75, 85-104.

Arienzo, M.M., Swart, P.K., Broad, K., Clement, A.C., Pourmand, A., Kakuk, B., 2017. Multi-proxy evidence of millennial climate variability from multiple Bahamian speleothems. Quaternary Science Reviews 161, 18-29.

Balthasar, U., Cusack, M., 2015. Aragonite-calcite seas - Quantifying the grey area. Geology 43, 99-102.

Bender, M.L., Fairbanks, R.G., Taylor, F.W., Matthews, R.K., Goddard, J.G., Broecker, W.S., 1979. Uranium-series dating of the Pleistocene reef tracts of Barbados, West Indies. Geological Society of America Bulletin 90, 577-594.

Broecker, W.S., Thurber, D.L., Goddard, J., Ku, T.L., Matthews, R.K., Mesolella, K.J., 1968. Milankovitch hypothesis supported by precise dating of coral reefs and deep sea sediments. Science 159, 297-310.

Burns, S.J., Fleitmann, D., Matter, A., Kramers, J., Al-Subbary, A.A., 2003. Indian Ocean climate and an absolute chronology over Dansgaard/Oeschger events 9 to 13. Science 301, 1365-1367.

Burton, E.A., Walter, L.M., 1987. Relative precipitation rates of aragonite and Mg calcite from seawater: temperature or carbonate ion control? Geology 15, 111-114.

Cabrol, P., Coudray, J., 1982. Climatic fluctuations influence in the genesis and diagenesis o carbonate speleothems in southwestern France. National Speleological Society Bulletin 44, 112-117.

Chen, J.H., Curran, H.A., White, B., Wasserburg, G.J., 1991. Precise chronology of the Last Interglacial period: ^{234}U-^{230}Th data from fossil coral reefs in the Bahamas. Geological Society of America Bulletin 103, 82-97.

Chen, J., Xiang, L., 2009. Controllable synthesis of calcium carbonate polymorphs at different temperatures. Powder Technology 189, 64-69.

Coyne, M.K., Jones, B., Ford, D.C., 2007. Highstands during Marine Isotope Stage 5: evidence from the Ironshore Formation of Grand Cayman, British West Indies. Quaternary Science Reviews 26, 536-559.

Dabkowski, J., Brou, L., Naton, H-G., 2015. New stratigraphic and geochemical data on the Holocene environment and climate from a tufa deposit at Direndall (Mamer Valley, Luxembourg). Holocene 25, 1153-1164.

Dansgaard, W., Johnsen, S., Clausen, H.B., Dahl-Jensen, D., Gundestrup, N., Hammer, C.U., Oeschger, H., 1984. North Atlantic climatic oscillations revealed by deep Greenland ice cores. In: Hansen, J.E., Takahashi, T. (Eds.), Climate Processes and Climate Sensitivity. American Geophysical Union, Washington DC, pp. 288-298.

Darbyshire, J., Bellamy, I., Jones, B., 1976. Results of investigations into the oceanography. In: J.H. Wickstead (Ed.), Cayman Islands Natural Resources Study Part Ill, Ministry of Overseas Development, London, 120 pp.

DeMets, C., Wiggins-Grandison, M., 2007. Deformation of Jamaica and motion of the Gonave microplate from GPS and seismic data. Geophysical Journal International 168, 362-378.

Deplazes, G., Luckge, A., Peterson, L.C., Timmermann, A., Hamann, Y., Hughen, K.A., Röhl, U., Laj, C., Cane, M.A., Sigman, D.M., Haug, G.H., 2013. Links between tropical rainfall and North Atlantic climate during the Last Glacial period. Nature Geoscience 6, 213-217.

Dixon, T.H., Farina, E., DeMets, C., Jansma, E., Mann, E., Calais, E., 1998. Relative motion between the Caribbean and North American plates and related plate boundary zone deformation from a decade of GPS observations. Journal of Geophysical Research-Solid Earth 103, 15157-15182.

Edwards, R. L., Chen, J.H., Ku, T-L., Wasserburg, G.J., 1987. Precise timing of the last interglacial period from mass spectrometric determination of thorium-230 in corals. Science 230, 1547-1553.

Elderfield, H., Ferretti, ., Greaves, M., Crowhurst, S. J., McCave, I. N., Hodell, D. A., Piotrowski, A. M., 2012. Evolution of ocean temperature and ice volume through the Mid-Pleistocene Climate Transition. Science 337, 704-709.

Emery, K.O., Milliman, J.D., 1980. Shallow water limestones from slope off Grand Cayman Island. Journal of Geology 88, 483-488.

Epstein, S., Buchsbaum, R., Lowenstam, H.A., Urey, H.C., 1953. Revised carbonate-water isotopic temperature scale. Bulletin of the Geological Society of America 64, 1315-1326.

Fairbanks, R.G., Matthews, R.K., 1978. The marine oxygen isotope record in Pleistocene coral, Barbados, West Indies. Quaternary Research 10, 181-196.

Fairchild, I.J., Smith, C.L., Baker, A., Fuller, L., Spötl, C., Mattey, D., McDermott, F., E.I.M.F., 2006. Modification and preservation of environmental signals in speleothems. Earth-Science Reviews 75, 105-153.

Fairchild, I.J., Frisia, S., Borsato, A., Tooth, A., 2007. Speleothems. In: Nash, D.J., McLaren, S.J. (Eds.), Geochemical Sediments and Landscapes. Blackwell Publishing, Oxford, pp. 200-245.

Fairchild I.J., Baker A., 2012. Speleothem science: from process to past Environments. Wiley-Blackwell, Oxford, 463 pp.

Farquhar, G.D., von Caemmerer, S., Berry, J.A., 1980. A biochemical model of photosynthetic CO_2 assimilation in leaves of C_3 species. Planta 149, 78–90.

Flügel, E., 2010. Microfacies of carbonate rocks: analysis, interpretation and application. Springer, Berlin, 984 pp.

Folk, R.L., 1965. Some aspects of recrystallization in ancient limestones. In: Pray, L.C., Murray, R.C. (Eds.), Dolomitization and Limestone Diagenesis. Society of Economic Paleontologists and Mineralogists, Special Publications 13, 14-48.

Ford, T.D., Pedley, H.M., 1996. A review of tufa and travertine deposits of the world. Earth-Science Reviews 41, 117-175.

Frisia, S., Borsato, A., Fairchild, I.J., McDermott, F., 2000. Calcite fabrics, growth mechanisms, and environments of formation in speleothems from the Italian Alps and Southwestern Ireland. Journal of Sedimentary Research 70, 1183-1186.

Frisia, S., Borsato, A., Fairchild, I.J., McDermott, F., Selmo, E.M., 2002. Aragonite-calcite relationships in speleothems (Grotte de Clamouse, France): environment, fabrics, and carbonate geochemistry. Journal of Sedimentary Research 72, 687-699.

Frisia S., Borsato A., 2010. Karst. In: Alonso-Zarza A.M., Tanner, L.H. (Eds.), Carbonates in Continental Settings: Facies, Environments, and Processes. Elsevier, Amsterdam, Developments in Sedimentology 61, pp. 269-318.

Frisia, S., Borsato, A., Drysdale, R.N., Paul, B., Greig, A., Cotte, M., 2012. A re-evaluation of the palaeoclimatic significance of phosphorus variability in speleothems revealed by high-resol - tion synchrotron micro XRF mapping. Climate of the Past 8, 2039-2051.

Frisia S., 2015. Microstratigraphic logging of calcite fabrics in speleothems as tool for palaeoclimate studies. International Journal of Speleology 44, 1-16.

Gillson, L., Waldron, S., Willis, K.J., 2004. Interpretation of soil $\delta^{13}C$ as an indicator of vegetation change in African savannas. Journal of Vegetation Science 15, 339-350.

Grossman, E.L., 2012. Oxygen isotope stratigraphy. In: Gradstein, F.M., Ogg, J.G., Schmitz, M.D., Ogg, G.M. (Eds.), The Geological Time Scale 2012. Elsevier, Amsterdam, pp. 181-206.

Hardie, L.A., 1996. Secular variation in seawater chemistry: an explanation for the coupled secular variation in the mineralogies of marine limestones and potash evaporites over the past 600 m.y. Geology 24, 279–283.

Harmon, R.S., Schwarcz, H.P., Ford, D.C., 1978. Late Pleistocene sea level history of Bermuda. Quaternary Research 9, 205-218.

Harmon, R.S., Land, L.S., Mitterer, R.M., Garrett, P., Schwarcz, H.P., Larson, G.J., 1981. Bermuda sea level during the Last Interglacial. Nature 289, 481-483.

Harmon, R.S., Mitterer, R.M., Kriausakul, N., Land, L.S., Schwarcz, H.P., Garrett, P., Larson, G.J., Vacher, H.L., Rowe, M., 1983. U/Th and amino acid racemization geochronology of Bermuda: implications for eustatic sea-level fluctuation over the past 250,000 years. Paleog - ography, Paleoclimatology, Paleoecology 44, 41-70.

Hays, P.D., Grossman, E.L., 1991. Oxygen isotopes in meteoric calcite cements as indicators of continental paleoclimate. Geology 19, 441-444.

Hearty, P.J., Neumann, A.C., 2001. Rapid sea-level and climate change at the close of the Last Interglaciation (MIS 5e): evidence from the Bahama Islands. Quaternary Science Reviews 20, 1881-1895.

Hearty, P.J., Hollin, J.T., Neumann, A.C., O'Leary, M.J., McCulloch, M., 2007. Global sea-level fluctuations during the last inte glaciation (MIS 5e). Quaternary Science Reviews 26, 2090-2112.

Hendy, C.H., Wilson, A.T., 1968. Paleoclimatic data from speleothems. Nature 219, 48-51.

Heinrich, H., 1988. Origin and consequences of cyclic ice rafting in the northeast Atlantic Ocean during the past 130,000 years. Quaternary Research 29, 142-152.

Henry, L.G., McManus, J.F., Curry, W.B., Roberts, N.L., Piotrowski, A.M., Keigwin, L.D., 2016. North Atlantic Ocean circulation and abrupt climate change during the last glaciation. Science 35, 470-474.

Hill, C.A., Forti, P., 1997. Cave Minerals of the World. National Speleological Society, Huntsville. 463 pp.

Holcombe, T.L., Ladd, J.W., Westbrook, G., Edgar, N.T., Bowland, C.L., 1990. Caribbean marine geology and basins of the plate interior. In: Dengo, G., Case, J.E. (Eds.), The Geology of North America, Vol. H. The Caribbean region: A Decade of North American Geology. Geological Society of America, Boulder, pp. 231-260.

Horsfield, W.T., 1972. A late Pleistocene sea level notch and its relation to block faulting on the north coast of Jamaica. Geological Society of Jamaica Journal 12, 18-22.

Jiménez de Cisneros, C., Caballero, E., Andreo, B., Durán, J.J., 2015. Climate Variability during the Middle-Late Pleistocene based on stalagmite from Órganos Cave (Sierra de Camorra, Southern Spain). In: Andreo, B., Carrasco, F., Durán, J.J., Jiménez, P., LaMoreaux, J. (Eds.), Hydrogeological and Environmental Investigations in Karst Systems, Environmental Earth Sciences 1: Springer-Verlag, Berlin, pp. 559-567.

Johnsen, S.J., Clausen, H.B., Dansgaard, W., Fuhrer, K., Gundestrup, N., Hammer, C.U., Iversen, P., Jouzel, J., Stauffe , B., Steffensen, J. ., 1992. Irregular glacial interstadials in a new Greenland ice core. Nature 359, 311-313.

Jones, B., Pemberton, S.G., 1987. Experimental formation of spiky calcite through organically mediated dissolution. Journal of Sedimentary Petrology 57, 687-694.

Jones, B., Ng, K.C., 1988. Anatomy and diagenesis of a Pleistocene carbonate breccia formed by the collapse of a seacliff, Cayman Brac, British West Indies. Bulletin of Canadian Petroleum Geology 36, 9-24.

Jones, B., Hunter, I.G., 1989. The Oligocene-Miocene Bluff Formation on Grand Cayman. Caribbean Journal of Science 25, 71-85.

Jones, B., Hunter, I.G., 1990. Pleistocene paleogeography and sea levels on the Cayman Islands, British West Indies. Coral Reefs 9, 81-91.

Jones, B., 1994. Geology of the Cayman Islands. In: Brunt, M.A., Davies, J.E. (Eds.), The Cayman Islands: Natural History and Biogeography. Kluwer, Dordrecht, pp. 13-49.

Jones, B., Hunter, I.G., 1994. Evolution of an isolated carbonate bank during Oligocene, Miocene and Pliocene times, Cayman Brac, British west Indies. Facies 30, 25-50.

Jones, B., Hunter, I.G., Kyser, T.K., 1994a. Stratigraphy of the Bluff Formation (Miocene-Pli - cene) and the newly defined Brac Formation (Oligocene), Cayman Brac, British West Indies. Caribbean Journal of Science 30, 30-51.

Jones, B., Hunter, I.G., Kyser, T.K., 1994b. Revised stratigraphic nomenclature for the Tertiary strata of the Cayman Islands. Caribbean Journal of Science 30, 53-68.

Jones, B., Kahle, C.F., 1995. Origin of endogenetic micrite in karst terrains: a case study from the Cayman Islands. Journal of Sedimentary Research 65, 283-293.

Jones, B., Ng, K.C., Hunter, I.G., 1997. Geology and hydrogeology of the Cayman Islands. In: Vacher, H.L., Quinn, T. (Eds.), Geology and Hydrogeology of Carbonate Islands. Developments in Sedimentology 54. Elsevier, Amsterdam, pp. 299-325.

Jones, B., 2010a. Speleothems in a wave-cut notch, Cayman Brac, British West Indies: the integrated product of subaerial precipitation, dissolution, and microbes. Sedimentary Geology 232, 15-34.

Jones, B., 2010b. Microbes in caves: agents of calcite corrosion and precipitation. In: Pedley, H.M., Rogerson, M. (Eds.), Tufas and Speleothems: Unravelling the Microbial and Physical Controls. Geological Society Special Publications 336, London, pp. 7-30.

Jones, B., Peng, X., 2016. Mineralogical, crystallographic, and isotopic constraints on the precipitation of aragonite and calcite at Shiqiang and other hot springs in Yunnan Province, China. Sedimentary Geology 345, 103-125.

Kendall, A.C., Broughton, P.L., 1978. Origin of fabrics in speleothems composed of columnar calcite crystals. Journal of Sedimentary Petrology 48, 519-538.

Kim, S.T., O'Neil, J.R., 1997. Equilibrium and nonequilibrium oxygen isotope effects in synthe - ic carbonates. Geochimica et Cosmochimica Acta 61, 3461-3475.

Kim, S.-T., O'Neil, J.R., Hillaire-Marcel, C., Mucci, A., 2007. Oxygen isotope fractionation between synthetic aragonite and water: influence of temperature and M^{2+} concentration. Geochimica et Cosmochimica Acta 71, 4704-4715.

Ku, T.L., Kimmel, M.A., Easton, W.H., O'Neill, T.J., 1974. Eustatic sea level 120,000 years ago on Oahu, Hawaii. Science 183, 959-962.

Labeyrie, L.D., Duplessy, J.C., Blanc, P.L., 1987. Variations in mode of formation and temperature of oceanic deep waters over the past 125000 years. Nature 327, 477-482.

Lachniet, M.S., 2009. Climatic and environmental controls on speleothem oxygen-isotope values. Quaternary Science Reviews 28, 412-432.

Lachniet, M.S., Johnson, L., Asmerom, Y., Burns, S.J., Polyak, V., Patterson, W.P., Burt, L., Azouz, A., 2009. Late Quaternary moisture export across Central America and to Greenland: evidence for tropical rainfall variability from Costa Rican stalagmites. Quaternary Science Reviews 28, 3348-3360.

Lea, D., Martin, P.A., Pak, D.K., Spero, H.J., 2002. Reconstructing a 350 ky history of sea level using planktonic Mg/Ca and oxygen isotope records from a Cocos Ridge core. Quaternary Science Reviews 21, 283-293.

Li, R., Jones, B., 2014. Calcareous crusts on exposed Pleistocene limestones: a case study from Grand Cayman, British West Indies. Sedimentary Geology 299, 88-105.

Liang, T., Jones, B., 2014. Deciphering the impact of sea-level changes and tectonic movement on erosional sequence boundaries in carbonate successions: a case study from Tertiary strata on Grand Cayman and Cayman Brac, British West Indies. Sedimentary Geology 305, 17-34.

Liang, T., Jones, B., 2015a. Petrographic and geochemical features of sinkhole-filling deposits associated with an erosional unconformity on Grand Cayman. Sedimentary Geology 315, 64-82.

Liang, T., Jones, B., 2015b. Ongoing, long-term evolution of an unconformity that originated as a karstic surface in the Late Miocene: a case study from the Cayman Islands, British West Indies. Sedimentary Geology 322, 1-18.

Lisiecki, L.E., Raymo, M.E., 2005. A Pliocene-Pleistocene stack of 57 globally distributed benthic $\delta^{18}O$ records. Paleoceanography 20, 1-17.

Macdonald, K.C. and Holcombe, T.L. 1978. Inversion of magnetic anomalies and sea floor spreading in the Cayman Trough. Earth and Planetary Science Letters 40, 407-414.

MacNeil, A., Jones, B., 2003. Dolomitization of the Pedro Castle Formation (Pliocene), Cayman Brac, British West Indies. Sedimentary Geology 162, 219-238.

Martín-García, R., Alonso-Zarza, A.M., Martín-Pérez, A., 2009. Loss of primary texture and geochemical signatures in speleothems due to diagenesis: evidence from Castañar Cave, Spain. Sedimentary Geology 221, 141-149.

Matley, C.A., 1926. The Geology of the Cayman Islands (British West Indies) and their relation to the Bartlett Trough. Quarterly Journal of the Geological Society 82, 352-387.

McDermott, F., 2004. Palaeo-climate reconstruction from stable isotope variations in speleothems: a review. Quaternary Science Reviews 23, 901- 918.

McDermott, F., Schwarcz, H. P., and Rowe, P., 2006. Isotopes in speleothems. In: Leng, M.J. (Ed.), Isotopes in Paleoenvironmental Research. Springer, Dordrecht, 185-226.

Milliman, J.D., Hook, J.A., Golubic, S., 1985. Meaning and usage of micrite cement and matrix - reply to discussion. Journal of Sedimentary Petrology 55, 777-784.

Muñoz-García, M.B., Cruz, J., Martín-Chivelet, J., Ortega, A.I., Turrero, M.J., López-Elorza, M., 2016. Comparison of speleothem fabrics and microstratigraphic stacking patterns in calcite stalagmites as indicators of paleoenvironmental change. Quaternary International 407, 74–85.

Mylroie, J.E., Carew, J.L., 1991. Erosional notches in Bahamian carbonates: bioerosion or groundwater dissolution? In: Bain, R.J. (Ed.), Proceedings of the Fifth Symposium on Geology of the Bahamas, Bahamian Field Station, Port Charlotte, pp. 85-90.

Neumann, A.C., Moore, W.S., 1975. Sea level events and Pleistocene coral ages in the northern Bahamas. Quaternary Research 5, 215-224.

Neumann, A.C., Hearty, P.J., 1996. Rapid sea-level changes at the close of the last interglacial (substage 5e) recorded in Bahamian island geology. Geology 24, 775-778.

Ng, K.C., 1990. Diagenesis of the Oligocene-Miocene Bluff Formation of the Cayman Islands – a petrographic and hydrogeochemical approach. Unpublished Ph.D. Thesis, University of Alberta, 344 pp.

O'Neil, J.R., Clayton, R.N., Mayeda, T.K., 1969. Oxygen isotope fractionation in divalent metal carbonates. Journal of Chemical Physics 51, 5547-5558.

Pedley, H.M., Rogerson, M., 2010. Tufas and Speleothems: Unravelling the Microbial and Physical Controls. Geological Society Special Publications 336, London, 368 pp.

Perfit, M.R., Heezen, B.C., 1978. The geology and evolution of the Cayman Trench. Geological Society of America Bulletin 89, 1155-1174.

Perrin, C., Prestimonaco, L., Servelle, G., Tilhac, R., Maury, M., Cabrol, P., 2014. Aragonite-calcite speleothems: identifying original and diagenetic features. Journal of Sedimentary Research 84, 245-269.

Pleydell, S.M., 1987. Aspects of Diagenesis and Ichnology in the Oligocene-Miocene Bluff Fo - mation of Grand Cayman Island, British West Indies. Unpublished M.Sc. Thesis, 209 pp.

Railsback, L.B., Brook, G.A., Chen, J., Kalin, R., and Fleisher, C.J., 1994. Environmental controls on the petrology of a late Holocene speleothem from Botswana with annual layers of aragonite and calcite. Journal of Sedimentary Research 64, 147-155.

Railsback L.B., Akers P.D., Wang L., Holdridge G.A., Voarintsoa N.R., 2013. Layer-bounding surfaces in stalagmites as keys to better paleoclimatological histories and chronologies. International Journal of Speleology 42, 167-180.

Richards, D.A., Dorale, J.A., 2003. Uranium-series chronology and environmental applications of speleothems. In: Bourdon, B., Henderson, G.M., Lundstrom, C.C., Turner, S.P. (Eds.), Uranium-series Geochemistry. Mineralogical Society of America 656, Washington, pp. 407-460.

Rosa, S., Madsen, H.E.L., 2011. Kinetics of mass crystallization of calcium carbonate at 25, 30 and 37 °C. Journal of Crystal Growth 318, 99-102.

Rosencrantz, E., Ross, M.I., Sclater, J.G., 1988. Age and spreading history of the Cayman Trough as determined from depth, heat flo , and magnetic anomalies. Journal of Geophysical Research-Solid Earth 93, 2141-2157.

Rowling, J., 2004. Studies on aragonite and its occurrence in caves, including New South Wales caves. Journal and Proceedings of the Royal Society of New South Wales 137, 123-149.

Sage, R.F., 2004. The evolution of C_4 photosynthesis. New Phytologist 161, 341-370.

Schellmann, G., Radtke, U., 2004. A revised morpho- and chronostratigraphy of the Late and Middle Pleistocene coral reef terraces on Southern Barbados (West Indies). Earth Science Reviews 64, 157-187.

Schmidt, M.W., Vautravers, M.J., Spero, H.J., 2006. Western Caribbean sea surface temperatures during the late Quaternary. Geochemistry. Geophysics. Geosystems 7, 1-17.

Self, C.A., Hill, C.A., 2003. How speleothems grow: an introduction to the ontogeny of cave minerals. Journal of Cave and Karst Studies 65, 130-151.

Shackleton N.J., Matthews, R.K., 1977. Oxygen isotope stratigraphy of Late Pleistocene coral terraces in Barbados. Nature 268, 618-620.

Shakun, J. D., Lea, D. W., Lisiecki, L. E., and Raymo, M. E., 2015. An 800-kyr record of global surface ocean $\delta^{18}O$ and implications for ice volume-temperature coupling. Earth and Planetary Science Letters 426, 58-68.

Sharp, Z., 2007. Principles of Stable Isotope Geochemistry. Pearson Prentice Hall, New York, 360 pp.

Shopov, Y.Y., Tsankov, L.T., Yonge, C.J., Krouse, H.P.R., Jull, A.J.T., 1997. Influence of the bedrock CO_2 on stable isotope records in cave calcites. Proceedings of the 12th International Congress of Speleology. Switzerland, 65-68.

Shourie, A. 1993. Depositional architecture of the late Pleistocene Ironshore Formation, Grand Cayman, British West Indies. Unpublished M.Sc. thesis, University of Alberta, 100 pp.

Siddall, M., Rohling, E.J., Almogi-Labin, A., Hemleben, C., Meischner, D., Schmelzer, I., Smeed, D., 2003. Sea-level fluctuations during the last glacial cycle. Nature 423, 853-858

Singurindy, O., Berkowitz, B., 2003. Flow, dissolution, and precipitation in dolomite. Water Resources Research 36, 1143.

Smith, D.S., 1987. The Genesis of speleothemic calcite deposits on Grand Cayman Island, British West Indies. Unpublished M.Sc. Thesis, University of Alberta, 171 pp.

Spötl, C., Unterwurzacher, M., Mangini, A., Longstaffe, ., 2002. Carbonate speleothems in the dry, inneralpine Vinschgau Valley, northernmost Italy: witnesses of changes in hydrology and climate since the Last Glacial Maximum. Journal of Sedimentary Research 72, 793-808.

Spötl C., Fohlmeister J., Cheng H. and Boch R., 2016. Modern aragonite formation at near-freezing conditions in an alpine cave, Carnic Alps, Austria. Chemical Geology 435, 60-70.

Spratt R.M., Lisiecki, L.E., 2016. A Late Pleistocene sea level stack. Climate of the Past 12, 1079-1092.

Svensson, A., Andersen, K.K., Bigler, M., Clausen, H.B., Dahl-Jensen, D., Davies, S.M., Johnsen, S.J., Muscheler, R., Parrenin, F., Rasmussen, S.O., Rothlisberger, R., Seierstad, I., Steffensen, J. ., Vinther, B.M., 2008. A 60,000 year Greenland stratigraphic ice core chronology. Climate of the Past 4, 47-57.

Taboroši, D., Stafford, K., 2003. Littoral Dripstone and flowstone - non-spelean carbonate s - ondary deposits. International Journal of Speleology 32, 85-106.

Taboroši, D., Hirakawa, K., Stafford, K., 2003. Speleothem-like calcite and aragonite deposits on a tropical carbonate coast. Cave and Karst Science 30, 23-32.

Tarhule-Lips, R.F.A., 1993. Speleogenesis on Cayman Brac, Cayman Islands, British West Indies. Unpublished M.Sc. Thesis, McMaster University, 223 pp.

Tarhule-Lips, R.F.A., 1999. Karst processes on Cayman Brac, a small oceanic island. Unpublished Ph.D. Thesis, McMaster University, 249 pp.

ten Brink, U.S., Coleman, D.F., Dillon, W.P., 2002. The nature of the crust under Cayman Trough from gravity. Marine and Petroleum Geology 19, 971-987.

Thompson, W.G., Curran, H.A., Wilson, M.A., White, B., 2011. Sea-level oscillations during the last interglacial highstand recorded by Bahamas corals. Nature Geoscience 4, 684-687.

Tucker, M. E., Wright, V.P., 1990. Carbonate Sedimentology. Blackwell, Oxford, 482 pp.

Uzelman, B.C., 2009. Sedimentology, diagenesis, and dolomitization of the Brac Formation (Lower Oligocene), Cayman Brac, British West Indies. Unpublished M.Sc. Thesis, University of Alberta, 120 pp.

Vézina, J.L., Jones, B., Ford, D., 1999. Sea level highstands over the last 500,000 years: evidence from the Ironshore Formation on Grand Cayman, British West Indies. Journal of Sedimentary Research 69, 317-327.

Waelbroeck, C., Labeyrie, L., Michel, E., Duplessy J.C., McManus J., 2002. Sea-level and deep water temperature changes derived from benthic foraminifera isotopic records. Quaternary Science Reviews 21, 295-305.

Wang, Y.J., Cheng, H., Edwards, R.L., An, Z.S., Wu, J.Y., Shen, C.C., Dorale, J.A., 2001. A high-resolution absolute-dated Late Pleistocene monsoon record from Hulu Cave, China. Science 294, 2345-2348.

Woodroffe, C.D., Stoddart, D.R., Harmon, R.S., Spence , T., 1983. Coastal morphology and Late Quaternary history, Cayman Islands, West Indies. Quaternary Research 19, 64-84.

Zhang, H., Cai, Y., Tana, L., Qina, S., Ana, Z., 2014. Stable isotope composition alteration produced by the aragonite-to-calcite transformation in speleothems and implications for paleoclimate reconstructions. Sedimentary Geology 309, 1-14.

Zhao, H and Jones, B. 2012a, Origin of “island dolostones”: A case study from the Cayman Formation (Miocene), Cayman Brac, British West Indies. Sedimentary Geology 243-244, 191-206.

Zhao, H and Jones, B. 2012b, Genesis of fabric-destructive dolostones: A case study of the Brac Formation (Oligocene), Cayman Brac, British West Indies. Sedimentary Geology, 267-268, 36-54.

Zhao, H.W., Jones, B., 2013. Distribution and interpretation of rare earth elements and yttrium in Cenozoic dolostones and limestones on Cayman Brac, British West Indies. Sedimentary Geology 284-285, 26-38.

APPENDIX A

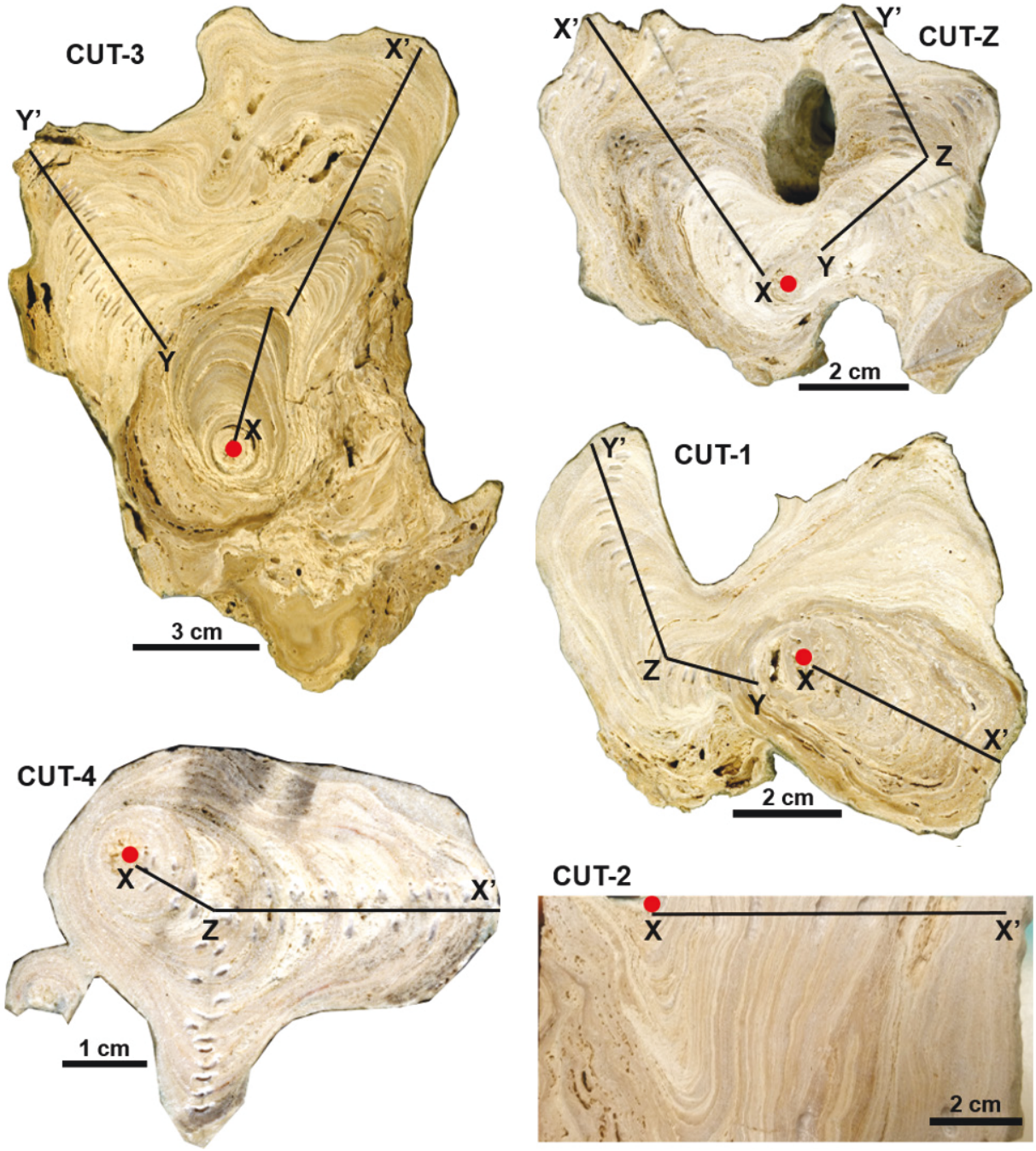

Fig. A.1 Sampling protocol of stable isotopes from five Cayman notch-speleothems (CU -3, CUT-Z, CUT-1, CUT-4, and CUT-Z). Black lines are sampling traces. The red dots on each sample are the start points.

Table A.1 Raw stable isotope results from five Cayman notch-speleothems (n = 224)

Transect number	Sample number	distance from start point (mm)	$\delta^{18}O$ (‰ VPDB)	$\delta^{13}C$ (‰ VPDB)
CUT-3 (X-X')	CUT3-01	1	-2.0	-3.4
CUT-3 (X-X')	CUT3-02	14	-3.8	-7.4
CUT-3 (X-X')	CUT3-03	36	-2.9	-6.4
CUT-3 (X-X')	CUT3-04	46	0.0	0.6
CUT-3 (X-X')	CUT3-05	65	-2.3	-5.1
CUT-3 (X-X')	CUT3-06	104	-3.7	-5.0
CUT-3 (X-X')	CUT3 X-1	7	-4.7	-10.2
CUT-3 (X-X')	CUT3 X-2	9	-1.9	-5.2
CUT-3 (X-X')	CUT3 X-3	22	-2.4	-7.6
CUT-3 (X-X')	CUT3 X-4	25	-2.8	-7.6
CUT-3 (X-X')	CUT3 X-5	29	-4.2	-6.3
CUT-3 (X-X')	CUT3 X-6	31	-2.8	-4.5
CUT-3 (X-X')	CUT3 X-7	33	-3.2	-5.2
CUT-3 (X-X')	CUT3 X-8	35	-3.4	-6.8
CUT-3 (X-X')	CUT3 X-9	38	-2.1	-3.1
CUT-3 (X-X')	CUT3 X-10	39	-1.9	-2.8
CUT-3 (X-X')	CUT3 X-11	40	-1.7	-1.7
CUT-3 (X-X')	CUT3 X-12	42	0.0	0.1
CUT-3 (X-X')	CUT3 X-13	44	-0.3	0.0
CUT-3 (X-X')	CUT3 X-14	45	-0.4	0.4
CUT-3 (X-X')	CUT3 X-15	48	-0.7	0.4
CUT-3 (X-X')	CUT3 X-16	50	-2.8	-5.7
CUT-3 (X-X')	CUT3 X-17	53	-1.7	-3.4
CUT-3 (X-X')	CUT3 X-18	55	-3.0	-7.4
CUT-3 (X-X')	CUT3 X-19	56	-1.3	-2.0
CUT-3 (X-X')	CUT3 X-20	57	-2.4	-2.8
CUT-3 (X-X')	CUT3 X-21	59	-0.9	-0.7
CUT-3 (X-X')	CUT3 X-22	60	-3.1	-5.2
CUT-3 (X-X')	CUT3 X-23	62	0.3	1.9
CUT-3 (X-X')	CUT3 X-24	56	-0.6	-2.0
CUT-3 (X-X')	CUT3 X-25	57	-2.5	-6.8
CUT-3 (X-X')	CUT3 X-26	58	-1.4	-2.5
CUT-3 (X-X')	CUT3 X-27	60	-3.2	-7.1
CUT-3 (X-X')	CUT3 X-28	61	-3.3	-7.7
CUT-3 (X-X')	CUT3 X-29	63	-1.7	-4.8
CUT-3 (X-X')	CUT3 X-30	67	-2.1	-5.6
CUT-3 (X-X')	CUT3 X-31	69	-1.4	-1.9
CUT-3 (X-X')	CUT3 X-32	71	-1.7	-1.9

CUT-3 (X-X')	CUT3 X-33	74	-2.3	-4.0
CUT-3 (X-X')	CUT3 X-34	76	-2.1	-3.3
CUT-3 (X-X')	CUT3 X-35	78	-2.7	-5.7
CUT-3 (X-X')	CUT3 X-36	80	-1.0	-0.7
CUT-3 (X-X')	CUT3 X-37	82	-1.3	-1.3
CUT-3 (X-X')	CUT3 X-38	85	-2.9	-6.0
CUT-3 (X-X')	CUT3 X-39	89	-3.8	-8.7
CUT-3 (X-X')	CUT3 X-40	90	-5.0	-9.6
CUT-3 (X-X')	CUT3 X-41	92	-3.3	-4.4
CUT-3 (X-X')	CUT3 X-42	94	-3.4	-5.4
CUT-3 (X-X')	CUT3 X-43	95	-4.7	-8.0
CUT-3 (X-X')	CUT3 X-44	97	-5.6	-9.1
CUT-3 (X-X')	CUT3 X-45	99	-5.2	-8.7
CUT-3 (X-X')	CUT3 X-46	101	-5.1	-9.1
CUT-3 (X-X')	CUT3 X-47	103	-4.9	-7.2
CUT-3 (X-X')	CUT3 X-48	105	-3.0	-3.0
CUT-3 (X-X')	CUT3 X-49	107	-4.3	-5.6
CUT-3 (X-X')	CUT3 X-50	109	-3.4	-5.2
CUT-3 (X-X')	CUT3 X-51	110	-3.8	-7.4
CUT-3 (X-X')	CUT3 X-52	111	-4.2	-8.1
CUT-3 (X-X')	CUT3 X-53	113	-4.7	-7.7
CUT-3 (X-X')	CUT3 X-54	115	-4.2	-8.3
CUT-3 (X-X')	CUT3 X-55	117	-4.1	-4.6
CUT-3 (Y-Y')	CUT3 Y-1	87	-0.2	-6.0
CUT-3 (Y-Y')	CUT3 Y-2	89	-1.8	-5.4
CUT-3 (Y-Y')	CUT3 Y-3	91	-3.6	-9.3
CUT-3 (Y-Y')	CUT3 Y-4	96	-3.6	-8.7
CUT-3 (Y-Y')	CUT3 Y-5	98	-3.1	-7.5
CUT-3 (Y-Y')	CUT3 Y-6	101	-3.4	-8.1
CUT-3 (Y-Y')	CUT3 Y-7	102	-3.5	-8.4
CUT-3 (Y-Y')	CUT3 Y-8	104	-4.0	-8.5
CUT-3 (Y-Y')	CUT3 Y-9	107	-3.6	-7.0
CUT-3 (Y-Y')	CUT3 Y-10	109	-3.4	-7.2
CUT-3 (Y-Y')	CUT3 Y-11	111	-4.5	-7.6
CUT-3 (Y-Y')	CUT3 Y-12	114	-3.2	-4.7
CUT-3 (Y-Y')	CUT3 Y-13	117	-4.1	-8.3
CUT-3 (Y-Y')	CUT3 Y-14	120	-3.4	-5.8
CUT-3 (Y-Y')	CUT3 Y-15	122	-3.8	-8.3
CUT-3 (Y-Y')	CUT3 Y-16	123	-4.1	-5.3
CUT-3 (Y-Y')	CUT3 Y-17	125	-2.4	-2.2
CUT-3 (Y-Y')	CUT3 Y-18	127	-3.9	-4.8

CUT-3 (Y-Y')	CUT3 Y-19	128	-2.9	-2.6
CUT-3 (Y-Y')	CUT3 Y-20	129	-5.8	-9.6
CUT-3 (Y-Y')	CUT3 Y-21	133	-5.1	-10.2
CUT-3 (Y-Y')	CUT3 Y-22	136	-5.5	-10.3
CUT-3 (Y-Y')	CUT3 Y-23	137	-4.2	-7.7
CUT-3 (Y-Y')	CUT3 Y-24	142	-3.9	-7.2
CUT-3 (Y-Y')	CUT3 Y-25	144	-3.9	-4.9
CUT-3 (Y-Y')	CUT3 Y-26	146	-3.5	-4.3
CUT-3 (Y-Y')	CUT3 Y-27	147	-1.6	-1.9
CUT-Z (X-X')	CUTZ X-1	5	-3.9	-5.8
CUT-Z (X-X')	CUTZ X-2	7	-1.9	-5.8
CUT-Z (X-X')	CUTZ X-3	10	-3.0	-6.9
CUT-Z (X-X')	CUTZ X-4	11	-3.0	-6.3
CUT-Z (X-X')	CUTZ X-5	12	-4.1	-8.1
CUT-Z (X-X')	CUTZ X-6	14	-3.0	-6.3
CUT-Z (X-X')	CUTZ X-7	15	-3.6	-7.7
CUT-Z (X-X')	CUTZ X-8	17	-3.3	-6.7
CUT-Z (X-X')	CUTZ X-9	20	-3.8	-7.5
CUT-Z (X-X')	CUTZ X-10	21	-4.0	-8.6
CUT-Z (X-X')	CUTZ X-11	24	-4.3	-8.9
CUT-Z (X-X')	CUTZ X-12	25	-3.6	-6.5
CUT-Z (X-X')	CUTZ X-13	27	-2.8	-3.9
CUT-Z (X-X')	CUTZ X-14	30	-2.9	-4.4
CUT-Z (X-X')	CUTZ X-15	32	-2.8	-4.3
CUT-Z (X-X')	CUTZ X-16	34	-3.9	-5.5
CUT-Z (X-X')	CUTZ X-17	36	-2.1	-4.9
CUT-Z (X-X')	CUTZ X-18	38	-1.4	-1.8
CUT-Z (X-X')	CUTZ X-19	40	-4.1	-7.6
CUT-Z (X-X')	CUTZ X-20	41	-2.2	-6.5
CUT-Z (X-X')	CUTZ X-21	42	-2.8	-7.7
CUT-Z (X-X')	CUTZ X-22	43	-2.6	-4.7
CUT-Z (X-X')	CUTZ X-23	44	-3.7	-6.7
CUT-Z (X-X')	CUTZ X-24	46	-4.9	-10.0
CUT-Z (X-X')	CUTZ X-25	48	-2.8	-5.6
CUT-Z (X-X')	CUTZ X-26	50	-4.1	-9.0
CUT-Z (X-X')	CUTZ X-27	52	-3.2	-6.0
CUT-Z (X-X')	CUTZ X-28	54	-2.7	-3.8
CUT-Z (X-X')	CUTZ X-29	57	-2.3	-3.0
CUT-Z (X-X')	CUTZ X-30	58	-2.9	-6.2
CUT-Z (X-X')	CUTZ X-31	59	-3.5	-8.2
CUT-Z (X-X')	CUTZ X-32	62	-2.2	-4.8

CUT-Z (X-X')	CUTZ X-33	64	-3.6	-4.3
CUT-Z (X-X')	CUTZ X-34	67	-2.7	-6.0
CUT-Z (X-X')	CUTZ X-35	70	-2.8	-4.7
CUT-Z (X-X')	CUTZ X-36	72	-1.8	-1.2
CUT-Z (X-X')	CUTZ X-37	74	-3.2	-3.9
CUT-Z (Y-Z-Y')	CUTZ Y-1	18	-2.7	-7.3
CUT-Z (Y-Z-Y')	CUTZ Y-2	19.5	-2.3	-6.7
CUT-Z (Y-Z-Y')	CUTZ Y-3	20	-2.8	-8.0
CUT-Z (Y-Z-Y')	CUTZ Y-4	23	-3.3	-8.0
CUT-Z (Y-Z-Y')	CUTZ Y-5	24	-2.7	-7.7
CUT-Z (Y-Z-Y')	CUTZ Y-6	25	-3.4	-9.0
CUT-Z (Y-Z-Y')	CUTZ Y-7	27	-2.5	-7.3
CUT-Z (Y-Z-Y')	CUTZ Y-8	28	-2.9	-7.0
CUT-Z (Y-Z-Y')	CUTZ Y-9	30	-2.8	-7.6
CUT-Z (Y-Z-Y')	CUTZ Y-10	32	-2.5	-7.3
CUT-Z (Y-Z-Y')	CUTZ Y-11	35	-3.3	-8.5
CUT-Z (Y-Z-Y')	CUTZ Y-12	37	-3.6	-9.4
CUT-Z (Y-Z-Y')	CUTZ Y-13	40	-3.0	-8.4
CUT-Z (Y-Z-Y')	CUTZ Y-14	42	-4.6	-8.1
CUT-Z (Y-Z-Y')	CUTZ Y-15	41	-0.6	-2.1
CUT-Z (Y-Z-Y')	CUTZ Y-16	44	-2.9	-7.7
CUT-Z (Y-Z-Y')	CUTZ Y-17	46	-2.5	-5.2
CUT-Z (Y-Z-Y')	CUTZ Y-18	48	-3.7	-9.0
CUT-Z (Y-Z-Y')	CUTZ Y-19	50	-3.0	-6.0
CUT-Z (Y-Z-Y')	CUTZ Y-20	52	-1.9	-5.0
CUT-Z (Y-Z-Y')	CUTZ Y-21	54	-4.0	-7.8
CUT-Z (Y-Z-Y')	CUTZ Y-22	56	-1.4	-4.5
CUT-Z (Y-Z-Y')	CUTZ Y-23	59	-3.7	-8.8
CUT-Z (Y-Z-Y')	CUTZ Y-24	63	-2.6	-6.9
CUT-Z (Y-Z-Y')	CUTZ Y-25	65	-3.3	-9.0
CUT-Z (Y-Z-Y')	CUTZ Y-26	68	-3.2	-8.2
CUT-Z (Y-Z-Y')	CUTZ Y-27	70	-2.5	-5.7
CUT-Z (Y-Z-Y')	CUTZ Y-28	72	-1.5	-2.9
CUT-Z (Y-Z-Y')	CUTZ Y-29	75	-2.4	-5.2
CUT-1 (X-X')	CUT1-01	2	-1.6	-3.7
CUT-1 (X-X')	CUT1-02	12	-1.8	-7.2
CUT-1 (X-X')	CUT1-03	35	-1.4	-6.3
CUT-1 (X-X')	CUT1-04	14	-1.5	-2.7
CUT-1 (X-X')	CUT1-05	55	-3.3	-5.1
CUT-1 (X-X')	CUT1-06	76	-2.6	-2.3
CUT-1 (X-X')	CUT1 X-1	0	-2.4	-8.2

CUT-1 (X-X')	CUT1 X-2	6	-1.3	-6.9
CUT-1 (X-X')	CUT1 X-3	11	-1.8	-7.1
CUT-1 (X-X')	CUT1 X-4	15	-2.1	-7.7
CUT-1 (X-X')	CUT1 X-5	23	-1.3	-6.9
CUT-1 (X-X')	CUT1 X-6	27	-0.9	-6.9
CUT-1 (X-X')	CUT1 X-7	31	-0.4	-7.2
CUT-1 (X-X')	CUT1 X-8	37	-1.3	-6.1
CUT-1 (X-X')	CUT1 X-9	40	-0.4	-6.5
CUT-1 (X-X')	CUT1 X-10	42	-0.7	-4.3
CUT-1 (X-X')	CUT1 X-11	45	-1.7	-6.3
CUT-1 (Y-Z-Y')	CUT1 Y-1	12	0.0	0.6
CUT-1 (Y-Z-Y')	CUT1 Y-2	15	-1.4	-3.0
CUT-1 (Y-Z-Y')	CUT1 Y-3	17	-1.9	-8.8
CUT-1 (Y-Z-Y')	CUT1 Y-4	22	-2.8	-8.1
CUT-1 (Y-Z-Y')	CUT1 Y-5	25	-0.2	-1.9
CUT-1 (Y-Z-Y')	CUT1 Y-6	27	-1.5	-7.9
CUT-1 (Y-Z-Y')	CUT1 Y-7	30	-1.4	-4.1
CUT-1 (Y-Z-Y')	CUT1 Y-8	34	-3.6	-5.4
CUT-1 (Y-Z-Y')	CUT1 Y-9	40	-4.0	-5.9
CUT-1 (Y-Z-Y')	CUT1 Y-10	44	-5.4	-9.2
CUT-1 (Y-Z-Y')	CUT1 Y-11	47	-4.2	-9.3
CUT-1 (Y-Z-Y')	CUT1 Y-12	50	-3.9	-6.6
CUT-1 (Y-Z-Y')	CUT1 Y-13	54	-4.4	-7.0
CUT-1 (Y-Z-Y')	CUT1 Y-14	57	-3.0	-6.0
CUT-1 (Y-Z-Y')	CUT1 Y-15	60	-1.8	-2.3
CUT-1 (Y-Z-Y')	CUT1 Y-16	63	-4.8	-6.9
CUT-1 (Y-Z-Y')	CUT1 Y-17	66	-2.8	-2.5
CUT-1 (Y-Z-Y')	CUT1 Y-18	69	-3.3	-4.9
CUT-1 (Y-Z-Y')	CUT1 Y-19	73	-2.6	-2.9
CUT-1 (Y-Z-Y')	CUT1 Y-20	75	-1.8	-2.0
CUT-1 (Y-Z-Y')	CUT1 Y-21	77	-2.2	-3.6
CUT-2 (X-X')	CUT2-01	6	-2.9	-6.1
CUT-2 (X-X')	CUT2-02	17	-0.3	0.3
CUT-2 (X-X')	CUT2-03	28	-3.3	-6.8
CUT-2 (X-X')	CUT2-04	40	-2.2	-4.1
CUT-2 (X-X')	CUT2-05	52	-2.8	-5.4
CUT-2 (X-X')	CUT2-06	61	-2.0	-8.2
CUT-2 (X-X')	CUT2-07	78	-4.9	-7.7
CUT-4 (X-Z-X')	CUT4 X-1	2	-6.1	-7.3
CUT-4 (X-Z-X')	CUT4 X-2	3	-6.2	-6.7
CUT-4 (X-Z-X')	CUT4 X-3	4	-6.5	-8.0

CUT-4 (X-Z-X')	CUT4 X-4	5	-6.0	-8.0
CUT-4 (X-Z-X')	CUT4 X-5	7	-5.5	-7.7
CUT-4 (X-Z-X')	CUT4 X-6	8	-5.0	-9.0
CUT-4 (X-Z-X')	CUT4 X-7	9	-5.3	-7.3
CUT-4 (X-Z-X')	CUT4 X-8	11	-5.2	-7.0
CUT-4 (X-Z-X')	CUT4 X-9	13	-4.0	-7.6
CUT-4 (X-Z-X')	CUT4 X-10	16	-4.2	-5.8
CUT-4 (X-Z-X')	CUT4 X-11	18	-5.4	-5.8
CUT-4 (X-Z-X')	CUT4 X-12	19	-5.9	-6.9
CUT-4 (X-Z-X')	CUT4 X-13	20	-4.2	-6.3
CUT-4 (X-Z-X')	CUT4 X-14	22	-4.1	-8.1
CUT-4 (X-Z-X')	CUT4 X-15	23	-5.2	-6.3
CUT-4 (X-Z-X')	CUT4 X-16	25	-4.8	-7.7
CUT-4 (X-Z-X')	CUT4 X-17	26	-5.3	-6.7
CUT-4 (X-Z-X')	CUT4 X-18	28	-4.4	-7.5
CUT-4 (X-Z-X')	CUT4 X-19	30	-3.9	-8.6
CUT-4 (X-Z-X')	CUT4 X-20	32	-5.6	-8.9
CUT-4 (X-Z-X')	CUT4 X-21	34	-5.0	-6.5
CUT-4 (X-Z-X')	CUT4 X-22	35	-4.3	-3.9
CUT-4 (X-Z-X')	CUT4 X-23	36	-4.3	-4.4
CUT-4 (X-Z-X')	CUT4 X-24	38	-4.8	-4.3
CUT-4 (X-Z-X')	CUT4 X-25	40	-5.8	-5.5